

Chemical Vapor Deposition Thin Films as Biopassivation Coatings and Directly Patternable Dielectrics

by

Hilton G. Pryce Lewis

M.S. in Chemical Engineering Practice
Massachusetts Institute of Technology, 1998

B. Sc. Eng. (Chemical)
University of Natal, South Africa, 1995

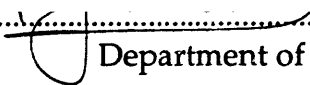
Submitted to the Department of Chemical Engineering
in Partial Fulfillment of the Requirements for the Degree of

DOCTOR OF PHILOSOPHY IN CHEMICAL ENGINEERING
AT THE
MASSACHUSETTS INSTITUTE OF TECHNOLOGY

June 2001

© 2001 Massachusetts Institute of Technology. All rights reserved.

Signature of Author



Department of Chemical Engineering
April 27, 2001

Certified by



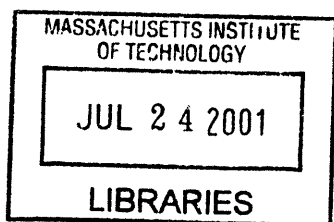
Karen K. Gleason
Professor of Chemical Engineering
Thesis Supervisor

Accepted by



Robert E. Cohen

St. Laurent Professor of Chemical Engineering
Chairman, Committee for Graduate Students



ARCHIVES

Chemical Vapor Deposition Thin Films as Biopassivation Coatings and Directly Patternable Dielectrics

by

Hilton Gavin Pryce Lewis

Submitted to the Department of Chemical Engineering
on April 27, 2001 in Partial Fulfillment of the
Requirements for the Degree of
Doctor of Philosophy in Chemical Engineering

ABSTRACT

Organosilicon thin films deposited by pulsed plasma-enhanced chemical vapor deposition (PPECVD) and hot-filament chemical vapor deposition (HFCVD) were investigated as potential biopassivation coatings for neural probes. It was found that organosilicon films from identical precursors differ in structure according to the method of deposition. For films produced from the cyclic siloxane precursor, hexamethylcyclotrisiloxane, pulsed plasma excitation reduced crosslink density over continuous excitation and produced flexible films resistant to prolonged saline soak testing. Deposition via a thermal process, HFCVD, allowed films of novel organosilicon structure to be formed from both hexamethylcyclotrisiloxane and its eight-membered analog, octamethylcyclotetrasiloxane. Characterization of these films was accomplished, and the effect of filament temperature on the chemical structure was elucidated. Silicon-silicon bonding and the retention of ring structures from the precursor was observed in HFCVD organosilicon films using Micro-Raman spectroscopy.

A direct dielectric patterning process was proposed for semiconductor manufacturing. In this process, a dielectric material is patterned directly and developed without the need for a sacrificial photoresist layer. HFCVD fluorocarbon films are under consideration as low-dielectric constant interlayer dielectrics, and direct patterning of these materials was demonstrated using e-beam irradiation and supercritical CO₂ development. The use of a gas-phase initiator species for HFCVD of fluorocarbon thin films was also demonstrated. Initiation enhanced deposition rates significantly and provided a means of selectively end-capping polymer chains present in the film structure.

Thesis Supervisor: Karen K. Gleason
Title: Professor of Chemical Engineering

For Mom and Dad

Acknowledgments

I dedicate this work to Mom and Dad. I would be nowhere without their unconditional love and support. They have always been role models for me in how to inspire and encourage selflessly; pulling rather than pushing. I want to thank them for everything they have given me, and tell them I love them. I also want to acknowledge my family back in South Africa: Jord, Trish, Sue, Ray, Cameron, Dylan, Judith, Sonny, and – of course – Ang in jolly old England. Little did I know five years could be so happy and sad at the same time. Also, to the memory of Gaga and Granny; I'm so glad I got to share in your lives for most of mine. Love you lots, miss you more.

It has been the utmost privilege for me to have worked closely with my advisor, Karen, during my time here. I made a very, very good choice, and it's tough to believe now that I almost wrote off the whole Ph.D. thing. Your guidance, diplomacy, and friendship is much appreciated, and will hopefully continue for many years to come. A stellar advisor begets a stellar research group, and I want to acknowledge the many witty, brilliant, sour, garrulous, overly fastidious, laconic, and plain old friendly personalities that have passed through the group over the years. Keep 'em coming! I want to especially thank Ken for many years of lengthy and enlightening conversation (animated on my part, incisive on his) and friendship. Many more to come, I hope. I'd also like to thank my "summer students", Tom and Jeff, who I credit with advancing my accomplishments in two giant leaps. Finally, I'd like to thank Todd Bailey for his warm interaction and fantastic parties!

Many friends have been made (and a few lost, unfortunately) during my time in Boston. Thanks to all those people who made my Ph.D. such fun. Special thanks to Inge and Bruno – you intimidating Europeans! You make things so much brighter and sunnier, and I relish the years we have together both in the past and to come. And, yes, Inge; Wendy and I **will** still talk to you...

My degree is in two parts: BW and AW. I am sure that everything I wrote after meeting you, Wendy, is that much more eloquent and cheery. I had to go a long way, and wait a long time, but I found you. Now we sit back and enjoy the ride. I love you, and can't wait for our new life together.

Finally, I want to acknowledge my Lord, Jesus Christ. Thank You for all that You've given me.

"But they that wait upon the Lord shall renew their strength; they shall mount up with wings as eagles; they shall run, and not be weary; they shall walk, and not faint." *Isaiah 40:31*.

Table of Contents

Abstract	2
Dedication	3
Acknowledgments	4
List of Figures	7
List of Tables	12
List of Notations	13
CHAPTER 1	14
Introduction	
1.1 Chemical Vapor Deposition (CVD)	15
1.2 Biopassivation Coatings	18
1.3 Directly Patternable Dielectrics	23
1.4 Scope of Thesis	25
1.5 References	25
CHAPTER 2	30
Pulsed-PECVD Films from D ₃ for Use as Insulating Biomaterials	
2.1 Abstract	31
2.2 Introduction	32
2.3 Experimental	34
2.4 Results and Discussion	35
2.5 Conclusions	46
2.6 References	47
CHAPTER 3	50
HFCVD of Organosilicon Thin Films from D ₃ and D ₄	
3.1 Abstract	51
3.2 Introduction	52
3.3 Experimental	53
3.4 Results and Discussion	54
3.5 Conclusions	75
3.6 References	75
CHAPTER 4	79
E-Beam Patterning of HFCVD Fluorocarbon Films Using Supercritical CO ₂ as Developer	
4.1 Abstract	80
4.2 Introduction	81
4.3 Experimental	82
4.4 Results and Discussion	83
4.5 Conclusion	86
4.6 References	86

CHAPTER 5	88
Perfluorooctane Sulfonyl Fluoride as an Initiator in HFCVD of Fluorocarbon Thin Films	
5.1 Abstract	89
5.2 Introduction	90
5.3 Experimental	91
5.4 Results and Discussion	92
5.5 Conclusions	99
5.6 References	99
CHAPTER 6	101
Hot-Wire Deposition of Organosilicon and Fluorocarbon Thin Films	
6.1 Abstract	102
6.2 Introduction	103
6.3 Experimental	103
6.4 Results and Discussion	105
6.5 Conclusions	109
6.6 References	109
CHAPTER 7	111
Conclusions and Future Work	
7.1 Conclusions	112
7.2 Future Work	114
7.3 References	114
APPENDIX A	115
Reactor Design and Construction	
A.1 Description	116
A.2 Main Chamber CAD Drawings	118
A.3 Bottom Plate CAD Drawing	121
A.4 Reactor Lid CAD Drawings	121
A.5 Rear Flange CAD Drawings	123
APPENDIX B	124
Additive Precursors Used in Combination with HFPO HFCVD	
B.1 List of Additive Precursors	125
B.2 Deposition Rates with Additive Precursors	125
B.3 New Chemistries Possible Using HFCVD with Dual Precursors	126

List of Figures

CHAPTER ONE

- Figure 1-1.** Schematic of a typical parallel-plate PECVD system.
- Figure 1-2.** Potential problem areas in the protection of implantable integrated circuits by thin layers of insulating biomaterials.
- Figure 1-3.** Direct dielectric patterning scheme.

CHAPTER TWO

- Figure 2-1.** Optical micrographs showing 750 μm loops of 3-mil copper wire coated with D_3 pulsed-PECVD film at (a) CW, (b) 10/60, (c) 50/300, and (d) 100/600. Film thickness is (a) 19 μm , (b) 9 μm , (c) 12 μm , and (d) 13 μm . Film deposited at 100/600 shows the most flexibility.
- Figure 2-2.** Coating on a University of Michigan probe deposited at 50/300, showing conformity of coating. Film is 20 μm at the thickest point.
- Figure 2-3.** FTIR spectra of (a) pulsed-PECVD film deposited at 100/600, and (b) PDMS secondary standard. Absorption spectra of pulsed-PECVD film has been normalized to standard thickness of 1,500 \AA .
- Figure 2-4.** FTIR spectral region from 600 cm^{-1} to 1,500 cm^{-1} for CW, 100/600 and 10/400 films. Respective duty cycles are 100%, 14% and 2.4%.
- Figure 2-5.** FTIR spectral region from 3,050 cm^{-1} to 2,800 cm^{-1} for CW, 100/600 and 10/400 films, showing CH_x correlated absorptions.
- Figure 2-6.** Possible crosslinking and/or branching nodes present in PECVD films. Non-branching M and D groups are shown for reference. Nodes of Type I involve only oxygen, while nodes of Type II involve both oxygen atoms and methylene groups.
- Figure 2-7.** Reaction pathways for the production of polymerization precursors from D_3 .

CHAPTER THREE

- Figure 3-1.** Arrhenius plot of D_3 and D_4 films produced by HFCVD. Straight lines were fitted by regression.
- Figure 3-2.** FTIR spectra of a. D_3 PECVD film deposited under continuous-wave excitation, and b. D_3 HFCVD film deposited at 1000°C.

- Figure 3-3.** FTIR spectra of D₃ HFCVD films deposited at filament temperatures of a. 860°C, b. 1000°C, and c. 1100°C.
- Figure 3-4.** FTIR spectra of D₄ HFCVD films deposited at filament temperatures of a. 800°C, b. 900°C, and c. 1000°C.
- Figure 3-5.** Micro-Raman spectra of a. D₃, b. D₄, c. PDMS, d. D₄ HFCVD film deposited at a filament temperature of 1000°C, and e. D₃ HFCVD film deposited at a filament temperature of 1100°C.
- Figure 3-6.** Micro-Raman spectra of D₃ HFCVD films deposited at filament temperatures of 860°C, 1000°C, and 1100°C.
- Figure 3-7.** Micro-Raman spectra of D₄ HFCVD films deposited at filament temperatures of 800°C, 900°C, and 1000°C.
- Figure 3-8.** ²⁹Si Solid-State CP-MAS NMR spectra of D₃ HFCVD film deposited at filament temperatures of 860°C, 1000°C, and 1100°C.
- Figure 3-9.** ²⁹Si Solid-State CP-MAS NMR spectra of D₄ HFCVD film deposited at filament temperatures of 800°C, 900°C, and 1000°C.
- Figure 3-10.** Atomic force micrograph of D₄ HFCVD film deposited at a filament temperature of 900°C. RMS roughness over image area is 1.1 nm. RMS roughness of bare silicon is 0.53 nm.
- Figure 3-11.** Reaction pathways for the production of polymerization precursor species in D₃ and D₄ HFCVD.

CHAPTER FOUR

- Figure 4-1.** FTIR spectra of hot-filament CVD fluorocarbon films from HFPO, showing the change in –OH and –COOH content as a result of varying process conditions. OH/CF₂ ratios were estimated by integrating the area of each absorption stretch in the FTIR spectra.
- Figure 4-2.** Contrast curves of samples 3, 4, 6, and 7, showing e-beam sensitivity following SCF CO₂ development. Sample 4 developed completely in positive-tone.
- Figure 4-3.** AFM image of 1.0 μm lines/spaces in sample 5. Left image is a top-down view, right plot is a cross-section through the line shown at left.

CHAPTER FIVE

- Figure 5-1.** Deposition rates of HFCVD fluorocarbon films from PFOSF and HFPO, showing the effect of a. adding PFOSF, and b. changing filament temperature. Trend lines in Figure 5-1a are included for visual clarification. Figure 5-1b shows data for PFOSF/HFPO ratios greater than 0.07, and is plotted in Arrhenius form. Regression fits illustrate kinetic regimes above and below $\sim 470^{\circ}\text{C}$.
- Figure 5-2.** Nuclear Magnetic Resonance (NMR) spectra of a. HFCVD film from the precursors HFPO and PFOSF, b. HFCVD film from the precursor HFPO with no PFOSF, and c. bulk PTFE. Concentrations of CF_3 , CF_2 , and CF are shown in mol %.
- Figure 5-3.** Atomic Force micrographs showing the effect of filament temperature on the morphology of HFCVD films from HFPO and PFOSF. Films were deposited at a PFOSF/HFPO ratio of 0.145 and filament temperatures of a. 435°C , b. 510°C , and c. 580°C . RMS roughnesses are also shown.
- Figure 5-4.** Proposed polymerization mechanism for HFCVD using HFPO and PFOSF.

CHAPTER SIX ---

- Figure 6-1.** Schematic of the HWCVD Chamber. Showing gas inlet through upper showerhead, pyrolysis on square filament array, and deposition onto a wafer substrate resting on the bottom electrode. Gas pump out is toward the back side of the chamber.
- Figure 6-2.** Solid state ^{19}F NMR of HWCVD fluorocarbon film (bottom) and PTFE (top).
- Figure 6-3.** FTIR of HWCVD fluorocarbon film (bottom) and PTFE (top).
- Figure 6-4.** Reactions for the pyrolysis of HFPO and polymerization of difluorocarbene.
- Figure 6-5.** FTIR of HWCVD organosilicon film (top) and PDMS (bottom).
- Figure 6-6.** HWCVD fluorocarbon low dielectric constant film directly patterned at 1.0 (left) and 0.25 (right) micron resolution.
- Figure 6-7.** Scanning electron micrograph of HWCVD porous fluorocarbon film at the edge of the silicon wafer substrate (bottom right). The tilt angle makes it possible to observe both the surface morphology (top left) and porosity through the thickness of the layer.

CHAPTER SEVEN ---

Figure 7-1. Compositional space available from CVD of organosilicon and fluorocarbon materials, as derived from ^{29}Si and ^{19}F NMR. This work filled in the top row of the matrix, and furthered our understanding of fluorocarbon HFCVD chemistry.

APPENDIX A

- Figure A-1.** Photographs of the dual-mode CVD reactor system known as *Pumpkin*.
- Figure A-2.** Front and rear view of chamber, showing feed port and pumping port.
- Figure A-3.** Top view of chamber, showing lid design, and filament orientation for HFCVD.
- Figure A-4.** Side view of chamber, showing water-cooled stage, pumping port and access door.
- Figure A-5.** Front view of chamber design.
- Figure A-6.** Front view of chamber design, rotated 30° clockwise as observed from above.
- Figure A-7.** Front view of chamber design, rotated 60° clockwise as observed from above.
- Figure A-8.** Front view of chamber design, rotated 90° clockwise as observed from above.
- Figure A-9.** Top view of chamber design, showing position of ports.
- Figure A-10.** Assembly view of main chamber design.
- Figure A-11.** Side cutaway view of original design of bottom plate. Note that copper tubing was replaced with a stainless steel reservoir 1-in. deep with inlet and outlet tubing in final construction.
- Figure A-12.** Side view of reactor lid, showing ¼-in. VCR and NW16 ports.
- Figure A-13.** Side cutaway view of reactor lid, showing ½-in. o-ring port and NW16 ports.
- Figure A-14.** Top view of reactor lid, showing all ports.
- Figure A-15.** Top and side views of rear flange.

APPENDIX B

Figure B-1. Typical deposition rates obtained using HFPO with secondary precursor species.

Figure B-2. C1s XPS spectra showing high surface concentrations of terminal CH₃ groups in PTFE films.

List of Tables

CHAPTER ONE

Table 1-1. Previous investigations of CW PECVD with organosilicon monomers.

CHAPTER TWO

Table 2-1. Results of wire coatings on 3-mil copper wire deposited from D₃ using pulsed-PECVD.

Table 2-2. Results of saline soak testing of pulsed-PECVD films deposited under a variety of pulse conditions.

Table 2-3. FTIR assignments from the literature.

CHAPTER THREE

Table 3-1. FTIR assignments from the literature.

Table 3-2. Raman assignments from the literature.

Table 3-3. Raman siloxane symmetric stretching mode (SSM) assignments for various chemical environments.

Table 3-4. ²⁹Si NMR structures and chemical shifts commonly observed in organosilicon CVD films.

Table 3-5. XPS elemental ratios for HFCVD films from D₃ and D₄.

CHAPTER FOUR

Table 4-1. Deposition conditions for CVD films that showed sensitivity to e-beam exposure.

CHAPTER SIX

Table 6-1. Typical process conditions for HWCVD.

CHAPTER SEVEN

Table 7-1. Silicon bonding environments in PPECVD and HFCVD organosilicon films.

APPENDIX B

Table B-1. Precursors used in combination with HFPO HFCVD.

List of Notations

κ	dielectric constant
AFM	atomic force microscopy
CP	cross polarization
CP-MAS	cross polarization with magic angle spinning
CVD	chemical vapor deposition
CW	continuous-wave plasma-enhanced chemical vapor deposition
D ₃	hexamethylcyclotrisiloxane
D ₄	octamethylcyclotetrasiloxane
EBDW	e-beam direct write lithography
EPL	e-beam projection lithography
ESH	environment, safety and health
ESR	electron spin resonance spectroscopy
FTIR	Fourier transform infrared spectroscopy
HFCVD	hot-filament chemical vapor deposition
HFPO	hexafluoropropylene oxide
HMDSO	hexamethyldisiloxane
IC	integrated circuit
ILD	interlayer dielectric
ITRS	International Technology Roadmap for Semiconductors
MAS	magic angle spinning
MW	molecular weight
NMR	nuclear magnetic resonance
OM	optical microscopy
OSG	organosilicate glass
PDMS	polydimethylsiloxane
PECVD	plasma enhanced chemical vapor deposition
PFOSF	perfluorooctane sulfonyl fluoride
PPECVD	pulsed plasma enhanced chemical vapor deposition
PTFE	poly(tetrafluoroethylene)
RF	radio-frequency
SCF	supercritical fluid
SEM	scanning electron microscope
TMS	tetramethylsilane
UV	ultraviolet
VTMS	vinyltrimethylsilane
XPS	x-ray photoelectron spectroscopy



CHAPTER 1

Introduction

1.1 Chemical Vapor Deposition (CVD)

CVD is a vacuum technology capable of producing thin, pinhole-free films on substrates of complex geometry.¹⁻³ In conventional, or thermal, CVD deposition takes place on a heated susceptor and substrate and the technique is most often used to produce inorganic materials such as SiO₂. Only in a few cases is it possible to produce organic thin films, due to their poor thermal stability and adsorption-dominated kinetics.³ For organic materials, a CVD process is required in which reactive species are generated in the gas phase and film growth proceeds via recombination on a cooled substrate. The method of activation to produce film growth precursors is thus a key differentiator in CVD of these types of materials. In this work, we have used both electrical (PECVD and PPECVD) and thermal activation (HFCVD).

Plasma-Enhanced Chemical Vapor Deposition (PECVD)

PECVD involves the formation of thin films on surfaces from a vapor phase precursor under the influence of a plasma (or glow discharge).⁴⁻¹¹ The plasma is a partially ionized gas usually formed by exposing a gaseous precursor to an electrical field at low pressure (<10 Torr). It consists of electrons, ions, free radicals, molecules in excited states, and photons of various energies. Plasmas used for etching and deposition, generally called "cold plasmas", are in a non-equilibrium state wherein the temperature of the electrons is much higher than that of the gas molecules. As a result, the temperature of the gas molecules is close to ambient and plasma chemistry can occur without thermal degradation of reactants and products. Plasma polymerization is a specific type of plasma chemistry which involves reactions between plasma species, between plasma and surface species, and between surface species. Reactive species are generated in the plasma by electron impact collisions, and thus overcome kinetic limitations that may exist in thermally activated processes. This allows monomers to be used that would not polymerize under conditions of conventional molecular addition polymerization, such as saturated alkanes or benzene. Plasma films are deposited on surfaces contacting the plasma of a precursor gas in the form of a thin film and/or powder. The discharge also supplies energetic radiation (e.g. positive ions and photons) that bombards surfaces exposed to the plasma. This alters the surface chemistry during deposition, and can result

in competitive ablation or etching of the growing film. Using PECVD, ultrathin, pinhole-free films that are highly coherent and adherent to a variety of substrates may be prepared from monomers not polymerizable by conventional means. Films are generally chemically inert, insoluble, mechanically tough, thermally stable and have been used or considered for a wide variety of electrical¹²⁻¹⁶, optical^{11,17-22} and biomedical^{6,9,23-37} applications, and as permselective membranes^{24,38-42} and protective coatings^{20,43-45}.

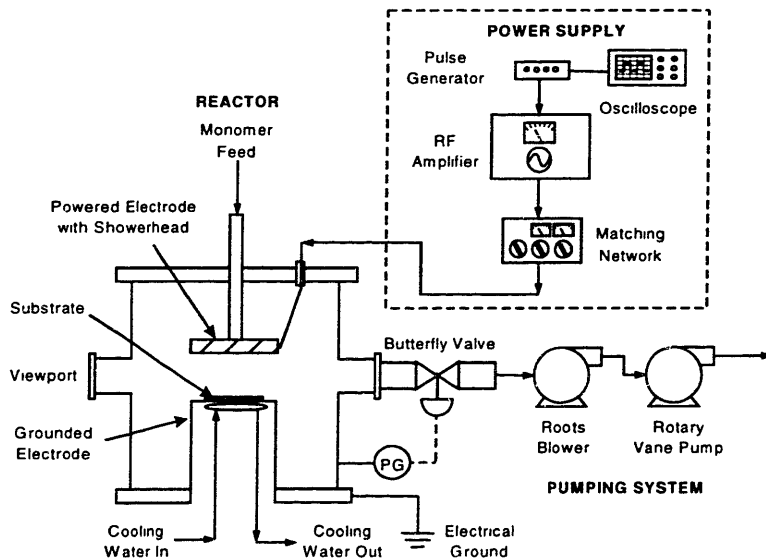


Figure 1-1. Schematic of a typical parallel-plate PECVD system.

A typical parallel plate plasma reactor system is shown in Figure 1-1. It consists of a deposition chamber with two electrodes located parallel to each other, a power generator, an impedance matching network and a vacuum pumping system. Radio-frequency (RF) power of 13.56 MHz is supplied to the top, or powered, electrode from an RF generator via the impedance matching network. The purpose of the matching network is to balance the impedance of the generator with that of the discharge, thereby maximizing power transfer to the discharge. In PECVD, substrates are usually placed on the bottom electrode, which is grounded and cooled. Discharge is normally confined to the space between the two electrodes. The primary process variables of consideration are the flow rate of the precursor gas, system pressure, RF discharge power and substrate temperature. The flow rate of feed gas and the system pressure determine the residence time of the monomer in the reactor. System pressure also determines the mean free path

length of species in the plasma, while the discharge power affects the degree of ionization in the plasma and the extent of monomer fragmentation. Substrate temperature affects adsorption and desorption kinetics and surface mobility of precursor species on the substrate surface.

Unlike conventional polymers, plasma films often have only limited polymeric character, and tend to form irregular three-dimensional crosslinked networks. UV irradiation and ion bombardment of the growing film, as well as the mechanism of plasma film growth itself, can result in the formation of trapped free radicals, or dangling bonds, in the film⁴⁶⁻⁴⁸. Upon exposure to atmosphere, these dangling bonds are oxidized, leading to concomitant changes in film structure and properties. This aging characteristic of plasma films makes them undesirable for use in some applications, particularly where electrical insulation is a requirement. The effect of ion bombardment is also to increase the crosslink density in plasma films, which often results in brittle, inflexible films.

Pulsed Plasma-Enhanced Chemical Vapor Deposition (PPECVD)

A promising method that has been applied in an effort to reduce dangling bond concentrations and crosslinking in plasma films is pulsed-PECVD, or PPECVD.^{24,37,46,49-62} In this technique, RF excitation is modulated on and off. When the RF power is on, both ions and reactive neutrals are produced in the gas phase. However, ions often have much shorter lifetimes than neutrals and the ratio of neutrals to ions increases during the period when RF power is off.^{51,52,54,63-65} Film deposition from reactive neutrals will thus be favored and the decrease in ion bombardment during the off period is anticipated to lead to a reduction in the number of dangling bonds and crosslinks.

Investigation of PPECVD using fluorocarbon precursors has been shown to produce flexible, conformal fluorocarbon films with reduced dangling bond concentration and lower crosslink density as compared to films obtained using continuous-PECVD^{55,58,60,61}. One of the goals of this project was to extend the PPECVD technique to organosilicon precursors, specifically the cyclic siloxane hexamethylcyclotrisiloxane (D₃). Coatings produced in this way were to be evaluated as potential encapsulant materials for biopassivation of neural probe devices.

Hot-Filament CVD (HFCVD)

In contrast to PECVD and PPECVD, HFCVD (also called pyrolytic CVD) generates reactive species through thermal activation at a hot surface – typically a heated wire. HFCVD has been used extensively in the deposition of diamond thin films^{66,67}, but has only recently been extended to polymer systems by our group.^{60,61,68,69} The substrate is cooled as in PECVD, but the lack of ion bombardment, UV, and electron irradiation in the non-plasma environment alters the chemistry of the growth process and limits the number of reaction pathways available for film growth. This makes it possible, for instance, to produce films that are spectroscopically indistinguishable from PTFE (commonly known as TeflonTM).^{60,61,68} Using the same precursor, hexafluoropropylene oxide (HFPO), in a PECVD process results in films in which carbon is present in a variety of bonding environments ranging from CF₃ to completely defluorinated quaternary carbon.^{48,53,58,60,70}

Much work has been done in characterizing fluorocarbon films produced using this method and understanding the chemistry of the HFCVD process with HFPO.^{60,61,68,71-73} At the start of this project, however, only preliminary work had been done in extending the HFCVD technique to organosilicon precursors.⁶⁹ One of the primary goals of this work was thus to elucidate the chemistry of the process and rigorously characterize these organosilicon materials. In particular, we wanted to compare and contrast organosilicon materials deposited from similar precursors using PPECVD and HFCVD

1.2 Biopassivation Coatings

Challenges for the Encapsulation of Implantable Devices

When a foreign object contacts blood or tissue fluids in the environment of the body, it is the surface of the object that the fluids first encounter. The immediate physiological response after exposure is usually the adsorption of biomolecules, particularly proteins. The chemical composition, topology, and morphology of this surface is thus extremely important in mediating the biologic response of the body to implantable devices of any kind. A coating of a biocompatible material on a biomedical device is a powerful method for altering the surface properties of the device without changing the bulk properties. Such a material can also serve to insulate and protect the

device from the demands of prolonged immersion in the environment of the body. Coatings which satisfy these criteria are termed *biopassivation coatings* and have been the subject of extensive review in the literature.^{6,9,35}

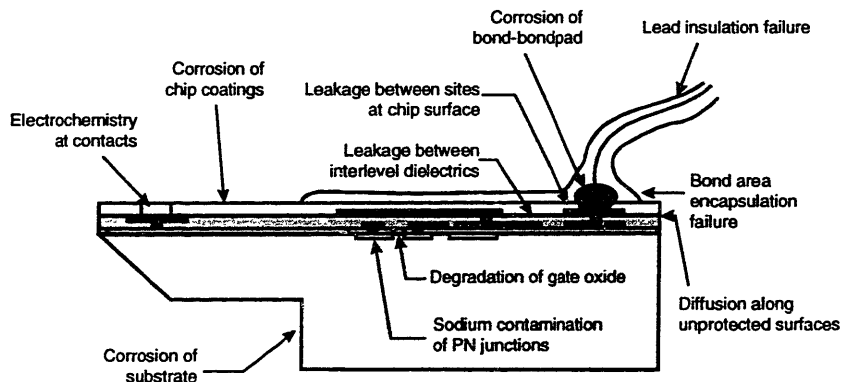


Figure 1-2. Potential problem areas in the protection of implantable integrated circuits by thin layers of insulating biomaterials.

Figure 1-2 illustrates some of the challenges for the protection of implantable integrated circuits (IC's) by insulating biomaterials. Coatings on such IC's need to be adherent, biocompatible and sterile and flexible enough to minimize static forces on the tissue. To fulfill the criteria of flexibility and conformity, the ability to prepare films ranging in composition from oily to highly crosslinked and brittle is required. The insulator should also have good dielectric properties and low permeability, and should be thermally stable at the temperature of assembly of the IC.

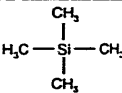
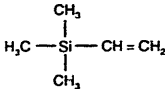
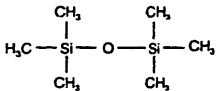
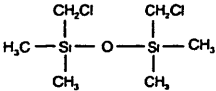
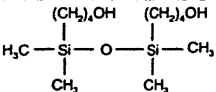
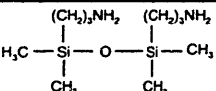
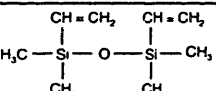
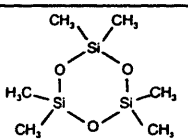
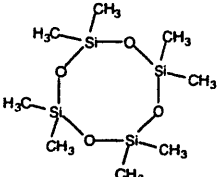
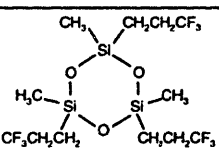
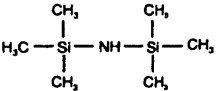
For devices in neural prosthetic applications, it is critical that biopassivation coatings be not only biocompatible, insulating, but also extremely thin. Neurological electrodes, for instance, have complex topologies with dimensions on the order of microns (10^{-6} m). Minimizing the thickness of these coatings is imperative to avoid any traumatic destruction of tissue in the nervous system.³⁵ Neurological electrodes also require conformal coatings on fine geometries on the micron scale. Conventional gel or liquid coating methods cannot be used for this purpose because high surface tension and capillary action tends to collapse these features. A gas-phase coating method, such as CVD, is necessary to obtain uniform, thin coatings with minimal damage to the substrate.

Organosilicon Thin Films as Biopassivation Coatings

Both PPECVD and HFCVD show promise as methods to tailor the composition of films to meet the foregoing criteria. In particular, organosilicon thin films deposited using these techniques are exciting candidates for biopassivation coatings. Previous work has confirmed their suitability as biocompatible materials.

Chawla investigated plasma-deposited films of D₃ and D₄ on Celgard[®]-2400 and Silastic[®] membranes and evaluated the adhesion of platelets and leucocytes using an *in vitro* loop²⁵ and an *ex vivo* shunt system with a canine model^{25,29}. It was determined that the number of platelets and leukocytes adhering to the silicone coated samples were less than on the untreated controls. Ishikawa *et al.* examined a number of organosilicon monomers, including D₃, and found that the number of platelets adhering to coated glass slides and the ATP released from these platelets in a human blood *in vitro* system was 10-30% less than the uncoated slides³¹. Hasirci investigated the deposition of HMDSO on activated charcoal, used in hemoperfusion, by PECVD. It was found that the silicone coating significantly reduced damage from the charcoal granules to platelets, erythrocytes and leucocytes in sheep's blood, without substantially reducing the absorptive capacity of the charcoal³². Cannon *et al.* detail the synthesis of a fine neurological electrode consisting of W-26 at.% Re wire coated with plasma-polymerized HMDSN. No *in vivo* biocompatibility and stability studies were reported, and some problems were experienced obtaining smooth pinhole-free coverage of the substrate²⁷. No subsequent work on this topic has been published by this group. More recently, Nichols reported the synthesis of a novel polymeric material, Plasmalene[®], as an hermetic coating on wire substrates. The polymer coatings were deposited by vacuum processes which included PECVD and thermal vapor deposition of methane and xylylene⁷⁴. Finally, Lin *et al.* have coated the inner surface of low-density polyethylene (LDPE) tubing with plasma-polymerized HMDSO and ammonia for possible use as an artificial blood vessel³⁴.

Table 1-1. Previous investigations of CW PECVD with organosilicon monomers.

Precursor	Structural Formula	Ref.
Tetramethylsilane (TMS)		75-78
Vinyltrimethylsilane (VTMS)		17,46,77,79
Hexamethyldisiloxane (HMDSO)		39,46,79-90
Tetramethyl-1,3-bis(chloromethyl)-disiloxane		82
Tetramethyl-1,3-bis(hydroxybutyl)-disiloxane		82
Tetramethyl- 1,3-bis(amino propyl)disiloxane		82
Divinyltetramethyldisiloxane		87,91
Hexamethylcyclotrisiloxane (D ₃)		24,25,29,92-94
Octamethylcyclotetrasiloxane (D ₄)		12,24,78,87,89,93,94
2,4,6-Tris (3,3,3-trifluoropropyl) methyl cyclotrisiloxane		75,95
Hexamethyldisilazane		27,75,76,91,94,96

Wróbel and Wertheimer give an excellent overview of the literature on plasma deposition of organosilicon materials¹³. CW PECVD has been investigated using a wide variety of monomers. Table 1-1 lists some of this work. In contrast, PPECVD has been investigated by only a few workers and in limited detail^{24,25,29,46,97}, and no previous work using a technique like HFCVD has been reported for any organosilicon precursors. Using

PPECVD, Yasuda *et al.* tested the monomers hexamethyldisilane (HMDS), tetramethyldisiloxane (TMDSO), hexamethyldisiloxane (HMDSO) and divinyltetramethyldisiloxane (DVTMDSO) with a 0.1ms on/ 0.9ms off pulse program in an electrodeless inductively-coupled plasma reactor. Results from electron spin resonance (ESR) spectroscopy indicated that the concentration of trapped free radicals in pulsed plasma polymers was significantly lower than that in continuous plasma polymers for all of the organosilicon monomers.⁴⁶ In other work using PPECVD, Chawla used hexamethylcyclotrisiloxane (D₃) and octamethylcyclotetrasiloxane (D₄) to prepare silicone coated membranes for possible use as blood oxygenators. Though it is not clearly described in his publications, Chawla used 30W pulsed RF power of 66ms on/66 ms off in a capacitively-coupled tubular reactor. According to Sipehia, this duty cycle was chosen to prevent excessive crosslinking in the film⁹⁸. None of these publications, however, analyzed the effect of the duty cycle on the structure and properties of the films. Only Panchalingam *et al.* used vinyltrimethylsilane (VTMS) to investigate the effect of systematic variations in the duty cycle on the chemistry and deposition rates of pulsed plasma films. Hence, there was considerable scope for further investigation in using PPECVD to produce organosilicon films with desirable and tunable properties.

The goal of this portion of the project was thus to investigate deposition of organosilicon thin films by PPECVD and HFCVD, with particular application to the coating of neurological electrodes and other implantable devices. It was desired to obtain films that had properties superior to their CW-PECVD counterparts, such as high deposition rates (>1000 Å/min), polymeric structure, low defect density, resistance to prolonged immersion in solution, and flexibility sufficient to resist cracking under stress. Examples of defects included non-uniformities in the film such as columnar structures, included contaminant particles, high dangling bond concentrations and excessive crosslinking. Thermal stability, good adhesion, and uniformity over non-planar substrates were also desirable properties. It was also important to understand the structure-property-processing relationship in the CVD process, and to determine the importance and effect of process variables on film chemistry.

1.3 Directly Patternable Dielectrics

Thin films produced by HFCVD and PPECVD also show promise as materials capable of undergoing patterning by lithographic means.^{76,91,99-109} In this portion of the project, we consider the use of fluorocarbon and organosilicon films deposited by HFCVD for producing nanometer-scale features in microelectronics manufacture. Both fluorine- and silicon- containing polymeric materials are under consideration as candidates in next-generation patterning technologies, such as 157 nm photolithography and e-beam projection lithography (EPL, e.g. SCALPEL, PREVAIL).^{107,109} Their transparency makes them ideal resist candidates for 157-nm lithography¹⁰⁷, and their low dielectric constant makes them strong contenders as interconnect materials¹⁴.

Direct Dielectric Patterning Process

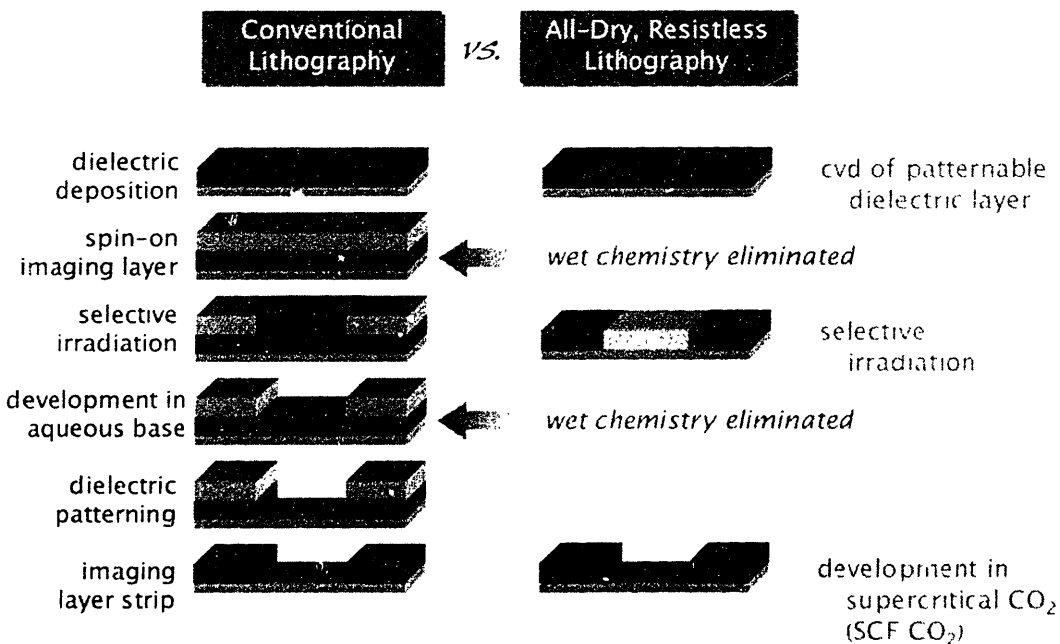


Figure 1-3. Direct dielectric patterning scheme.

The objective of this work – a collaboration between MIT and Cornell University – is thus to merge the role of resist and low-k dielectric. Specifically, we propose a direct dielectric patterning process in which a material is deposited by CVD, exposed, and developed using no wet chemistry, as illustrated in Figure 1-3.

In this process, an irradiation-sensitive CVD film is exposed using e-beam or a 157-nm source, and developed using supercritical CO₂ as a dry developing medium. The patterned film then serves as a low-k interconnect material. This technology would greatly simplify future device manufacture by reducing the number of steps involved in patterning. Supercritical CO₂ also offers many processing advantages over wet development, including improved resolution and the prevention of pattern collapse.¹¹⁰ This is due to its good selectivity, high diffusivity, and low surface tension. Furthermore, in conventional photolithographic patterning, the photoresist is applied using liquid spin-on techniques. This results in significant quantities of waste materials and exposes workers to hazardous volatile organic compounds (VOCs). Development is accomplished in aqueous base and presents similar potential hazards. The process outlined in Figure 1-3 thus also offers many environment, safety, and health (ESH) benefits over conventional processing.

HFCVD Fluorocarbon Thin Films as Directly Patternable Dielectrics

After an initial screening of organosilicon and fluorocarbon candidate materials produced by both PPECVD and HFCVD, efforts were concentrated on patterning of PTFE-like films deposited by HFCVD from the precursor HFPO.^{60,61,68} PTFE has the lowest dielectric constant of any bulk material ($k \sim 2.0$), and is under consideration as an interlayer dielectric (ILD) to replace SiO₂ in semiconductor manufacture. It is highly transparent at 157-nm¹⁰⁵, but insoluble in the aqueous developers currently used. In collaboration with Cornell University, e-beam exposure was used to induce molecular contrast in films produced by HFCVD, and development was tested using supercritical CO₂. The goal was not only to show successful proof-of-concept of the process scheme illustrated in Figure 1-3, but also to deepen our understanding of the HFCVD process through the use of secondary precursors supplementary to the primary precursor, HFPO. One particular additive, perfluorooctane sulfonyl fluoride (PFOSF), allowed us to demonstrate initiation in the HFCVD process in a manner analogous to that observed in classical polymer chemistry. The successful use of an initiator species is a novel result, and suggests that many conventional polymer techniques may have application in the HFCVD method.

1.4 Scope of Thesis

Chapter 2 describes the PPECVD of organosilicon films from D₃ for use as biopassivation coatings.

Chapter 3 describes the HFCVD of organosilicon films from D₃ and D₄, including extensive characterization of the structure and chemistry of these films.

Chapter 4 describes the successful use of e-beam exposure and supercritical CO₂ development to pattern fluorocarbon films from the HFCVD of HFPO.

Chapter 5 describes the use of an initiator molecule, PFOSF, to alter the deposition chemistry of HFCVD from HFPO.

Chapter 6 gives an overview of the progress made in using HFCVD to produce fluorocarbon and organosilicon thin films.

1.5 References

1. W. E. Mutter, US Patent No. 3,319,311 (1967).
2. K. F. Jensen, in *Microelectronics Processing : Chemical Engineering Aspects*, D. W. Hess and K. F. Jensen, Editors, p. 377, American Chemical Society, Washington, DC (1989).
3. A. Kubono and N. Okui, *Prog. Polym. Sci.*, **19**, 389 (1994).
4. B. N. Chapman, *Glow Discharge Processes*, Wiley and Sons, Inc., New York, (1980).
5. H. V. Boenig, *Plasma Science and Technology*, Cornell U. P., Ithaca, New York, (1982).
6. W. R. Gombotz and A. S. Hoffman, *Crit. Rev. Biocompat.*, **4**, 1 (1987).
7. D. W. Hess and D. B. Graves, in *Microelectronics Processing : Chemical Engineering Aspects*, D. W. Hess and K. F. Jensen, Editors, p. 377, American Chemical Society, Washington. DC (1989).
8. R. d'Agostino, Ed. *Plasma Deposition, Treatment, and Etching of Polymers*, Academic Press, San Diego, CA (1990).
9. B. D. Ratner, A. Chilkoti, and G. P. Lopez, in *Plasma Deposition, Treatment, and Etching of Polymers*, R. d'Agostino, Editor, p. 463, Academic Press, San Diego, CA (1990).
10. F. F. Shi, *J. Macromol. Sci. - Rev. Macromol. Chem. Phys.* , **C36**, 795 (1996).
11. L. Martinu and D. Poitras, *J. Vac. Sci. Technol. A*, **18**, 2619 (2000).
12. Z. Ogumi, Y. Uchimoto, and Z. Takehara, *J. Electrochem. Soc.*, **136**, 625 (1989).
13. A. M. Wróbel and M. R. Wertheimer, in *Plasma Deposition, Treatment, and Etching of Polymers*, R. d'Agostino, Editor, p. 163, Academic Press, San Diego, CA (1990).
14. W. W. Lee and P. S. Ho, *MRS Bulletin*, **22**, 19 (1997).
15. M. J. Loboda, *Microelect. Eng.*, **50**, 15 (2000).

16. L. Peters, *Semicond. Int.*, **23**, 108 (2000).
17. P. K. Tien, G. Smolinsky, and R. J. Martin, *Appl. Opt.*, **11**, 637 (1972).
18. P. K. Tien, *Rev. Mod. Phys.*, **49**, 361 (1977).
19. T. Wydeven, *Appl. Opt.*, **16**, 717 (1977).
20. E. Zehender, B. Blaich, H. Stein, and K. Kerner, US Patent No. 4,085,248 (1978).
21. R. M. Kubacki, US Patent No. 4,096,315 (1978).
22. T. J. Wydeven and J. R. Hollahan, US Patent No. 4,137,365 (1979).
23. D. E. Ocumpaugh and H. L. Lee, in *Biomedical Polymers*, p. 101, Marcel Dekker, New York (1971).
24. A. S. Chawla, *Artif. Organs*, **3**, 92 (1979).
25. A. S. Chawla, *Trans. Am. Soc. Artif. Intern. Organs*, **XXV**, 287 (1979).
26. G. Akovali and M. Y. Bolük, *Polym. Prepr.*, **21**, 59 (1980).
27. J. G. Cannon, R. O. Dillon, R. F. Bunshah, P. H. Crandall, and A. M. Dymond, *J. Biomed. Mater. Res.*, **14**, 279 (1980).
28. A. R. Ozdural, J. Hameed, M. Y. Boluk, and E. Piskin, *ASAIO J.*, **3**, 1980 (1980).
29. A. S. Chawla, *Biomaterials*, **2**, 83 (1981).
30. A. S. Chawla and R. Sipehia, *J. Biomed. Mater. Res.*, **18**, 537 (1984).
31. Y. Ishikawa, S. Sasakawa, M. Takase, Y. Iriyama, and Y. Osada, *Makromol. Chem., Rapid Commun.*, **6**, 495 (1985).
32. N. Hasirci, *J. Appl. Polym. Sci.*, **34**, 2457 (1987).
33. V. Panchalingam, B. Poon, H.-H. Huo, C. R. Savage, R. B. Timmons, and R. C. Eberhart, *J. Biomater. Sci. Polym. Edn.*, **5**, 131 (1993).
34. J.-C. Lin and S. L. Cooper, *J. Appl. Polym. Sci., Appl. Polym. Symp.*, **54**, 157 (1994).
35. M. F. Nichols, *Crit. Rev. Biomed. Eng.*, **22**, 39 (1994).
36. L. Caburet, K. Asfardjani, O. Dessaux, P. Goudmand, and C. Jama, US Patent No. 5,576,068 (1996).
37. H. G. Pryce Lewis, D. J. Edell, and K. K. Gleason, *Chem. Mater.*, **12**, 3488 (2000).
38. O. Görbig, S. Nehlsen, and J. Müller, *J. Membr. Sci.*, **138**, 115 (1998).
39. J. Sakata and M. Yamamoto, *J. Appl. Polym. Sci., Appl. Polym. Symp.*, **42**, 339 (1988).
40. H. Matsuyama, T. Shiraishi, and M. Teramoto, *J. Appl. Polym. Sci.*, **54**, 1665 (1994).
41. S. Roualdes, N. Hovnanian, A. van der Lee, J. Sanchez, and J. Durand, *J. Phys. IV France*, **9**, 1147 (1999).
42. R. K. Sathir and Z. N. Sanjana, *J. Mater. Sci.*, **26**, 4261 (1991).
43. E. Knut and W. Zultzke, US Patent No. 4,762,730 (1988).
44. F. Verzaro and D. Ferry, US Patent No. 5,569,497 (1996).
45. R. H. Petrnoch, B. J. Knapp, F. M. Kimock, and B. K. Daniels, US Patent No. 5,618,619 (1997).
46. H. Yasuda and T. Hsu, *J. Polym. Sci., Polym. Chem. Ed.*, **15**, 81 (1977).

47. A. M. Wróbel and G. Czeremuszkina, *Thin Solid Films*, **216**, 203 (1992).
48. C. B. Labelle, S. J. Limb, and K. K. Gleason, *J. Appl. Phys.*, **82**, 1784 (1997).
49. K. Nakajima, A. T. Bell, and M. Shen, *J. Appl. Polym. Sci.*, **23**, 2627 (1979).
50. J. W. Vinzant, M. Shen, and A. T. Bell, *Am. Chem. Soc., Plasma Polym.*, **108**, 79 (1979).
51. A. Kono, M. Haverlag, G. M. W. Kroesen, and F. J. de Hoog, *J. Appl. Phys.*, **70**, 2939 (1991).
52. S. Samukawa and S. Furuoya, *Appl. Phys. Lett.*, **63**, 2044 (1993).
53. C. R. Savage, R. B. Timmons, and J. W. Lin, in *Adv. Chem. Ser.*, 236, p. 745, American Chemical Society, Washington, DC (1993).
54. P. Jiang, D. J. Economou, and C. B. Shin, *Plasma Chem. Plasma Process.*, **15**, 383 (1995).
55. S. J. Limb, K. K. Gleason, D. J. Edell, and E. F. Gleason, *J. Vac. Sci. Technol. A*, **15**, 1814 (1997).
56. N. M. Mackie, N. F. Dalleska, D. G. Castner, and E. R. Fisher, *Chem. Mater.*, **9**, 349 (1997).
57. L. M. Han, R. B. Timmons, D. Bogdal, and J. Pielichowski, *Chem. Mater.*, **10**, 1422 (1998).
58. K. K. S. Lau and K. K. Gleason, *J. Phys. Chem. B*, **102**, 5977 (1998).
59. C. B. Labelle and K. K. Gleason, *J. Vac. Sci. Technol. A*, **17**, 445 (1999).
60. S. J. Limb, K. K. S. Lau, D. J. Edell, E. F. Gleason, and K. K. Gleason, *Plasmas Polym.*, **4**, 21 (1999).
61. K. K. S. Lau and K. K. Gleason, *J. Fluorine Chem.*, **104**, 119 (2000).
62. E. J. Winder and K. K. Gleason, *J. Appl. Polym. Sci.*, **78**, 842 (2000).
63. S. G. Hansen, G. Luckman, and S. D. Colson, *Appl. Phys. Lett.*, **53**, 1588 (1988).
64. A. Bouchoule and P. Ranson, *J. Vac. Sci. Technol. A*, **9**, 317 (1991).
65. L. J. Overzet, B. A. Smith, J. Kleber, and S. K. Kanakasabapathy, *Jpn. J. Appl. Phys.*, **36**, 2443 (1997).
66. C. Wolden, S. Mitra, and K. K. Gleason, *J. Appl. Phys.*, **72**, 3750 (1992).
67. G. H. Song, C. Sun, R. F. Huang, and L. S. Wen, *J. Vac. Sci. Technol. A*, **18**, 860 (2000).
68. S. J. Limb, C. B. Labelle, K. K. Gleason, D. J. Edell, and E. F. Gleason, *Appl. Phys. Lett.*, **68**, 2810 (1996).
69. M. C. Kwan and K. K. Gleason, *CVD*, **3**, 299 (1997).
70. C. I. Butoi, N. M. Mackie, J. L. Barnd, E. R. Fisher, L. J. Gamble, and D. G. Castner, *Chem. Mater.*, **11**, 862 (1999).
71. K. K. S. Lau, J. A. Caulfield, and K. K. Gleason, *Chem. Mater.*, **12**, 3032 (2000).
72. K. K. S. Lau, K. K. Gleason, and B. L. Trout, *J. Chem. Phys.*, **113**, 4103 (2000).
73. K. K. S. Lau, J. A. Caulfield, and K. K. Gleason, *J. Vac. Sci. Technol. A*, **18**, 2404 (2000).
74. M. F. Nichols, *Biomed. Sci. Instrum.*, **29**, 77 (1993).
75. P. Favia, R. d'Agostino, and F. Fracassi, *Pure Appl. Chem.*, **66**, 1373 (1994).
76. M. W. Horn, S. W. Pang, and M. Rothschild, *J. Vac. Sci. Technol. B*, **8**, 1493 (1990).
77. N. Inagaki and M. Taki, *J. Appl. Polym. Sci.*, **27**, 4337 (1982).
78. I. Tajima and M. Yamamoto, *J. Polym. Sci., A, Polym. Chem.*, **25**, 1737 (1987).

47. A. M. Wróbel and G. Czeremuszkín, *Thin Solid Films*, **216**, 203 (1992).
48. C. B. Labelle, S. J. Limb, and K. K. Gleason, *J. Appl. Phys.*, **82**, 1784 (1997).
49. K. Nakajima, A. T. Bell, and M. Shen, *J. Appl. Polym. Sci.*, **23**, 2627 (1979).
50. J. W. Vinzant, M. Shen, and A. T. Bell, *Am. Chem. Soc., Plasma Polym.*, **108**, 79 (1979).
51. A. Kono, M. Haverlag, G. M. W. Kroesen, and F. J. de Hoog, *J. Appl. Phys.*, **70**, 2939 (1991).
52. S. Samukawa and S. Furuoya, *Appl. Phys. Lett.*, **63**, 2044 (1993).
53. C. R. Savage, R. B. Timmons, and J. W. Lin, in *Adv. Chem. Ser.*, 236, p. 745, American Chemical Society, Washington, DC (1993).
54. P. Jiang, D. J. Economou, and C. B. Shin, *Plasma Chem. Plasma Process.*, **15**, 383 (1995).
55. S. J. Limb, K. K. Gleason, D. J. Edell, and E. F. Gleason, *J. Vac. Sci. Technol. A*, **15**, 1814 (1997).
56. N. M. Mackie, N. F. Dalleska, D. G. Castner, and E. R. Fisher, *Chem. Mater.*, **9**, 349 (1997).
57. L. M. Han, R. B. Timmons, D. Bogdal, and J. Pielichowski, *Chem. Mater.*, **10**, 1422 (1998).
58. K. K. S. Lau and K. K. Gleason, *J. Phys. Chem. B*, **102**, 5977 (1998).
59. C. B. Labelle and K. K. Gleason, *J. Vac. Sci. Technol. A*, **17**, 445 (1999).
60. S. J. Limb, K. K. S. Lau, D. J. Edell, E. F. Gleason, and K. K. Gleason, *Plasmas Polym.*, **4**, 21 (1999).
61. K. K. S. Lau and K. K. Gleason, *J. Fluorine Chem.*, **104**, 119 (2000).
62. E. J. Winder and K. K. Gleason, *J. Appl. Polym. Sci.*, **78**, 842 (2000).
63. S. G. Hansen, G. Luckman, and S. D. Colson, *Appl. Phys. Lett.*, **53**, 1588 (1988).
64. A. Bouchoule and P. Ranson, *J. Vac. Sci. Technol. A*, **9**, 317 (1991).
65. L. J. Overzet, B. A. Smith, J. Kleber, and S. K. Kanakasabapathy, *Jpn. J. Appl. Phys.*, **36**, 2443 (1997).
66. C. Wolden, S. Mitra, and K. K. Gleason, *J. Appl. Phys.*, **72**, 3750 (1992).
67. G. H. Song, C. Sun, R. F. Huang, and L. S. Wen, *J. Vac. Sci. Technol. A*, **18**, 860 (2000).
68. S. J. Limb, C. B. Labelle, K. K. Gleason, D. J. Edell, and E. F. Gleason, *Appl. Phys. Lett.*, **68**, 2810 (1996).
69. M. C. Kwan and K. K. Gleason, *CVD*, **3**, 299 (1997).
70. C. I. Butoi, N. M. Mackie, J. L. Barnd, E. R. Fisher, L. J. Gamble, and D. G. Castner, *Chem. Mater.*, **11**, 862 (1999).
71. K. K. S. Lau, J. A. Caulfield, and K. K. Gleason, *Chem. Mater.*, **12**, 3032 (2000).
72. K. K. S. Lau, K. K. Gleason, and B. L. Trout, *J. Chem. Phys.*, **113**, 4103 (2000).
73. K. K. S. Lau, J. A. Caulfield, and K. K. Gleason, *J. Vac. Sci. Technol. A*, **18**, 2404 (2000).
74. M. F. Nichols, *Biomed. Sci. Instrum.*, **29**, 77 (1993).
75. P. Favia, R. d'Agostino, and F. Fracassi, *Pure Appl. Chem.*, **66**, 1373 (1994).
76. M. W. Horn, S. W. Pang, and M. Rothschild, *J. Vac. Sci. Technol. B*, **8**, 1493 (1990).
77. N. Inagaki and M. Taki, *J. Appl. Polym. Sci.*, **27**, 4337 (1982).
78. I. Tajima and M. Yamamoto, *J. Polym. Sci., A, Polym. Chem.*, **25**, 1737 (1987).

79. M. J. Vasile and G. Smolinsky, *J. Electrochem. Soc.*, **119**, 451 (1972).
80. M. R. Alexander, R. D. Short, F. R. Jones, M. Stollenwerk, J. Zabold, and W. Michaeli, *J. Mater. Sci.*, **31**, 1879 (1996).
81. R. A. Assink, A. K. Hays, R. W. Bild, and B. L. Hawkins, *J. Vac. Sci. Technol. A*, **3**, 2629 (1985).
82. S. Cai, J. Fang, and X. Yu, *J. Appl. Polym. Sci.*, **44**, 135 (1992).
83. I. H. Coopes and H. J. Griesser, *J. Appl. Polym. Sci.*, **37**, 3413 (1989).
84. V. Krishnamurthy, I. L. Kamel, and Y. Wei, *J. Appl. Polym. Sci.*, **38**, 605 (1989).
85. M. Kusabiraki, *J. Appl. Polym. Sci., Appl. Polym. Symp.*, **46**, 473 (1990).
86. S. Y. Park and N. Kim, *J. Appl. Polym. Sci., Appl. Polym. Symp.*, **46**, 91 (1990).
87. C. Rau and W. Kulisch, *Thin Solid Films*, **249**, 28 (1994).
88. S. Sahli, M. A. Djouadi, S. Hadj-Moussa, F. Mansour, M. S. Aida, and Y. Segui, *Mater. Chem. Phys.*, **33**, 106 (1993).
89. J. Sakata, M. Yamamoto, and M. Hirai, *J. Appl. Polym. Sci.*, **31**, 1999 (1986).
90. I. Tajima and M. Yamamoto, *J. Polym. Sci., Polym. Chem. Ed.*, **23**, 615 (1985).
91. V. S. Nguyen, J. Underhill, S. Fridmann, and P. Pan, *J. Electrochem. Soc.*, **132**, 1925 (1985).
92. M. Kryszewski, A. M. Wróbel, and J. Tyczkowski, *Am. Chem. Soc., Plasma Polym.*, **108**, 220 (1979).
93. Y. Osada and M. Hashidzume, *J. Polym. Sci., Polym. Lett. Ed.*, **19**, 369 (1981).
94. A. M. Wróbel, M. Kryszewski, and M. Gazicki, *J. Macromol. Sci. - Chem.*, **A20**, 583 (1983).
95. P. Favia, G. Caporiccio, and R. d'Agostino, *J. Polym. Sci., A, Polym. Chem.*, **32**, 121 (1994).
96. J. S. Svardved and K. Kristiansen, *Vacuum*, **27**, 235 (1977).
97. V. Panchalingam, X. Chen, C. R. Savage, R. B. Timmons, and R. C. Eberhart, *J. Appl. Polym. Sci., Appl. Polym. Symp.*, **54**, 123 (1994).
98. R. Sipehia, Personal Communication, (1998).
99. H. Sugiyama, A. Mizushima, and K. Nate, *J. Appl. Polym. Sci.*, **44**, 1591 (1992).
100. R. Dagani, *Chemical and Engineering News*, **71**, 6 (1993).
101. A. M. Joshi, T. W. Weidman, A. D. Johnson, J. F. Miner, and D. E. Ibbotson, in *Advances in Resist Technology and Processing X*, p. 709,, (1993).
102. T. W. Weidman and A. M. Joshi, *Appl. Phys. Lett.*, **62**, 372 (1993).
103. O. Joubert, T. W. Weidman, A. M. Joshi, and R. L. Kostelak, *Microelect. Eng.*, **30**, 275 (1996).
104. H. W. P. Koops, S. Babin, M. Weber, G. Dahm, A. Holopkin, and M. Lyakhov, *Microelect. Eng.*, **30**, 539 (1996).
105. T. M. Bloomstein, M. W. Horn, M. Rothschild, R. R. Kuz, S. T. Palmacci, and R. D. Goodman, *J. Vac. Sci. Technol. B*, **15**, 2112 (1997).
106. O. Nalamasu, T. I. Wallow, F. M. Houlihan, E. Reichmanis, A. G. Timko, G. Dabbagh, R. A. Cirelli, R. S. Hutton, and A. E. Novembre, *Future Fab International*, 159 (1998).

107. R. R. Kunz, T. M. Bloomstein, D. E. Hardy, R. B. Goodman, D. K. Downs, and J. E. Curtin, *J. Vac. Sci. Technol. B*, **17**, 3267 (1999).
108. R. Kwong, W.-S. Huang, W. Moreau, R. Lang, C. Robinson, D. R. Medeiros, A. Aviram, R. C. Guarnieri, and M. Angelopoulos, *Mater. Res. Soc. Symp. Proc.*, **584**, 147 (2000).
109. K. Patterson, M. Somervell, and C. G. Willson, *Solid State Technology*, **March, 2000** (2000).
110. C. K. Ober, A. H. Gabor, P. Gallagher-Wetmore, and R. D. Allen, *Adv. Mater.*, **9**, 1039 (1997).



CHAPTER 2

Pulsed-PECVD Films from D_3 For Use as Insulating Biomaterials

HG Pryce Lewis, DJ Edell, and KK Gleason, *Chem. Mat.*, 12, 3488 (2000)

2.1 Abstract

Thin films produced by plasma-enhanced chemical vapor deposition (PECVD) have potential application as conformal coatings on implantable devices with complex topologies and small dimensions. Coatings on such devices need to be biocompatible, insulating, and flexible enough to minimize static forces on the surrounding tissue. In this study, we describe the use of pulsed-PECVD to deposit thin films from hexamethylcyclotrisiloxane (D_3). Pulsed-PECVD is a method in which plasma excitation is modulated to favor deposition from neutral and radical species. Thin, conformal coatings were demonstrated on nonplanar substrates suitable for implantation, such as copper wires and neural probes. Coatings were resistant to prolonged immersion in warm saline solution, and wire coatings produced by pulsed-PECVD showed more flexibility than analogous coatings deposited by continuous-wave (CW) excitation. Using Fourier Transform Infra-Red (FTIR) spectroscopy, it was demonstrated that the mode of plasma excitation is important in determining film structure. Both CW and pulsed-PECVD showed evidence of crosslinking via ternary (T) and quaternary (Q) silicon atoms bonded to more than two oxygen atoms. Methylene groups were observed only in CW films, and may constitute part of a carbon crosslinking unit of the form $Si-(CH_2)_n-Si$, where $n \geq 1$. Methylene was not detectable in the pulsed-PECVD films, suggesting that formation of carbon crosslinks requires a longer plasma decomposition period. The presence of two distinct crosslinking structures in CW films leads to a highly networked structure and results in brittle coatings on thin wires. A higher proportion of terminal methyl groups was also observed in CW films, suggesting that pulsed-PECVD films may retain more precursor ring structure than CW films.

2.2 Introduction

Polymeric thin films produced by plasma-enhanced chemical vapor deposition (PECVD) offer several advantages over films produced by conventional polymerization. Thin, pinhole-free films that are highly coherent and adherent to a variety of substrates may be prepared from monomers not polymerizable by conventional means. Films are generally chemically inert, insoluble, mechanically tough, thermally stable and have been used in a wide variety of electrical, optical and biomedical applications, and as permselective membranes and protective coatings.¹⁻¹¹ In particular, plasma deposited films have potential application as conformal coatings on implantable devices with complex topologies and small dimensions, such as neurological electrodes.¹² Coatings on such devices need to be biocompatible, adherent, and flexible enough to minimize static forces on the surrounding tissue. The insulator should also have good dielectric properties and low permeability. In this work, we describe progress made towards a material that satisfies the foregoing properties.

Previous work has confirmed the suitability of PECVD organosilicon films for use as biomaterials. Chawla has investigated plasma-deposited films of hexamethylcyclotrisiloxane and octamethylcyclotetrasiloxane on Celgard[®]-2400 and Silastic[®] membranes and determined that the coatings reduced the adhesion of platelets both *in vitro*⁶ and *ex vivo* with a canine model.⁷ Ishikawa *et al.* examined coatings from a number of organosilicon precursors and found that the coatings reduced the adhesion of platelets on glass slides by 10-30%.⁸ Hasirci investigated the deposition of hexamethyldisiloxane on activated charcoal by PECVD and found that the organosilicon coating significantly reduced damage to platelets, erythrocytes and leucocytes in sheep's blood.⁹ Cannon *et al* detailed the synthesis of a fine neurological electrode consisting of W-26 at.% Re wire 125- μ m in diameter coated with plasma-polymerized hexamethyldisilazane. No *in vivo* biocompatibility and stability studies were reported, and some problems were experienced obtaining smooth pinhole-free coverage of the substrate.¹⁰ More recently, Nichols reported the synthesis of a novel polymeric material, Plasmalene[®], as an hermetic coating on wire substrates. The polymer coatings were deposited by vacuum processes which included PECVD and thermal vapor deposition of

methane and xylene. Encapsulant coatings were deposited on 75- μm wire substrates and demonstrated good mechanical durability and low leakage currents.¹³

Unlike conventional polymers, plasma polymers do not consist of chains with a regular repeat unit, but tend to form an irregular three-dimensional crosslinked network. UV irradiation and ion bombardment of the growing film can result in the formation of trapped free radicals, or dangling bonds, in the film.¹⁴ Upon exposure to atmosphere, these dangling bonds can be oxidized, leading to concomitant changes in film structure and properties. The effect of ion bombardment is also to increase the crosslink density in plasma films, which often results in brittle, inflexible films. In an effort to reduce dangling bond concentrations and crosslinking, we have used pulsed-PECVD to deposit coatings from an organosilicon precursor. In this technique, electrical power is repeatedly pulsed on and off. During the on-time, both ions and reactive neutrals are produced in the gas phase. During the off-time, the ratio of neutrals to ions increases due to the shorter lifetimes of ions: film deposition from reactive neutrals will thus be favored and a decrease in ion bombardment is anticipated.¹⁵⁻¹⁷ Fragmentation of the precursor gas is also expected to be less since it is exposed to a lower average electron energy, and the dynamics of competing reactions can be altered by varying on- and off-times. Indeed, investigation of pulsed-PECVD using fluorocarbon precursors has been shown to produce flexible, conformal PTFE-like films with reduced dangling bond concentration and lower crosslink density as compared to films obtained using continuous-wave (CW) excitation.¹⁸⁻²³ By contrast, only a few authors have documented the use of pulsed-PECVD with organosilicon precursors.^{6,14,24}

In the present study, PECVD was used to deposit coatings from the precursor hexamethylcyclotrisiloxane to assess their potential as insulating biomaterials. Films of different structure were obtained by varying the mode and timing of plasma excitation. By using pulsed-PECVD it was possible to optimize the flexibility of coatings produced on thin copper wires and produce films robust enough to withstand prolonged exposure to warm saline solution.

2.3 Experimental

A custom-built parallel-plate PECVD system was employed, with a powered upper electrode and a grounded lower electrode. For continuous-wave (CW) runs, 100 W of power was applied continuously for the duration of the run. Lower values of CW power were explored, but the resulting films suffered from incorporation of particulates most likely generated by the cracking and flaking of film deposited on the upper electrode during long deposition periods. This problem was not as severe for the shorter deposition periods used for the 100 W CW runs. For pulsed-PECVD runs, a peak RF power of 300 W was applied during on-time excitation. Power modulation was achieved using a pulse generator. On-times were varied from 10 to 100 ms and off-times from 0 to 600 ms to achieve duty cycles – defined as the fraction of total time during which power is applied – from 2.4% to 100%. Notation such as 10/100 will be used to denote the on/off timing for a pulsed plasma film.

During an initial screening period, films were deposited on planar substrates at duty cycles of 100%, 33%, 20%, 14%, 9%, and 3% and investigated by soak testing. For lower duty cycles, on/off timing was limited by the frequency range of the pulse generator, and low duty cycles are thus characterized by shorter on-times than higher duty cycles. For instance, an on-time of 10 ms was used for a duty cycle of 3%, while 100 ms was used for a duty cycle of 33%. As a bridging condition, and to allow comparison of the effect of on-time and off-time, three different pulse cycles of 100/600, 50/300, and 10/60 were used for a duty cycle of 14%. Based on these preliminary results, films were deposited on wire substrates at selected duty cycles of 100%, 33%, 14%, and 8%. Analyses were then performed on both planar and wire substrates. Deposition times ranged from 50 minutes (for CW and high duty cycles) to 75 minutes (for low duty cycles).

Silicon wafer substrates were placed on the lower electrode, and the lower electrode temperature was maintained near ambient by cooling water. Coatings were produced on 3-mil copper wires (0.003" diameter), which were strung across an aluminum ring placed on the lower electrode. After deposition, film thickness was estimated from optical micrographs of wire cross-sections. Pressure in the reactor was maintained at 500 mTorr by a butterfly valve. The precursor used was

hexamethylcyclotrisiloxane (D_3), a cyclic organosilicon compound consisting of three dimethylsiloxane (D) units of the form $-\text{Si}(\text{CH}_3)_2\text{O}-$. The precursor was vaporized in a heated vessel and delivered through a needle valve. The needle valve was calibrated by isolating the chamber from the vacuum pump and observing the pressure rise over time as the precursor flowed into the chamber. A precursor flow rate of 8 sccm was used for all runs. Argon was used as a diluent and the flow rate was maintained at approximately 40 sccm by a mass-flow controller.

To assess the insulation performance of coatings under conditions approximating that of the human body, films on silicon wafer substrates were subjected to soak testing. For each chosen condition, five identical samples were produced: four for bulk resistivity measurements and one for thickness measurements and film characterization. All five samples were deposited at the same time in the reactor. Once coated with the PECVD film, silicone o-rings were glued to the surface of the silicon pieces to delineate an area of 0.28cm^2 to be exposed to saline solution. Wires were attached to the backside of the silicon pieces using silver epoxy on a freshly scratched surface. All areas other than the test area were then coated with silicone to provide electrical isolation. The four samples for soak testing were then immersed in saline at the bottom of a test tube, heated to 80°C and plugged into the electrometer system. Current-voltage sweeps were run continuously from -5 V to $+5\text{ V}$, relative to a platinum ball electrode. For film characterization, infrared spectroscopy was performed using a Nicolet Magna 860 FTIR spectrometer in transmission mode. All spectra were normalized to a standard thickness of $1,500\text{ \AA}$.

2.4 Results and Discussion

Wire Coatings. Wire coatings were produced under CW excitation and at various duty cycles, and thickness was measured for each wire sample. Table 2-1 indicates that deposition rate depends strongly on duty cycle. Previously reported deposition rates for organosilicon films produced by RF PECVD are typically in the range $100 - 1100\text{ \AA}\cdot\text{min}^{-1}$.^{4-7,11,25,26} To test the flexibility of each coating, coated wires were twisted around a mandrel $750\text{ }\mu\text{m}$ in diameter and observed under an optical microscope. Wire coatings deposited at the duty cycles indicated in Table 2-1 (i.e. 100%, 33%, 14%, and 8%) were all examined for flexibility.

Table 2-1. Results of wire coatings on 3-mil copper wire deposited from D₃ using pulsed-PECVD.

duty cycle (%)	plasma excitation ^a	equivalent power (W)	thickness (μm)	deposition rate (Å·min ⁻¹)
100	CW	100	19	3,800
33	100/200	100	25	4,200
14	10/60	43	9	1,800
	50/300	43	12	2,400
	100/600	43	13	2,600
8	50/600	23	6	790

^a CW denotes continuous-wave excitation. 100/600 denotes 100-ms on time, 600-ms off time.

Figure 2-1 shows the results of this testing for a CW coating and three coatings deposited at the same duty cycle of 14% but with different on- and off-times. Coatings deposited under continuous-wave excitation (Figure 2-1a) showed considerable cracking and flaking under tension, while coatings deposited at a lower duty cycle of 14% showed improved flexibility (Figure 2-1b through 2-1d). In particular, cracking and flaking was reduced as the on-time and off-time were increased, as illustrated by the good flexibility of the 100/600 film. Indeed, of all the coatings tested, only the coating deposited at 100/600 did not crack, despite being more than 50% thicker than the 50/600 film (a duty cycle of 8%). This suggested that, though thickness may be important in determining flexibility, the effect of pulsing plasma excitation is more significant. Coatings on wires were conformal, as illustrated by a cross-sectional ESEM of film deposited on a University of Michigan (UM) probe (Figure 2-2).

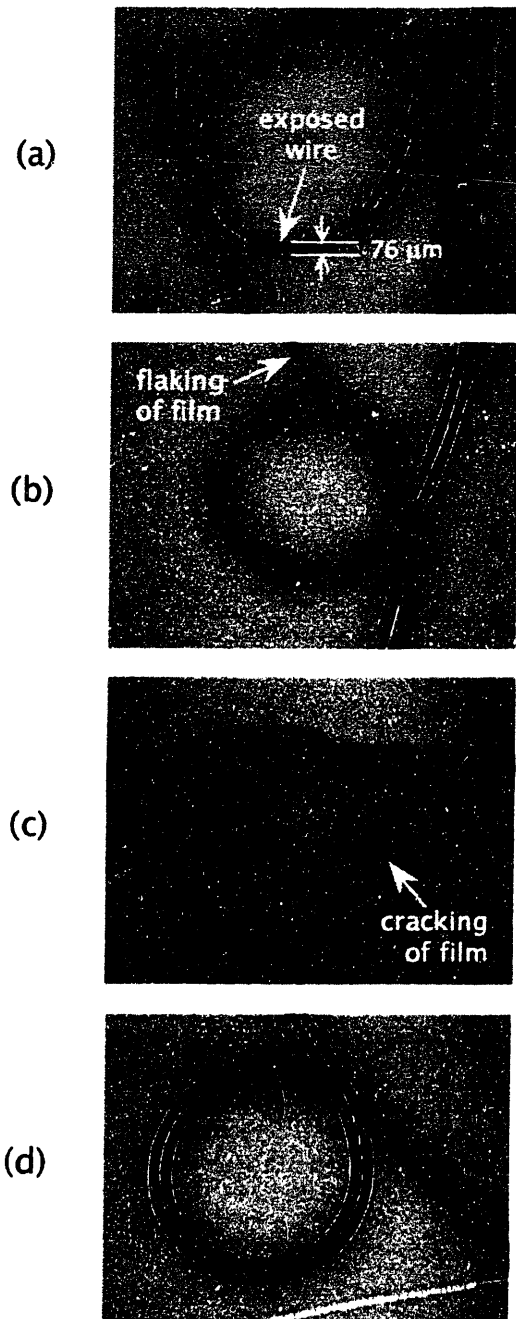


Figure 2-1. Optical micrographs showing 750 μm loops of 3-mil copper wire coated with D_3 pulsed-PECVD film at (a) CW, (b) 10/60, (c) 50/300, and (d) 100/600. Film thickness is (a) 19 μm , (b) 9 μm , (c) 12 μm , and (d) 13 μm . Film deposited at 100/600 shows the most flexibility.

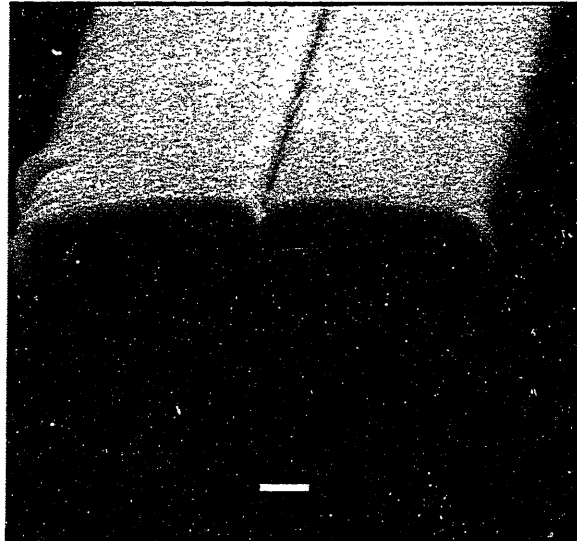


Figure 2-2. Coating on a University of Michigan probe deposited at 50/300, showing conformity of coating. Film is 20 μm at the thickest point.

Soak Testing. Multiple samples of pulsed-PECVD films were placed under saline soak at 80°C and the leakage current was monitored over time. Results to date (Table 2-2) indicate that many of the films still survive after nearly a year under soak. Films are robust and appear to adhere well to silicon surfaces. In particular, the 100/600 film that showed good flexibility has proved resistant to prolonged exposure to warm saline solution. Bulk resistivities for these films are lower than observed for high-quality silicones (typically $10^{16} \Omega\cdot\text{cm}$), but are acceptable for our applications. Failure mode was determined by examination of failed films under an optical microscope. The failure mode observed for the pulsed-PECVD samples appeared to be defect inclusion, where a pinhole or particulate caused a loss in insulating characteristics, while the CW films failed primarily through cracking.

Table 2-2. Results of saline soak testing of pulsed-PECVD films deposited under a variety of pulse conditions.

duty cycle (%)	plasma excitation	no. of samples tested	years under soak	survival rate (%)	average resistivity ^a ($\Omega\cdot\text{cm}$)
100	CW	8	1.23	88	$4.5\cdot 10^{12}$
	CW	4	0.90	100	$3.3\cdot 10^{13}$
33	100/200	4	0.90	75	$2.3\cdot 10^{13}$
20	100/400	8	1.23	75	$1.6\cdot 10^{13}$
	100/400	8	0.90	100	$4.7\cdot 10^{13}$
14	10/60	8	0.90	75	$5.8\cdot 10^{13}$
	50/300	4	0.73	75	$2.9\cdot 10^{13}$
	100/600	4	0.90	100	$4.7\cdot 10^{13}$
9	10/100	8	1.23	88	$4.6\cdot 10^{13}$
	10/100	4	0.90	100	$2.0\cdot 10^{14}$
3	10/250 ^b	4	0.90	50	$9.1\cdot 10^{12}$
average				84	$4.6\cdot 10^{13}$

^a Error in resistivity for each sample over time was small, typically less than 5%.

^b The 10/250 film was considerably thinner than other samples tested, which may account for its poor soak performance.

Film Structure. The FTIR spectrum of a 100/600 film is compared to that of the bulk polymer polydimethylsiloxane (PDMS) in Figure 2-3. Major assignments have been made in Table 2-3 based on the literature.^{26,31}

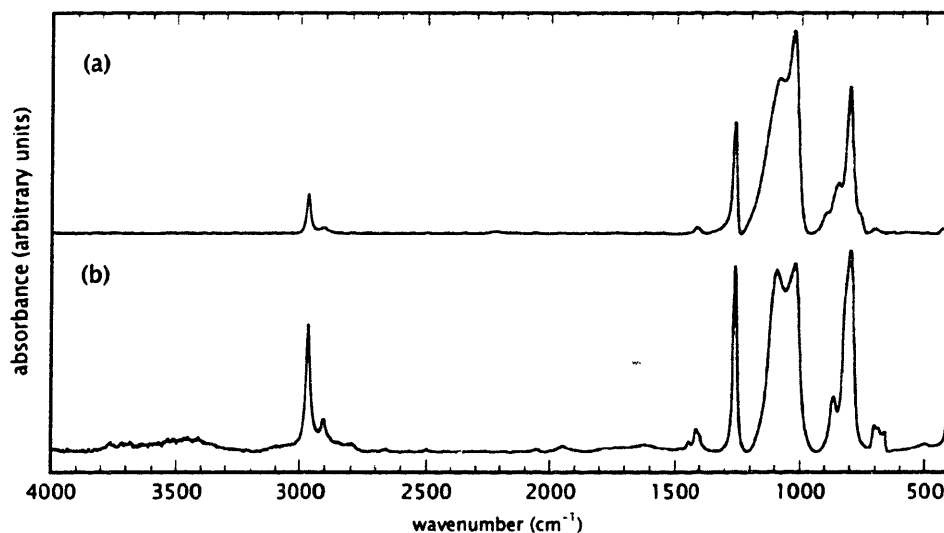


Figure 2-3. FTIR spectra of (a) pulsed-PECVD film deposited at 100/600, and (b) PDMS secondary standard. Absorption spectra of pulsed-PECVD film has been normalized to standard thickness of 1,500 Å.

Table 2-3. FTIR assignments from the literature.

wavenumber (cm ⁻¹)	mode ^a	comment	references
2964 – 2967	v ^A _{CH}	in sp ³ CH ₃	26,28,30
2933	v ^A _{CH}	in sp ³ CH ₂	26,30
2907 – 2909	v ^S _{CH}	in sp ³ CH ₃	26,28,30
2878	v ^S _{CH}	in sp ³ CH ₂	26,30
1463	δ ^A _{CH2}		26,30
1413	δ ^A _{CH3}	in SiMe _x	26,28,30,31
1263	δ ^S _{CH3}	in SiMe _x	26,28,29,31
1028 – 1120	v ^A _{SiOSi}		26,28,30,31
895	v _{Si-C, ρCH3}	in SiMe ₂	26,28,29,31
803	v _{Si-C, ρCH3}	in SiMe ₂	26,28,29,31
845 – 850	v _{Si-C, ρCH3}	in SiMe ₃	26,28,29,31
760	v _{Si-C, ρCH3}	in SiMe ₃	26,28,29,31
780	v _{Si-C}	in SiMe ₁	26,29

^a v, δ and ρ denote stretching, bending and rocking modes respectively, a and s denote asymmetric and symmetric vibrations.

The spectrum for the pulsed-PECVD film bears some resemblance to that obtained previously for PECVD films from organosilicon precursors.²⁶ Of particular note is the strong doublet centered around 1090 cm⁻¹, identified as the asymmetric stretching mode (ASM) of a polymeric siloxane backbone. The ratio of the two peaks of this doublet has been correlated with the length of chains or size of rings in the polymethylsiloxane network.^{26,32} In particular, for a series of linear and cyclic polymethylsiloxanes of increasing chain length or ring size, a doublet was observed in FTIR spectra only when chain lengths exceeded two siloxane units and ring size exceeded eight siloxane units. Hence, the films produced by pulsed-PECVD show some polymeric character.³² Strong absorptions are observed near 800 cm⁻¹ and 850 cm⁻¹ and have been assigned to di- and tri-methyl substituted silicon atoms. The strong band at 1,263 cm⁻¹ represents the bending mode for a silicon-bonded methyl group. Absorptions correlated to CH_x groups are observed at higher wavenumbers. For this sample, only sp³-hybridized carbon bonding is observed. Comparison of the FTIR spectra reveals that plasma excitation timing can strongly influence film structure. Films deposited at duty cycles of 100% (CW), 14% (100/600) and 2.4% (10/400) show the most variation both in the silicon-correlated and carbon-correlated regions (Figures 2-4 and 2-5).

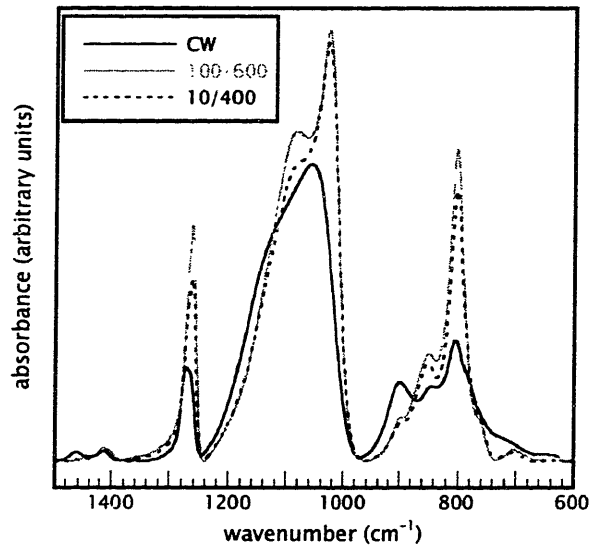


Figure 2-4. FTIR spectral region from 600 cm^{-1} to $1,500\text{ cm}^{-1}$ for CW, 100/600 and 10/400 films. Respective duty cycles are 100%, 14% and 2.4%.

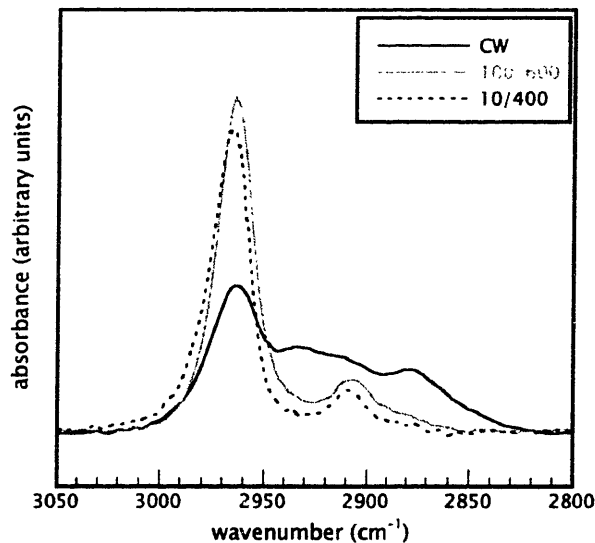


Figure 2-5. FTIR spectral region from $3,050\text{ cm}^{-1}$ to $2,800\text{ cm}^{-1}$ for CW, 100/600 and 10/400 films, showing CH_x correlated absorptions.

The spectra of films deposited at duty cycles ranging from 33% to 8% bore a close resemblance to that of the 100/600 film. Of particular note is the 100/200 film, which was deposited at the same equivalent power as the CW film (100 W), where equivalent power is obtained by multiplying duty cycle by peak power. The FTIR spectrum of the 100/200 film (not shown) resembles that of the 100/600 film rather than

that of the CW film. Thus, the difference in structure between CW and pulsed-PECVD films is attributed to the effect of pulsing rather than that of equivalent power.

In the region from 600 cm^{-1} to 1500 cm^{-1} (Figure 2-4), the spectrum of the CW film shows a shift to higher wavenumbers for the ASM and an increase in the intensity of the peak at 900 cm^{-1} . The peak at 900 cm^{-1} is in the region usually assigned to the stretching and bending modes for SiMe_2 . Typically, this peak has been reported at lower wavenumbers than observed here, as for instance in the work of Rau *et al*²⁶, who observed the peak at 885 cm^{-1} . It is odd that an increase in intensity for this peak is coupled with a reduction in intensity for the peak also associated with SiMe_2 at 803 cm^{-1} for the CW film, although this may be due to steric effects. Since no literature was found to suggest any other assignment, the SiMe_2 assignment is thus made tentatively. A band of low intensity at 780 cm^{-1} is more pronounced for the CW film and corresponds to SiMe_1 stretching. This suggests the presence of silicon atoms which may be involved in crosslinking and/or branching. We have identified two categories of crosslinks and/or branches: Type I, which consists of siloxane sidechains originating from nodes where silicon is attached to more than two oxygen atoms; and Type II, which consists of carbon sidechains originating from methylene-substituted multi-oxygen nodes. These categories are illustrated structurally in Figure 2-6. Here, M, D, T and Q represent silicon atoms with increasing numbers of oxygen substituents, and DCH_2 , $\text{D}(\text{CH}_2)_2$ and TCH_2 represent D and T groups with methylene substituents. Note that Figure 2-6 is not intended to be a rigorous summary of the silicon bonding environments present in our PECVD films. Indeed, hydrogen substituted versions of M through Q (typically referred to as MH, DH, etc.) have been observed in ^{29}Si solid-state NMR analysis of these films, and other structural variations are possible.

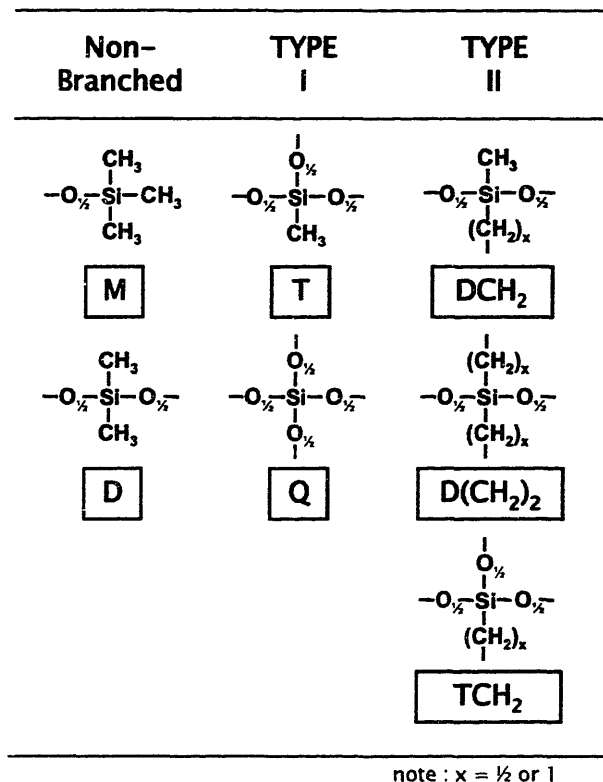


Figure 2-6. Possible crosslinking and/or branching nodes present in PECVD films. Non-branching M and D groups are shown for reference. Nodes of Type I involve only oxygen, while nodes of Type II involve both oxygen atoms and methylene groups.

Both CW and pulsed-PECVD films show a lower methyl content than PDMS (compare Figures 2-3a and 2-3b). This confirms, as does the hardness of the films, that crosslinking groups are present in the films. Indeed, T and Q groups have been clearly observed in PECVD organosilicon films by other workers³³ and in our own laboratory using solid-state ²⁹Si NMR spectroscopy. Crosslinks of Type I are thus present in both CW and pulsed-PECVD films. In the CW film, absorptions associated with methylene groups are observed at 2,933 cm⁻¹ and 2,878 cm⁻¹ (Figure 2-5). This is consistent with an absorption of low intensity at 1,463 cm⁻¹, also attributed to the presence of the methylene group, as well as the lower relative intensity of the methyl band at 1,263 cm⁻¹ for the CW film. Additional analyses on several of these films, including XPS and solid-state ²⁹Si NMR, have indicated that pulsed-PECVD films are more oxidized than their CW counterparts and contain more T and Q groups. For instance, a 10/60 film analyzed using ²⁹Si SSNMR showed 0.6% more T groups and 3.2% more Q groups than a CW film.

Considering the enhanced flexibility observed in pulsed-PECVD films, this suggests that methylene is present in CW films primarily in the form of carbon crosslinks rather than as carbon sidechains. These carbon crosslinks are of Type II and originate from DCH_2 , $\text{D}(\text{CH}_2)_2$ and TCH_2 nodes. Whether methylene is bonded as $\text{Si-CH}_2\text{-Si}$ or $\text{Si}-(\text{CH}_2)_2\text{-Si}$ is uncertain. Previous workers have argued that even a small absorption at $1,360\text{ cm}^{-1}$ is evidence of the former, but no assignment has been made in this work.²⁶ The lack of methylene crosslinking groups in pulsed-PECVD films suggests that there may be more pathways available for incorporation of oxygen during pulsed excitation than during CW excitation. With just a single type of crosslinking group, reasonable mechanical flexibility can still be retained.

The intensities of both the SiMe_3 absorptions (at 845 cm^{-1}) and the SiMe_2 absorptions (at 803 cm^{-1}) are lower in the CW film than in the pulsed-PECVD films. However, the ratio of the intensities of SiMe_3 to SiMe_2 is higher for the CW film than for the pulsed-PECVD films. This suggests that there are more terminal groups per polymeric siloxane (or D) unit in the CW film. Two main differences in structure are postulated to account for this. First, polymeric segments in the CW film may be shorter on average than those in the pulsed-PECVD film. These segments could be main chains or sidechain branches attached to a main chain. Second, since ring structures preclude the possibility of SiMe_3 groups, the CW film may have less ring structure overall than the pulsed-PECVD films. A more highly branched structure in CW films would also be consistent with an increase in the ratio of endgroups to backbone groups. The poor flexibility of CW coatings, however, suggests that these films are highly networked, rather than highly branched.

Mechanisms of plasma polymerization have been considered by various authors, notably Wróbel *et al*,¹ who provide a good overview of plasma-polymerized organosilicon materials. They argue that the dominant mode of precursor fragmentation is methyl abstraction, and that the active species in polymerization are primarily ionic in nature. In particular, an ionic mechanism for the ring expansion of D_3 during oligomerization is proposed.^{34,35}

The thermal decomposition of cyclic polydimethylsiloxanes has also been investigated.³⁶⁻³⁸ Davidson and Thompson, in particular, considered the pyrolysis of D_4

and estimated kinetic parameters for some proposed decomposition pathways. Based on their work, we have identified possible reaction pathways for the production of polymerization precursors from the decomposition of D_3 , as shown in Scheme 1.

1. $D_3 \leftrightarrow D_2 + D_1$ *decomposition*
2. $D_3 \rightarrow Me\cdot + Me_5O_3Si_3\cdot$ *methyl abstraction*
3. $D_3 \rightarrow l\text{-}D_3$ *ring opening*

Scheme 2-1. Reaction pathways for the production of polymerization precursors from D_3 .

D_1 in reaction 3 is the intermediate dimethylsilanone, $Me_2Si=O$. It is a potential film growth species that could lead to structures analogous to linear PDMS chains. The abstraction of a methyl group from D_3 , as represented by reaction 2, may take place via electron impact, and may result in a ionic silicon species rather than the radical species proposed for thermal decomposition. The presence of ionic silicon species in plasmas has been predicted and confirmed by other workers.³⁹⁻⁴² Mass spectrometry has been used to directly sample the reaction species from an RF plasma consisting of a mixture of vinyltrimethylsilane (VTMS) and argon. The distribution of ionic and neutral products indicated that successive dissociation and ionization of VTMS by low energy electron impact was the dominant mode of energy transfer at high pressures (> 0.5 Torr).^{42,43} These results suggest that ion and radical chemistries may both be important in organosilicon plasmas.^{1,34}

In their pyrolysis experiments, Davidson and Thompson observed reaction 2 to be much faster than reaction 1. The Si-O bond in cyclosiloxanes has been found to be exclusively stable to homolytic cleavage, and the ring-opening of D_3 to form the biradical $\cdot Me_2Si(OSiMe_2)_2O\cdot$ by reaction 3 unlikely.⁴⁴ The radical or ion produced by reaction 2 may thus be of some importance in plasma polymerization. Its existence suggests that film growth may involve the incorporation of oligomeric cyclic groups in addition to linear chains. It is interesting to speculate that the right-hand peak of the ASM near $1,020\text{ cm}^{-1}$ may be due to the presence of bound six-membered D_3 -like rings within the film. In a series of IR spectra of cyclic polymethylsiloxanes from D_3 up to D_8 , Wright et al.

observed that the ASM consisted of a single peak for ring structures smaller than D₅. This peak was offset at 1,020 cm⁻¹ for D₃ due to higher ring strain. By this reasoning, the FTIR data indicate that films of lower duty cycle incorporate a higher proportion of six-membered D₃-like rings into their structure. Specifically, the FTIR spectrum for the 10/400 film in Figure 2-1 bears a closer resemblance to that of the precursor than the 100/600 film. The FTIR spectrum for high molecular-weight PDMS (Figure 2-3b), however, does show an ASM doublet with a peak close to 1,020 cm⁻¹, making it difficult to differentiate between the presence of long chains and bound D₃ rings.³² To form a network of rings, at least two methyl abstraction events are required per precursor molecule. In previous work, we have investigated films deposited from D₄ using pyrolytic CVD. From elemental analysis, we observed that 1.9 methyl groups were lost per D₄ molecule, offering strong evidence for the incorporation of precursor-like rings into the film structure.⁴⁵ For PECVD films, the destructive nature of the plasma means that both linear and ring structures are likely to coexist even for films deposited at low duty-cycle films. It is not yet clear whether the characterization techniques available to us are capable of separating these different structural forms.

2.5 Conclusions

Pulsed-PECVD of D₃ offers a means of producing thin conformal, and insulating coatings at reasonable rates with adequate resistance to prolonged immersion in warm saline solution. Deposition was demonstrated on nonplanar substrates suitable for implantation, such as copper wires and neural probes. Wire coatings produced by pulsed-PECVD show more flexibility than CW coatings.

Both CW and pulsed-PECVD show evidence of crosslinking via T and Q groups. The carbon in pulsed-PECVD films is predominately bonded as CH₃, indicating retention of methyl groups from the D₃ precursor. By contrast, both CH₃ and CH₂ groups are observed in CW films. These methylene units, when bonded to D, T, or Q groups, constitute a crosslinking node we have designated as Type II. Type II crosslinks are characterized by carbon bridges of the form Si-(CH₂)_n-Si (n ≥ 1). The presence of crosslinking groups of both Type I and Type II in CW films leads to a highly networked structure, and results in brittle coatings on thin wires. Methylene was not detectable in the

pulsed-PECVD films, suggesting that formation of Type II crosslinks requires a longer plasma decomposition period.

Endgroups and sidechain terminations of the form SiMe_3 are prevalent in the CW film, indicating short chains and/or highly branched structures. In the pulsed-PECVD film, SiMe_2 is the predominate mode of methyl incorporation, consistent with enhanced retention of the precursor structure under conditions where plasma fragmentation processes are limited. Films with primarily SiMe_2 bonding must be either long linear siloxane chains and/or networks of interconnected ring structures. Polymerization of dimethylsilanone is one mechanism which could result in the growth of long linear chains. Six-membered D_3 rings and larger may be present in films produced by pulsed-PECVD, where neutral chemistry is more likely to compete with ionic chemistry and precursor fragmentation is expected to be less. This could explain the higher proportion of terminal methyl groups observed in FTIR of CW films, since these groups do not appear in siloxane ring structures.

Acknowledgements. We gratefully acknowledge the support of the NIH under contract NO1-NS-9-2323 and the NSF/SRC Engineering Research Center for Environmentally Benign Semiconductor Manufacturing in funding this work. In addition, this work made use of MRSEC Shared Facilities supported by the NSF under award DMR-9400334.

2.6 References

1. A. M. Wróbel and M. R. Wertheimer, in *Plasma Deposition, Treatment, and Etching of Polymers*, R. d'Agostino, Editor, p. 163, Academic Press, San Diego, CA (1990).
2. F. F. Shi, *Surf. Coat. Tech.*, **82**, 1 (1996).
3. Z. Ogumi, Y. Uchimoto, and Z. Takehara, *J. Electrochem. Soc.*, **136**, 625 (1989).
4. M. Kusabiraki, *J. Appl. Polym. Sci., Appl. Polym. Symp.*, **46**, 473 (1990).
5. P. K. Tien, G. Smolinsky, and R. J. Martin, *Appl. Opt.*, **11**, 637 (1972).
6. A. S. Chawla, *Artif. Organs*, **3**, 92 (1979).
7. A. S. Chawla, *Biomaterials*, **2**, 83 (1981).

8. Y. Ishikawa, S. Sasakawa, M. Takase, Y. Iriyama, and Y. Osada, *Makromol. Chem., Rapid Commun.*, **6**, 495 (1985).
9. N. Hasirci, *J. Appl. Polym. Sci.*, **34**, 2457 (1987).
10. J. G. Cannon, R. O. Dillon, R. F. Bunshah, P. H. Crandall, and A. M. Dymond, *J. Biomed. Mater. Res.*, **14**, 279 (1980).
11. H. Matsuyama, A. Kariya, and M. Teramoto, *J. Appl. Polym. Sci.*, **51**, 689 (1994).
12. M. F. Nichols, *Crit. Rev. Biomed. Eng.*, **22**, 39 (1994).
13. M. F. Nichols, *Biomed. Sci. Instrum.*, **29**, 77 (1993).
14. H. Yasuda and T. Hsu, *J. Polym. Sci., Polym. Chem. Ed.*, **15**, 81 (1977).
15. A. Bouchoule and P. Ranson, *J. Vac. Sci. Technol. A*, **9**, 317 (1991).
16. S. G. Hansen, G. Luckman, and S. D. Colson, *Appl. Phys. Lett.*, **53**, 1588 (1988).
17. A. Kono, M. Haverlag, G. M. W. Kroesen, and F. J. de Hoog, *J. Appl. Phys.*, **70**, 2939 (1991).
18. C. B. Labelle, S. J. Limb, and K. K. Gleason, *J. Appl. Phys.*, **82**, 1784 (1997).
19. S. J. Limb, K. K. S. Lau, D. J. Edell, E. F. Gleason, and K. K. Gleason, *Plasmas Polym.*, **4**, 21 (1999).
20. K. K. S. Lau and K. K. Gleason, *J. Fluorine Chem.*, **104**, 119 (2000).
21. C. R. Savage, R. B. Timmons, and J. W. Lin, in *Adv. Chem. Ser.*, 236, p. 745, American Chemical Society, Washington, DC (1993).
22. V. Panchalingam, B. Poon, H.-H. Huo, C. R. Savage, R. B. Timmons, and R. C. Eberhart, *J. Biomater. Sci. Polym. Edn.*, **5**, 131 (1993).
23. N. M. Mackie, N. F. Dalleska, D. G. Castner, and E. R. Fisher, *Chem. Mater.*, **9**, 349 (1997).
24. V. Panchalingam, X. Chen, C. R. Savage, R. B. Timmons, and R. C. Eberhart, *J. Appl. Polym. Sci., Appl. Polym. Symp.*, **54**, 123 (1994).
25. M. J. Vasile and G. Smolinsky, *J. Electrochem. Soc.*, **119**, 451 (1972).
26. C. Rau and W. Kulisch, *Thin Solid Films*, **249**, 28 (1994).
27. D. R. Anderson, in *Analysis of Silicones*, A. L. Smith, Editor, 41, p. 407, Wiley, New York (1974).
28. H. Kriegsmann, in *Advances in Molecular Spectroscopy; Proceedings*, A. Mangini, Editor, **3**, p. 1000, Pergamon Press, New York (1962).
29. L. J. Bellamy, *The Infra-red Spectra of Complex Molecules*, 2nd ed., p. 334, John Wiley & Sons, Inc., New York, (1958).
30. K. M. McNamara, B. E. Williams, K. K. Gleason, and B. E. Scruggs, *J. Appl. Phys.*, **76**, 2466 (1994).
31. R. E. Richards and H. W. Thompson, *J. Chem. Soc.*, 124 (1949).
32. N. Wright and M. J. Hunter, *J. Am. Chem. Soc.*, **69**, 803 (1947).
33. I. Tajima and M. Yamamoto, *J. Polym. Sci., A, Polym. Chem.*, **25**, 1737 (1987).
34. A. M. Wróbel, M. Kryszewski, and M. Gazicki, *J. Macromol. Sci. - Chem.*, **A20**, 583 (1983).

35. M. Kryszewski, A. M. Wróbel, and J. Tyczkowski, *Am. Chem. Soc., Plasma Polym.*, **108**, 220 (1979).
36. I. M. T. Davidson and J. F. Thompson, *Chem. Comm.*, 251 (1971).
37. I. M. T. Davidson and J. F. Thompson, *J. Chem. Soc., Faraday Trans. 1*, **71**, 2260 (1975).
38. L. E. Gusel'nikov, N. S. Nametkin, T. K. Islamov, A. A. Sobtsov, and V. M. Vdovin, *Izvest. Akad. Nauk SSSR, Ser. Khimi.*, **20**, 84 (1971).
39. A. K. Hays, in *Plasma Processing*, J. Dieleman, R. G. Frieser, and G. S. Mathad, Editors, **82-6**, p. 75, The Electrochemical Society (1981).
40. A. K. Hays, *Thin Solid Films*, **84**, 401 (1981).
41. G. Smolinsky and M. J. Vasile, *Int. J. Mass Spectrom. Ion Phys.*, **12**, 147 (1973).
42. M. J. Vasile and G. Smolinsky, *Int. J. Mass Spectrom. Ion Phys.*, **13**, 381 (1974).
43. M. J. Vasile and G. Smolinsky, *Int. J. Mass Spectrom. Ion Phys.*, **12**, 133 (1973).
44. M. G. Voronkov, *J. Organomet. Chem.*, **557**, 143 (1998).
45. M. C. Kwan and K. K. Gleason, *CVD*, **3**, 299 (1997).



CHAPTER 3

HFCVD of Organosilicon Thin Films from D₃ and D₄

HG Pryce Lewis, TB Casserly, KK Gleason, submitted to *J. Electrochem. Soc.*

3.1 Abstract

A non-plasma technique, hot-filament chemical vapor deposition (HFCVD), is an alternative method to produce organosilicon films of novel structure. Films are deposited onto room temperature substrates from the precursors hexamethylcyclotrisiloxane (D_3) and octamethylcyclotetrasiloxane (D_4) at high rates (>1 micron/min). Filament temperature can be used to control film structure, and the limited reaction pathways available via thermal decomposition make it possible to elucidate the chemistry of the growth process. During film growth, there appears to be competition between reaction pathways for the incorporation of cyclic and linear siloxane structures. For both D_3 and D_4 HFCVD films, Infrared, Raman, and Nuclear Magnetic Resonance spectroscopies indicate the incorporation of ring structures consisting of three siloxane units (oR_3). The concentration of these structures increases as filament temperature is raised, and is especially pronounced for films from D_3 . In comparison, films from D_4 show a greater degree of incorporation of linear, unstrained structures over the range of filament temperatures studied. In contrast to PECVD organosilicon films, crosslinking in HFCVD films occurs predominantly via silicon-silicon bonding and not from ternary or quaternary siloxane bonds.

3.2 Introduction

Organosilicon thin films produced by chemical vapor deposition have attracted considerable interest in a wide variety of applications, ranging from biocompatible coatings for medical implants to permselective membranes.¹⁻⁹ In particular, organosilicon films are presently under consideration as low-k interlayer dielectric (ILD) candidates for future semiconductor processing. These materials, termed organosilicate glasses (OSGs), are typically carbon-doped oxides or siloxanes deposited by CVD or plasma-enhanced CVD.¹⁰⁻¹² Research in this field has primarily focused on the use of plasma-enhanced chemical vapor deposition (PECVD) for producing organosilicon films with desirable properties (see Wróbel and Wertheimer¹ for an extensive review).

A plasma-based deposition technique, however, has inherent deficiencies. Plasma polymers tend to show high dielectric loss as compared to conventional polymers, as well as an aging effect upon exposure to the atmosphere. It has been proposed that exposure of the growing film to UV irradiation and ion bombardment during the deposition process can result in the formation of trapped free radicals, or dangling bonds, in the film.¹³ These defect sites are then subject to oxidation upon exposure to the atmosphere. The effect of ion bombardment is also to increase the crosslink density in plasma films, which often results in brittle, inflexible films. Pulsed-PECVD is a technique that can be used to minimize plasma exposure during film growth. In this method, plasma excitation is modulated to alter the dynamics of competing deposition pathways, allowing for greater compositional control and lower crosslink density in the resulting films.¹³⁻¹⁷ Using pulsed-PECVD with the precursor hexamethylcyclotrisiloxane (D_3), we have demonstrated flexible, conformal coatings on nonplanar substrates suitable for implantation.³

Hot-filament chemical vapor deposition (HFCVD, also known as pyrolytic CVD) does not suffer from the UV irradiation and ion bombardment associated with plasma exposure. In addition, HFCVD allows for more control over precursor fragmentation pathways than PECVD. Thermal activation is limited to the gas phase and independent control of the substrate temperature can be exercised. Indeed, HFCVD using hexafluoropropylene oxide as the precursor gas has been shown to produce fluorocarbon

films with low dangling bond density and having a chemical structure which is spectroscopically similar to polytetrafluoroethylene (PTFE).^{17,18}

In this study, we consider the structure of films produced by HFCVD using the precursors hexamethylcyclotrisiloxane, $[(\text{CH}_3)_2\text{SiO}]_3$, and octamethylcyclotetrasiloxane, $[(\text{CH}_3)_2\text{SiO}]_4$, commonly known as D₃ and D₄. Previously, we demonstrated that polymeric thin films could be deposited from D₄ by HFCVD at rates of up to 25,000 Å·min⁻¹ depending on filament temperature.¹⁹ In this work, we show that filament temperature (T_f) has a strong influence on composition for both D₃ and D₄ HFCVD films, and postulate a structure for these novel films.

3.3 Experimental

Films were deposited on silicon wafer substrates in a custom built vacuum chamber. Thermal excitation was accomplished by resistively heating tantalum wire (diameter 0.5 mm) strung on a filament holder. Springs on the holder maintained wire tension to compensate for thermal expansion and prevent drooping. The filament wire was mounted in a parallel array designed to minimize thermal gradients between individual wires and offer uniform heating over an area the size of a wafer. The filament holder straddled a cooled stage on which a silicon wafer substrate was placed. A filament to substrate standoff of 1.3 cm was used. Pure precursor was vaporized in a heated vessel and delivered through a needle valve to maintain flow rates of approximately 14 sccm for D₃ and 11 sccm for D₄. Pressure in the reactor was maintained at 300 mTorr by a butterfly valve. No diluent gas was used.

Filament temperature was measured using an 2.2 μm infrared pyrometer. For oxidized tantalum, a spectral emissivity of 0.20 was estimated from direct contact thermocouple measurements. Given the difficulties of direct measurement at high temperatures, reported temperatures are probably accurate to ±50°C. However, temperatures were consistent from run to run and there was little variation in power requirements for heating the wire. Substrate temperature was maintained below 60°C by backside water cooling. Films were deposited on 4-inch silicon wafers at filament temperatures ranging from 800°C to 1200°C. Deposition rates were monitored *in situ*

using interferometry and checked using profilometry at the center of each wafer after deposition.

For film characterization, infrared spectroscopy was performed using a Nicolet Magna 860 FTIR spectrometer operating in transmission mode. All spectra were normalized to a standard thickness of 1500 Å and baseline corrected for purposes of comparison. Resonant Raman spectra were obtained using a Kaiser Optical Systems Hololab 5000R Modular Research Micro-Raman Spectrograph, with 785 nm laser line excitation and 15 mW power at the sampling stage under 50x magnification. High resolution solid-state NMR spectra were acquired on a homebuilt NMR spectrometer²⁰ equipped with a 6.338 T Oxford superconducting magnet and a 3.2 mm Chemagnetics probe with spinning capabilities up to 25 kHz. Magic angle spinning (MAS) and cross-polarization (CP) from the proton spin bath were used to resolve isotropic chemical shifts and reduce acquisition time. Approximately 10 mg of film was scraped off the wafer and packed into a zirconia rotor, which was spun at 7 kHz. 14,512 acquisitions were performed for signal averaging. A ¹H-²⁹Si CP time of 5 ms was chosen to maximize the overall signal intensity. Experiments confirmed that the contact time between the silicon and proton spin baths was sufficient to provide uniform ²⁹Si polarization. Indeed, a direct comparison of NMR spectra acquired with direct- and cross-polarization confirmed that CP spectra were quantitative. All NMR spectra were referenced to tetramethylsilane (TMS) and are plotted in ppm. X-Ray Photoelectron Spectroscopy (XPS) was performed on a Kratos AXIS ULTRA spectrometer using a monochromatized aluminum K- α source. Atomic force microscopy (AFM) was performed on a Digital Instruments Dimension 3000. Images were taken under tapping mode with a standard etched silicon tip.

3.4 Results and Discussion

Deposition Rate. As shown in Figure 3-1, the deposition rate appears to follow an Arrhenius-type relationship as a function of filament temperature. The highest deposition rate observed was 15,740 Å/min, for D₄ at a filament temperature of 1050°C. No film deposition was detected at filament temperatures below 800°C with either precursor. At the higher filament temperatures, run times were limited to 1.5 minutes to

produce thin films appropriate for subsequent characterization. These temperatures are consistent with other studies of the vacuum pyrolysis of D_4 .²¹ Regression of the data in Figure 3-1 yielded apparent activation energies of 218 ± 35 kJ/mol for D_3 , and 301 ± 102 kJ/mol for D_4 (at a 90% confidence level).

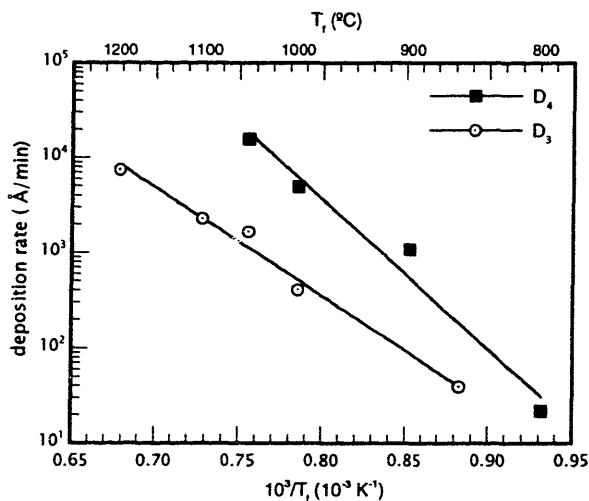


Figure 3-1. Arrhenius plot of D_3 and D_4 films produced by HFCVD. Straight lines were fitted by regression.

Fourier-Transform Infra-Red (FTIR) Spectroscopy. A comparison of the FTIR spectra of D_3 films deposited using HFCVD and continuous-wave excitation PECVD is shown in Figures 3-2a and 3-2b. The spectra for the CW PECVD film (Figure 3-2a) was taken from previous work by our group.³ Assignments have been made from the literature and are shown in Table 3-1. Comparison of these spectra indicates that the HFCVD film differs structurally from the PECVD film. Only sp^3 -carbon bonding is observed in the HFCVD film, and no crosslinking of Type II, i.e. via carbon-crosslinks, is evident.³ Carbon is thus preserved primarily as methyl, giving rise to the distinct pair of symmetric and asymmetric CH stretches at 2907 and 2964 cm^{-1} . The asymmetric stretching mode (ASM) of the siloxane group (SiOSi) shows two distinct peaks for the HFCVD film, a characteristic observed in the IR signatures of polydimethylsiloxanes with chain lengths of more than two siloxane units or ring sizes of larger than eight units.^{22,23} Below 1000 cm^{-1} , absorption bands associated with SiMe_2 rocking and stretching are observed at 878 and 805 cm^{-1} , and those associated with SiMe_3 rocking

near 840 cm^{-1} . Qualitatively, the PEVD films appears to have a higher $\text{SiMe}_3/\text{SiMe}_2$ ratio, suggesting that the HFCVD films is less branched than its PECVD analog.³

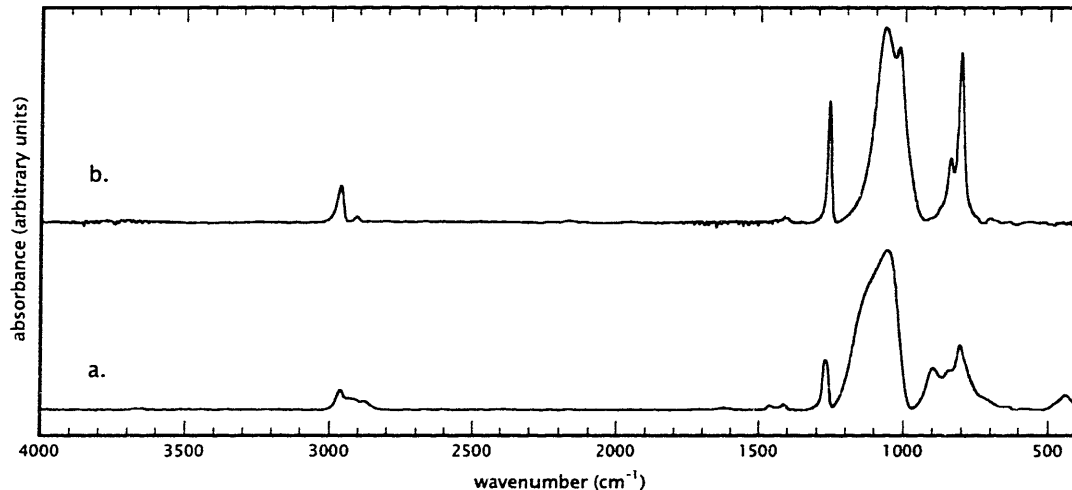


Figure 3-2. FTIR spectra of a. D_3 PECVD film deposited under continuous-wave excitation, and b. D_3 HFCVD film deposited at 1000°C .

Table 3-1. FTIR assignments from the literature.

wavenumber (cm^{-1})	mode ^a	comment	ref.
2963 – 2965	$\nu^{\text{A}}_{\text{CH}}$	in sp^3CH_3	24-27
2935	$\nu^{\text{A}}_{\text{CH}}$	in sp^3CH_2	26,27
2907	$\nu^{\text{S}}_{\text{CH}}$	in sp^3CH_3	24-27
2878	$\nu^{\text{S}}_{\text{CH}}$	in sp^3CH_2	26,27
1463	$\delta^{\text{A}}_{\text{CH}_2}$		26,27
1412	$\delta^{\text{A}}_{\text{CH}_3}$	in SiMe_x	23-27
1262	$\delta^{\text{S}}_{\text{CH}_3}$	in SiMe_x	23-25,27,28
1020 – 1075	$\nu^{\text{A}}_{\text{SiOSi}}$		23-27
878	$\rho^{\text{S}}_{\text{CH}_3}$	in SiMe_2	23,24,27,28
804 – 806	$\nu^{\text{A}}_{\text{Si-C}}, \rho^{\text{A}}_{\text{CH}_3}$	in SiMe_2	23-25,27,28
839 – 845	$\rho^{\text{A}}_{\text{CH}_3}$	in SiMe_3	23,24,27,28

^a ν , δ and ρ denote stretching, bending and rocking modes respectively, a and s denote asymmetric and symmetric vibrations.

FTIR spectra of films deposited at filament temperatures of 860°C , 1000°C , and 1200°C using D_3 , and 800°C , 900°C , and 1000°C using D_4 , are also shown (Figures 3-3 and 3-4, respectively). The region around the ASM has been expanded for detail. Strong absorptions associated with SiMe_2 (805 cm^{-1}), methyl in SiMe_x (1412 cm^{-1}), and the ASM ($1020\text{-}1075\text{ cm}^{-1}$) are apparent. The peak at about 880 cm^{-1} observed in the low

filament temperature D_4 film is usually associated with the symmetric CH_3 rocking mode in $SiMe_2$. The disappearance of this band at higher filament temperatures may be due to the conformational constraints present in a more highly networked structure. Similar effects in this infrared region have been observed in temperature-dependent spectroscopy studies of other organosilicon compounds.^{29,30}

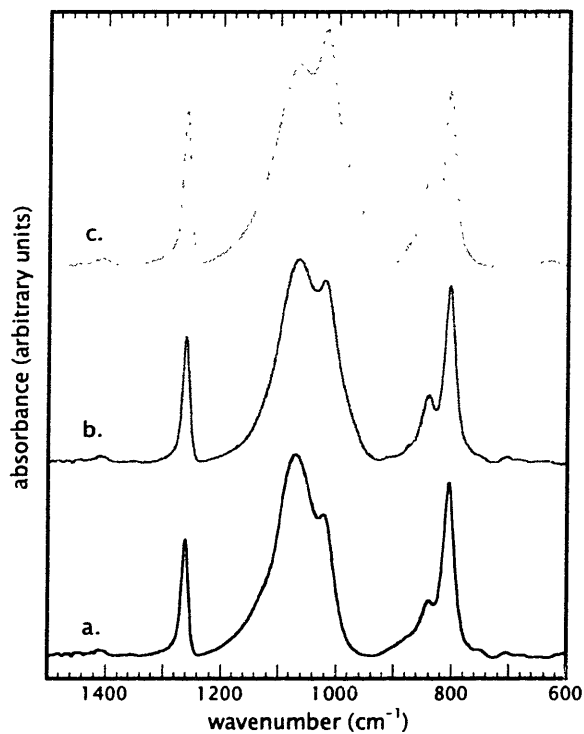


Figure 3-3. FTIR spectra of D_3 HFCVD films deposited at filament temperatures of a. 860°C, b. 1000°C, and c. 1100°C.

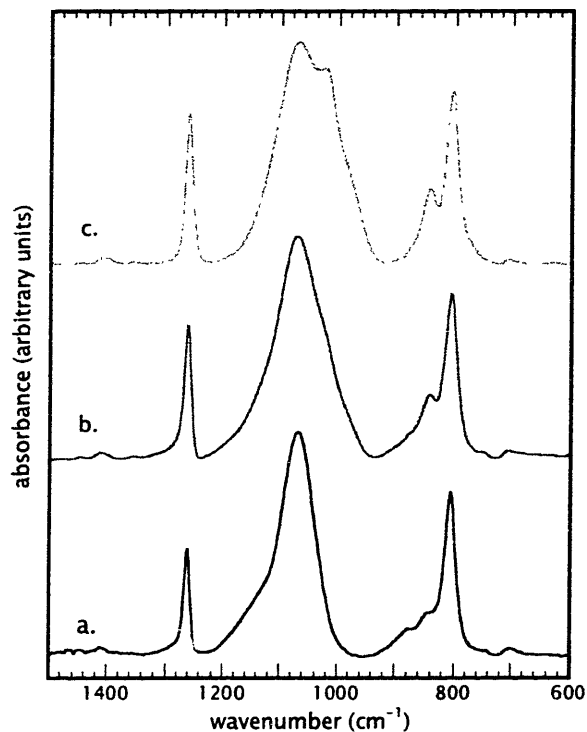


Figure 3-4. FTIR spectra of D₄ HFCVD films deposited at filament temperatures of a. 800°C, b. 900°C, and c. 1000°C.

Conventionally^{23,27,28}, the peak around 845 cm⁻¹ is assigned to an asymmetric CH₃-rocking mode in SiMe₃, with an accompanying symmetric CH₃-rocking mode at 760 cm⁻¹. The SiMe₃ group is a chain or branch termination group that is associated with an M group in siloxanes.³ The relative intensities of the SiMe₂ and SiMe₃ bands depends on the length of chains in open-chain regions of the film structure, and the strength of the SiMe₃ peak is an indication that chains are either short or highly branched.^{22,25} The SiMe₃/SiMe₂ ratio also increased only slightly as filament temperature was increased, suggesting that the chain length and branching was similar for both sets of films. Other data obtained for these films, particularly from NMR analysis, show only small quantities of M groups in the films, with the highest concentrations appearing in low filament-temperature D₃ and high filament-temperature D₄ films. This implies that short chain segments or branches of similar length are present in low concentrations in almost all the films produced.

Significant changes in the relative intensities of the peaks of the ASM band are observed for both D₃ and D₄ films. The D₃ film shows a doublet for all three filament

temperatures, with the shoulder on the doublet switching from the low- to high-wavenumber side at higher filament temperatures (compare Figures 3-3a and 3-3c). By contrast, the D₄ film deposited at a filament temperature of 800°C showed only a singlet, and the IR spectra resembled that of the precursor D₄.^{22,23} Unlike D₄, however, which is a liquid at room temperature, the film was solid and contiguous and came off the wafer in flakes when scraped with a razor. Little SiMe₃ was detected in this film. The D₄ film deposited at higher filament temperature showed behavior similar to that of the D₃ film. As filament temperature was increased, the low-wavenumber peak of the ASM doublet increased in intensity, exceeding that of the high-wavenumber peak above 1050°C (spectra not shown), as in the case of the D₃ film.

The ASM doublet of the film deposited from D₃ at a filament temperature of 1100°C (Figure 3-3c) resembles that observed in FTIR analyses of other organosilicon PECVD films.^{3,27,31} Typically for these films, the low-wavenumber peak was more intense than the high-wavenumber peak. This ASM signature is also observed in spin-on methyl silsesquioxane (MSQ) films.³² For bulk polydimethylsiloxane (PDMS), the intensities of these peaks are approximately equal at room temperature.³³ To our knowledge, no IR spectra with an ASM doublet similar to that observed in Figures 3-3a, 3-3b and 3-4c have been reported for organosilicon films deposited by CVD from comparable precursors. The configuration of the ASM doublet is likely to be conformational in origin. For PDMS, the splitting of the doublet has been attributed to coupling between adjacent chain segments.²⁵ In other work using Raman spectroscopy, the splitting of the symmetric SiOSi stretching mode has been correlated to the crystalline state of PDMS.³⁴

The intensity ratio of the two peaks of the ASM doublet has been correlated with the length of chains or size of rings in the polymethylsiloxane network.^{22,23,27} In particular, for a series of linear and cyclic polymethylsiloxanes of increasing chain length or ring size, a doublet was observed in FTIR spectra only when chain lengths exceeded two siloxane units and ring size exceeded five siloxane units. The ASM singlet for D₃ was offset at 1,020 cm⁻¹ compared to larger ring structure. The peak at 1,020 cm⁻¹ may thus be associated with an increasing proportion of six-membered D₃-like rings in the film structure. This is in the same region as the low-wavenumber peak of the ASM

doublet in PDMS, however, making it difficult to differentiate between the presence of chains and bound D₃ rings using IR analysis.²⁵

Raman Spectroscopy. Though some work has been done in characterizing pure organosilicon compounds using Raman spectroscopy, little has been reported on the use of Raman for characterizing more complex organosilicon materials, such as those produced by CVD. Figure 3-5 compares the Raman spectra of the pure compounds D₃, D₄, and PDMS with that of HFCVD films grown from D₃ and D₄ using high filament temperatures. Assignments in Table 3-2 have been made based on the literature.^{24,25,29,35} The symmetric siloxane stretching mode (SSM), which is weak in FTIR spectra, is strong in the Raman spectra. The position of the symmetric siloxane Raman band is shifted to higher wavenumbers for D₃ due to ring strain, and bands associated with ring deformation can be observed for both D₃ and D₄.²⁵ Raman spectroscopy is thus a sensitive probe for observing ring structure. Indeed, Raman spectroscopy is capable of identifying siloxane ring “defects” in SiO₂ films produced by sol-gel³⁶⁻³⁹ and CVD processes.⁴⁰ Raman spectra for these materials exhibit specific bands corresponding to ring structures comprised of different numbers of silicon atoms. In particular, Raman bands at 605 cm⁻¹ and 495 cm⁻¹ in silica have been attributed to rings with three and four siloxane units, termed R₃ and R₄ respectively.^{36,37,39,40}

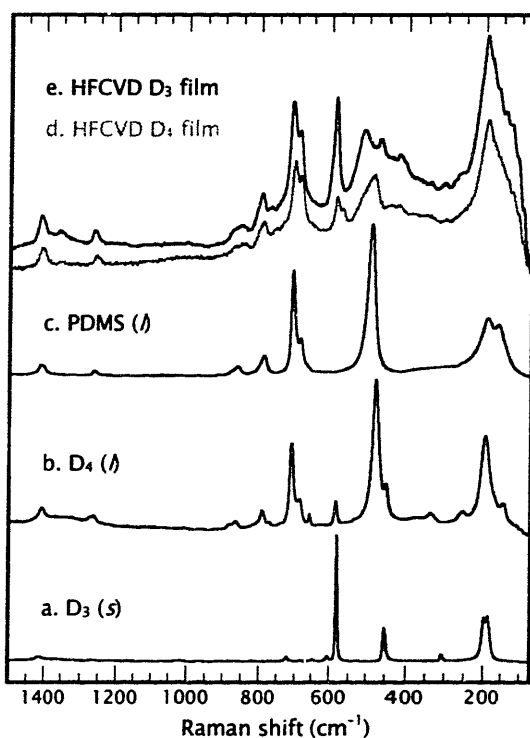


Figure 3-5. Micro-Raman spectra of a. D₃, b. D₄, c. PDMS, d. D₄ HFCVD film deposited at a filament temperature of 1000°C, and e. D₃ HFCVD film deposited at a filament temperature of 1100°C.

Table 3-2. Raman assignments from the literature.

Raman shift (cm ⁻¹)	mode ^a	comment	ref.
1410	$\delta_{\text{CH}_3}^{\text{A}}$		24,29,41
1260 – 1265	$\delta_{\text{CH}_3}^{\text{S}}$		24,29,41
795	$\nu_{\text{SiC}}^{\text{A}}$	In SiC ₂	24,29,35,41
707 – 712	$\nu_{\text{SiC}}^{\text{S}}$	In SiC ₂	24,29,35,41
690	$\rho_{\text{CH}_3}^{\text{A}}$		29,35,41
581	$\nu_{\text{SiOSi}}^{\text{S}}$	In D ₃	25,35,42
489	$\nu_{\text{SiOSi}}^{\text{S}}$	In PDMS	24,41
476	$\nu_{\text{SiOSi}}^{\text{S}}$ and/or ring deformation	In D ₄	35,41
450	Ring deformation	In D ₃ and D ₄	35,41
424 – 426	Possible Si-Si stretch		43
190 – 194	$\delta_{\text{SiC}}^{\text{S}}$	in SiC ₂	25,35
160	$\delta_{\text{SiC}}^{\text{S}}$ and twist	In PDMS	25
145	$\delta_{\text{SiC}}^{\text{S}}$	In D ₄	25

^a ν , δ and ρ denote stretching, bending and rocking modes respectively, a and s denote asymmetric and symmetric vibrations.

As observed in Figure 3-5, the HFCVD films differ from the pure compounds the Raman shift region from 400 cm^{-1} to 600 cm^{-1} . Both HFCVD films show a peak in the range 586 – 590 cm^{-1} which is not observed in PDMS or other linear siloxane compounds.²⁵ This is close to the band assigned to the siloxane symmetric stretching mode (SSM) at 581 cm^{-1} in pure D_3 . During an experiment in which polarization of the Raman beam was changed from the parallel to the perpendicular mode, the band in the HFCVD film was also found to be polarized, which is consistent with results observed for the SSM in D_3 .^{25,35} This band may thus be evidence of a bound D_3 -like ring structure in the film. The 5 – 10 cm^{-1} shift from the position of this band in D_3 may be conformational in origin and a result of the strain of being locked into a semi-networked structure. Such shifts are possible, and Table 3-3 shows Raman assignments for the SSM mode in different chemical environments.

Table 3-3. Raman siloxane symmetric stretching mode (SSM) assignments for various chemical environments.

structure	Raman shift (cm^{-1})	comment	ref.
R_3	600-608	In vitreous and/or CVD silica.	36-40
$o\text{R}_3$	586-590	In D_3 and D_4 HFCVD films.	
D_3	581-587	In D_3 .	25,35,42
D	489-497	In PDMS.	24,41
R_4	490-495	In vitreous and/or CVD silica.	36-40
$o\text{R}_4$ and/or $l\text{D}$	485	In D_3 and D_4 HFCVD films.	
D_4	475-480	In D_4 .	24,29,35,41

In the highly networked environment of vitreous and chemical vapor-deposited silica, the characteristic vibrational mode of the three-membered planar ring of siloxane units, R_3 , has been observed at shifts as high as 608 cm^{-1} .^{36,38,44} By contrast, the SSM mode is typically observed from 581-587 cm^{-1} for unconstrained D_3 . The band around 590 cm^{-1} for the HFCVD falls between these extremes, and is thus assigned to an $o\text{R}_3$ group. The nomenclature is intended to represent an organically substituted ring consisting of three siloxane units, which is bound into the film structure. By analogy, there may also be rings consisting of four siloxane units bound into the film structure

(νR_4). Table 3-3 shows that the peak at 485 cm^{-1} observed primarily in D_4 HFCVD films falls between the SSM bands for D in PDMS, R_4 in silica, and unperturbed D_4 . This suggests that the band is associated with νR_4 groups and/or unstrained siloxane units in the film. The unstrained siloxane units may be present in linear structures or in ring structures larger than four units, and are designated as $1D$. The predominance of these groups in the D_4 films, particularly at low filament temperature, suggest that they are unique to the pyrolysis chemistry of D_4 and may be the four siloxane-unit ring analog, νR_4 .

The HFCVD films also show a peak at 425 cm^{-1} not observed in any of the pure compounds. No assignment could be found for this peak in the literature, but it is in the region associated with a silicon-silicon stretching mode.⁴³ The Si-Si stretch gives a strong Raman band at $400 - 405\text{ cm}^{-1}$ for hexamethyldisilane, and is highly sensitive to silicon substituents. For polar substituents, shifts can be large. For example, the Si-Si stretching mode for $FMe_2SiSiMe_2F$ has been reported at 433 cm^{-1} , a shift of 30 cm^{-1} from the unsubstituted disilane.⁴⁵ Hence, this peak is tentatively assigned to an Si-Si bond in the film structure.

Figure 3-6 and 3-7 show the effect of filament temperature as probed by Raman spectroscopy. In Figure 3-6, films deposited from D_3 show an increasing concentration of νR_3 units and Si-Si bonds as filament temperature is increased, and the D_3 film deposited at 1100°C shows significant ring incorporation. FTIR spectra for these films show a similar increase in intensity in the low-wavenumber peak of the ASM doublet (see Figure 3-3), suggesting that this peak at 1020 cm^{-1} is indeed associated with three siloxane-unit ring structures. By contrast, films deposited from D_4 show a strong peak at 485 cm^{-1} , assigned to the presence of νR_4 and/or unstrained D units. A slight increase in νR_3 incorporation is observed as T_f increases, but this band does not dominate as it does in D_3 films. Hence, the D_3 and D_4 films differ structurally at high filament temperatures, despite the similarities in structures suggested by FTIR.

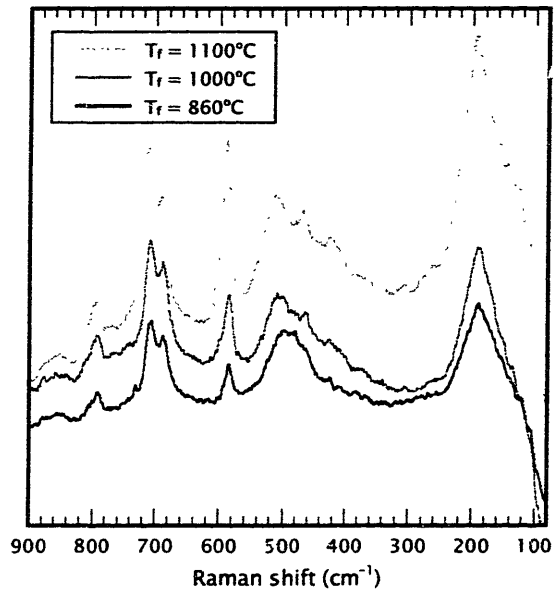


Figure 3-6. Micro-Raman spectra of D_3 HFCVD films deposited at filament temperatures of 860°C, 1000°C, and 1100°C.

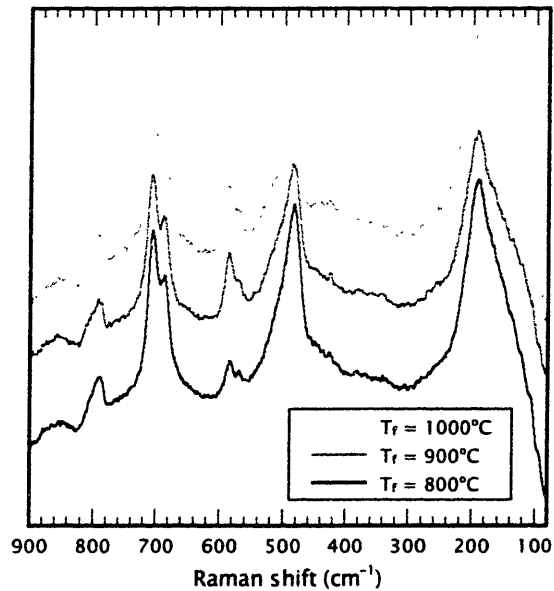


Figure 3-7. Micro-Raman spectra of D_4 HFCVD films deposited at filament temperatures of 800°C, 900°C, and 1000°C.

Nuclear Magnetic Resonance (NMR) Spectroscopy. ^{29}Si CP-MAS NMR spectra were obtained for the D_3 and D_4 HFCVD films and are shown in Figures 3-8 and 3-9. Typical chemical shifts reported in the literature for organosilicon CVD films are included in Table 3-4.^{20,31,46-49}

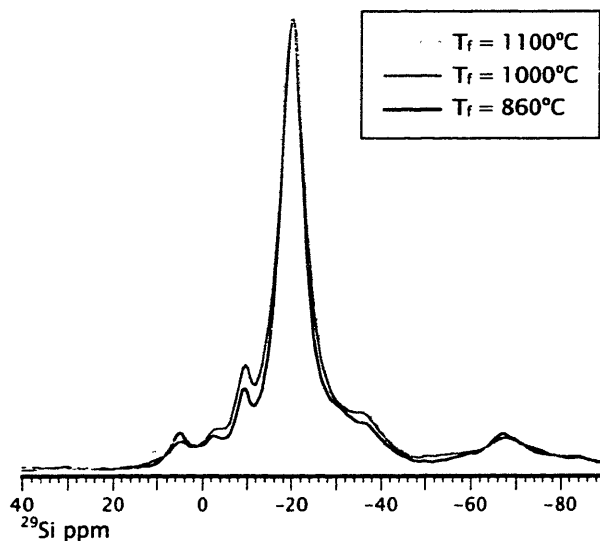


Figure 3-8. ^{29}Si Solid-State CP-MAS NMR spectra of D_3 HFCVD film deposited at filament temperatures of 860°C , 1000°C , and 1100°C .

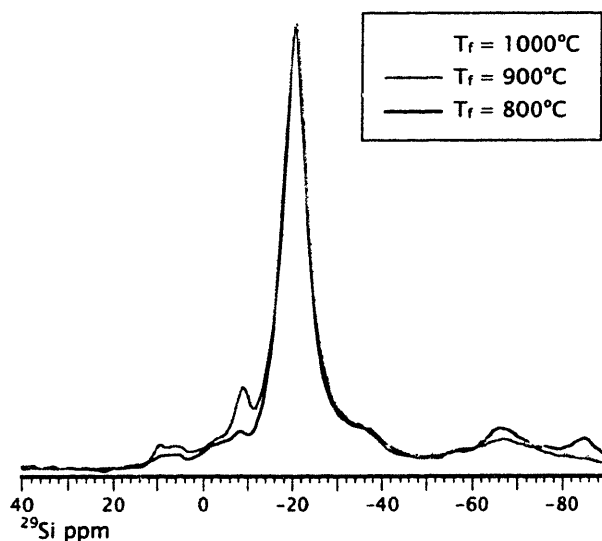


Figure 3-9. ^{29}Si Solid-State CP-MAS NMR spectra of D_4 HFCVD film deposited at filament temperatures of 800°C , 900°C , and 1000°C .

Table 3-4. ^{29}Si NMR structures and chemical shifts commonly observed in organosilicon CVD films.

symbol	structure	chemical shift (ppm)	ref.
M	$(\text{SiO})\text{Si}^+(\text{CH}_3)_3$	+6	31,49,51
M^{H}	$(\text{SiO})\text{Si}^+(\text{H})(\text{CH}_3)_2$	-6	47,49,51
		-10 in D_3	
D	$(\text{SiO})_2\text{Si}^+(\text{CH}_3)_2$	-20 in D_4	31,46,48,49,51
		-22 in PDMS	
D^{H}	$(\text{SiO})_2\text{Si}^+(\text{H})(\text{CH}_3)$	-34 to -37	46,47,49,51,52
T	$(\text{SiO})_3\text{Si}^+(\text{CH}_3)$	-67	31,46,49,51
T^{H}	$(\text{SiO})_3\text{Si}^+(\text{H})$	-84	20,47
Q	$(\text{SiO})_4\text{Si}^+$	-105 to -110	31,46,48,49,51

As suggested by Table 3-4, films deposited by other CVD methods commonly show a wide variety of bonding environments, including the presence of M, D, T, and Q groups as well as their hydrogenated analogs.^{31,49,53} By contrast, only two primary peaks were observed in these HFCVD films. The major peak at -19 ppm is assigned to the D unit, $(\text{SiO})_2\text{Si}^+(\text{CH}_3)_2$.^{31,46,48,49} The chemical shift for this moiety depends on the conformation of the siloxane chain, typically varying from -22 ppm for PDMS to -10 ppm for D_3 (due to ring strain). The lack of a doublet for this resonance analogous to that observed in FTIR is probably due to the longer time scales used for signal averaging in NMR. The closest assignment for the peak at -9 ppm suggested by the literature was for M^{H} [$(\text{SiO})\text{Si}^+(\text{H})(\text{CH}_3)_2$], which is typically reported at -6 ppm.^{47,49} However, there is little evidence of Si-H bonding (usually observed near 2140 cm^{-1}) in FTIR spectra of the HFCVD films. Since the Si-H stretching vibration has a high oscillator strength⁵⁴, even low concentrations of this moiety should yield a visible peak in FTIR spectra. Furthermore, CP contact time experiments produced no change in the relative intensities of the major peaks at -9 ppm and -19 ppm. It is anticipated that silicon directly bonded to hydrogen would increase cross-polarization rate. Thus, the peak at -9 ppm is not indicative of an M^{H} structure. Rather, as suggested by Raman spectroscopy, this peak is assigned to the presence of oR_3 ring structures in the film. This assignment is close to the reported shift of -10 ppm for the D unit in the strained molecule D_3 .^{46,48,51} The major peak at -19 ppm is then associated with oR_4 and/or unstrained siloxane units. The shift

of +3 ppm from an unstrained D group suggests that this unit may be primarily present in the form of a ring structure rather than a linear chain.⁴⁸

For both D₃ and D₄ films, the peak at -9 ppm increases in intensity as filament temperature increases (see Figures 3-8 and 3-9). While this peak is present in the D₃ films over the whole range of filament temperatures, it is of very low intensity in the D₄ film deposited at a filament temperature of 800°C. This is consistent with Raman data, which shows very little *oR*₃ in this film. The M peak at 5-6 ppm is also more intense in the D₃ film deposited at filament temperature of 860°C than in its 1100°C counterpart. Since M is more likely to be associated with linear structures in the film, a lower M content at high filament temperatures is consistent with the higher content of ring structures suggested by Raman spectroscopy. Both D₃ and D₄ films show a low and constant concentration of T groups, and almost no Q group. T and Q groups are conventional crosslinking and/or branching groups in organosilicon materials, and are observed in significant concentrations in films produced using PECVD.^{3,31,49,53} The absence of these groups suggests that crosslinking in the film must be associated with some other bonding structure. Based on the evidence of Si-Si bonding observed in Raman spectroscopy, it is postulated that crosslinking in these films occurs preferentially in the form of Si-Si bonding.

X-Ray Photoelectron Spectroscopy (XPS). Elemental ratios obtained using XPS analysis are reported in Table 3-5. The O:Si ratio is fairly constant for all films except the D₄ film deposited at a filament temperature of 800°C, which shows a high O:Si ratio of 1.23. The higher O:Si ratio for the this film is consistent with ²⁹Si NMR data indicating a greater concentration of T groups.

Table 3-5. XPS elemental ratios for HFCVD films from D₃ and D₄.

Precursor	T _f (°C)	O/Si	C/Si
D ₃	860	1.19	1.63
	1000	1.14	1.42
	1100	1.12	1.38
D ₄	800	1.23	1.86
	900	1.10	1.44
	1000	1.12	1.34

A C:Si ratio of less than 2.0 indicates that all films are deficient in carbon as compared to the precursor molecules. C1s high-resolution scans confirm that carbon is present exclusively as methyl. The methyl content appears to depend on filament temperature, with a significant loss of methyl at high filament temperatures for both D₃ and D₄ films. In all but one film, Si2p high-resolution scans showed no evidence of silicon oxidation states other than 2+, confirming that very little T and Q is present in the films. For the D₃ film deposited at a filament temperature of 1100°C, the Si2p and C1s high-resolution scans show slight shouldering on the main peaks. One source for this shouldering may be the slight increase in T group concentration observed in ²⁹Si NMR (Figure 3-8). However, this is inconsistent with the low O/Si ratio reported for this film, and similar shouldering is not observed in the D₄ film deposited at filament temperature of 800°C which shows a greater O/Si ratio. More likely, the shouldering is a shift associated with Si-Si bonding that becomes visible when the concentration of this moiety is high. The origin of the shouldering in the C1s scan is uncertain but is unlikely to originate from carbonyl or methylene moieties in the films, as these would be visible using other spectroscopic techniques (e.g. FTIR).

Atomic Force Microscopy (AFM). AFM indicated that the films were very smooth. A typical micrograph is shown in Figure 3-10, in this case for a D₄ film deposited at a filament temperature of 900°C. RMS roughnesses for all films were of the order of 1.0 nm. The RMS roughness of the silicon substrate was 0.53 nm.⁵⁵ This in contrast to fluorocarbon films deposited using HFVCD, which often show significant morphology.⁵⁶ This morphology is possible due to the lack of ion and electron bombardment which tends to cause densification and film damage in films grown via PECVD. The smoothness of our films deposited using a similar HFCVD process suggests that there is efficient packing on the molecular level in the organosilicon films.

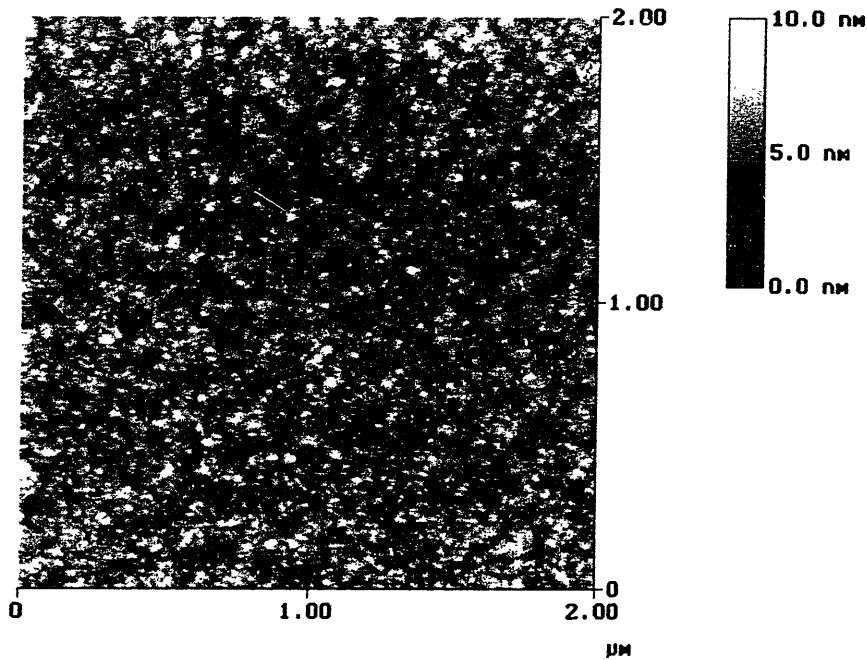


Figure 3-10. Atomic force micrograph of D₄ HFCVD film deposited at a filament temperature of 900°C. RMS roughness over image area is 1.1 nm. RMS roughness of bare silicon is 0.53 nm.

Reaction Chemistry. Possible pathways for the production of film growth species under thermal excitation are shown in Figure 3-11. Reactions 1 through 3 describe respectively the molecular rearrangement of D₄ to produce D₃ and the intermediate species dimethylsilanone (D₁, Me₂Si=O), methyl abstraction from the ring to produce a radical ring species, and ring-opening to produce a linear diradical group. Reactions 4 through 6 are analogous pathways for D₃.

Reaction	Description
(1) $D_4 \leftrightarrow D_3 + \text{Me}_2\text{Si}=\text{O}$	<i>Intramolecular Rearrangement</i>
(2) $D_4 \rightarrow \text{Me}^\bullet + \text{[cyclic D}_4\text{]} \rightarrow 2\text{Me}^\bullet + \text{[cyclic D}_3\text{]} \rightarrow \dots$	<i>Methyl Abstraction</i>
(3) $D_4 \leftrightarrow \bullet\text{O}(\text{Me}_2\text{SiO})_3\text{Me}_2\text{Si}^\bullet$ or $\text{O}(\text{Me}_2\text{SiO})_3\text{Me}_2\text{Si}^\bullet$	<i>Ring Opening</i>
(4) $D_3 \leftrightarrow D_2 + \text{Me}_2\text{Si}=\text{O}$	<i>Intramolecular Rearrangement</i>
(5) $D_3 \rightarrow \text{Me}^\bullet + \text{[cyclic D}_3\text{]} \rightarrow 2\text{Me}^\bullet + \text{[cyclic D}_2\text{]} \rightarrow \dots$	<i>Methyl Abstraction</i>
(6) $D_3 \leftrightarrow \bullet\text{O}(\text{Me}_2\text{SiO})_2\text{Me}_2\text{Si}^\bullet$ or $\text{O}(\text{Me}_2\text{SiO})_2\text{Me}_2\text{Si}^\bullet$	<i>Ring Opening</i>

Figure 3-11. Reaction pathways for the production of polymerization precursor species in D_3 and D_4 HFCVD.

Previous studies have investigated the gas-phase pyrolysis of D_3 and D_4 over a temperature range from 400 to 1100°C and a pressure range from 10^{-4} to 1.0 Torr.^{21,57-60} For the pyrolysis of D_4 , the only products observed were D_3 and D_5 , with the rate of formation of D_5 decreasing rapidly above 2% decomposition until D_3 was the only product at high conversions.^{59,60} The formation of the intermediate D_1 was postulated to explain the observed results, and the presence of D_5 explained by recombination of D_1 with D_4 . Other authors have postulated the existence of D_1 ^{58,61,62}, and evidence for its existence has been collected in matrix IR studies of the vacuum pyrolysis of D_4 ²¹. In the latter study, temperatures of 900°C to 1,050°C were used, closer to those used in our work, and significant conversion of D_4 to D_3 was also noted at these higher temperatures. D_1 may result from the intramolecular rearrangement of D_4 at high temperatures, and similar thermal rearrangements have been observed in other dimethylsiloxanes. It has been suggested that these involve the formation of a bicyclic transition state, accounting for the predominant cleavage of the Si-O bond over the weaker Si-C bond.^{21,58,62-66}

D_1 may be a growth precursor for the organosilicon films, with a polymerization mechanism analogous to that postulated for the diradical difluorocarbene (CF_2) during HFCVD of fluorocarbon films.⁶⁷ Indeed, heterogeneous loss of D_1 has been postulated to account for discrepancies in the mass balance in previous pyrolysis studies of D_4 .⁶⁰ For the early stages of this pyrolysis (<4% decomposition), an activation energy of 301 ± 6.3 kJ/mol was reported for Reaction 1.⁶⁰ This is close to the apparent activation energy of 301 ± 102 kJ/mol estimated for D_4 in the present work, and suggests that Reaction 1 may be the predominant pathway for the pyrolysis of D_4 at low filament temperatures. It is illuminating to apply the reported rate law to our CVD system. At low filament temperatures (e.g. 800°C), where the conversion of D_4 is likely to be less than 4% and 569°C may be representative of temperatures in the gas phase some distance from the filament, the conversion of D_4 using this rate law is calculated to be 0.3%. Assuming a film density²⁷ of 1.3 g/cm³, the production of D_1 could yield film growth at a rate of 108 Å/min on a 4-inch wafer. By comparison, the measured deposition rate at 800°C was 22 Å/min. At higher filament temperatures (above 1,000°C), the conversion of D_4 exceeds 4% and the rate law no longer applies. Hence, film growth by D_1 generated via Reaction 1 is possible, and could lead to a linear siloxane backbone structure. This may explain the higher C/Si ratio in XPS and the lack of ASM doublet structure in FTIR for the D_4 film deposited at a filament temperature of 800°C.

In contrast to D_4 , the pyrolysis of D_3 is not expected to yield significant quantities of D_1 . The D_2 ring is highly unstable^{62,68} and the elimination of D_1 from D_3 as shown in Reaction 4 is known to be highly endothermic.^{60,64} The lack of this pathway for producing growth species may explain the lower deposition rates observed for D_3 , despite the molecule's planar strained conformation and typically high reactivity in heterolytic reactions. Instead, the rupture of the silicon-methyl bond via Reaction 5 is likely to predominate. In preliminary studies, Davidson *et al.* reported on the kinetics of this reaction for the loss of one methyl group between 578°C and 662°C.⁶⁰ Calculations at 662°C analogous to those performed for Reaction 1 showed that a loss of one methyl group from D_3 via Reaction 5 could account for a conversion of 0.6% of the precursor, and could yield film growth at a rate of 762 Å/min. If only one methyl group were lost per D_3 molecule, the oR_3 ring structure could be incorporated into the film as a terminal

group. Additional methyl abstraction processes may also occur after the initial loss, resulting in incorporation of the oR_3 structure as a polymeric (loss of two methyl groups) or networked unit (loss of three methyl groups). Incorporation requires bonding of the oR_3 group to another oR_3 group and/or a D_1 unit, and, in the absence of free oxygen, involves a silicon-silicon bond. This may be the origin of the assigned silicon-silicon group observed in Raman spectroscopy. By similar reasoning, methyl abstraction from D_4 , as shown in Reaction 2, and subsequent incorporation of the oR_4 group is possible. However, no kinetic data has been found for Reaction 2.

Ring-opening is also possible for both D_3 and D_4 , as illustrated in Reactions 3 and 6. However, direct homolytic cleavage of the Si-O bond in cyclosiloxanes to produce diradicals of the form $\cdot SiMe_2(OSiMe_2)_nO\cdot$ is unlikely.^{62,64} Free radical polymerization of diradical species produced by Reactions 3 and 6 is thus improbable. Ionic polymerization also seems unlikely in an HFCVD environment, where ions are expected to be short-lived. Such pathways are more likely in a plasma environment, where ionic species formed from the ring-opening of cyclic dimethylsiloxanes have been postulated to explain growth mechanisms in organosilicon PECVD from similar precursors^{1,69-71} Furthermore, if the ring-opening reaction were the primary contributor to the production of film growth species, it is anticipated that greater ring strain in D_3 would be reflected in higher growth rates for that precursor. Instead, Figure 3-1 shows that deposition rates for D_4 are consistently higher than for D_3 . For comparison, ring strains of 10.5 kJ/mol for D_3 and 1.00 kJ/mol for D_4 have been reported.⁶⁸ Hence, polymerization of linear species produced via Reactions 3 and 6 does not appear to be a dominant mode of film growth.

Film growth in D_3 and D_4 HFCVD films is thus believed to occur mainly through the combination of growth precursors generated via Reactions 1, 2, and 5. For D_4 , there is competition between the generation of D_1 via Reaction 1 and the generation of oR_4 groups from methyl abstraction in Reaction 2. Since Reaction 1 produces D_3 , there is an additional pathway for the incorporation of oR_3 groups generated via Reaction 5. At low filament temperatures, Reaction 1 may dominate, resulting in film growth primarily from D_1 species. At higher filament temperatures, however, evidence of oR_3 incorporation suggests that Reaction 5 starts to compete. For D_3 , Reaction 5 is the predominant source of potential growth precursors in the form of oR_3 structures. However, it does not appear

to be the only source, as all films from D_3 show some evidence of incorporation of oR_4 and/or ID units in the film structure. Pyrolysis studies of D_3 have shown evidence of appreciable concentrations of D_4 in the pyrolyzate, and it was found that the concentration of D_4 in the pyrolyzate decreased as pyrolysis temperature increased.^{57,58} At low filament temperatures, where D_4 concentrations are higher, there is probably a significant contribution of Reaction 1 to the chemistry. At higher temperatures, where D_3 concentrations are high, Reaction 1 is probably less favorable and D_4 reacts preferentially via the methyl abstraction process in Reaction 2. This may explain the shift observed in the Raman peak assigned to oR_4 and/or ID as filament temperature increases (Figure 3-6). For the 860°C film, this peak is centered close to 495 cm^{-1} , but shifts to about 505 cm^{-1} for filament temperatures above 1000°C. There also appears to be a new peak that appears near 465 cm^{-1} above this temperature. Most likely, the peak centered around 495 cm^{-1} is indicative of a linear siloxane unit derived from the polymerization of D_1 . The two peaks that appear at higher temperature are indicative of an oR_4 unit (at 505 cm^{-1}) and a larger structure such as oR_5 (at 465 cm^{-1}). The five-membered siloxane ring, oR_5 , could originate from D_5 via methyl abstraction processes analogous to those in Reactions 2 and 5.

It is thus postulated that growth of the D_3 HFCVD occurs in two distinct regimes: at low filament temperatures, there is growth primarily from linear polymeric units (ID) and by the incorporation of rings consisting of three siloxane units (oR_3); at high filament temperatures, there is growth primarily from three- and higher-membered siloxane rings (oR_3 , oR_4 , oR_5 , and higher). This growth model is consistent with previous studies of D_3 pyrolysis, in which it was observed that as temperature increased, the composition of the pyrolyzate changed from a linear polymeric mixture of molecular weight 1810 to a mixture of cyclic components consisting mainly of D_3 , D_4 , and D_5 .⁵⁷

Film Structure. The physical properties of D_3 and D_4 HFCVD films show evidence of crosslinking. In particular, as-deposited films are found to be insoluble in common solvents, and form visible flakes when scraped off the wafer. In contrast, a polymethylsiloxane polymer with a composition of 30% T and 70% D groups – corresponding to a C:Si ratio of 1.70 – is a liquid at ambient conditions, and more

crosslinked polymethylsiloxanes remain resinous up to a composition of about 90% T and 10% D groups – a C:Si ratio of 1.10.⁶⁸ The HFCVD films show higher C:Si ratios of between 1.90 and 1.30, but are coherent, hard, and show no evidence of tackiness. Qualitatively, films deposited at higher temperatures are observed to be harder than those deposited at lower temperatures, suggesting higher crosslink densities. However, the concentration of T and Q groups observed in NMR even at high filament temperatures is not sufficient to explain the lack of resinous character in the films. Some other type of crosslinking group must be present.

Spectroscopic evidence suggests that this networking occurs via silicon-silicon bonding. This bonding could originate during film growth from ring structures that have lost methyl groups, as illustrated in Reactions 2 and 5 in Figure 3-11. These reactions produce cyclic structural units capable of silicon-silicon bonding. Ring structures are then “tiled” into the film structure and observed as the moieties σR_3 and σR_4 . Analogous silicon-silicon bonding of cyclic structures has been observed in radiation-induced crosslinking of D_4 ,⁷² and other occurrences of Si-Si bonding have also been reported for similar organosilicon materials.⁷³ Raman data confirm that, for both D_3 and D_4 films, there is a simultaneous increase in intensity for bands assigned to σR_3 and silicon-silicon bonding as filament temperature is raised. Reactions 2 and 5 thus appear to be the dominant pathway for silicon-silicon bonding.

Increased crosslink density by silicon-silicon bonding is expected to occur at the expense of methyl groups. This is confirmed by XPS data from Table 3-5, which show a decrease in methyl content as filament temperature is increased, with no corresponding change in oxygen content. From the data, it is possible to speculate on the average number of silicon-silicon bonds per structural unit. To form part of a polymeric chain, at least two methyl abstraction events are required per structural unit. For the case where only three-membered siloxane rings are incorporated, data from Table 3-5 correspond to an average loss of 2.0 methyl groups per ring. For the case where only four-membered rings are incorporated, these data correspond to an average loss of 2.6 methyl groups per ring. A loss of at least three methyl groups per ring is necessary to produce a networked structure. The data are thus consistent with incorporation of both σR_3 and σR_4 units in HFCVD films .

3.5 Conclusions

Hot-filament CVD is a technique that is capable of producing smooth organosilicon thin films of unique structure at high deposition rates. Filament temperature can be used as a control variable for varying film structure. During the growth process, there appears to be competition between pathways for the incorporation of three-membered and higher-order siloxane ring structures, and pathways for the incorporation of linear structures in the films. For both D_3 and D_4 , there is greater incorporation of ring structures consisting of three siloxane units (oR_3) as filament temperature is increased. The incorporation of these structures is more pronounced for films grown from D_3 . D_3 films also shows evidence of higher-order ring structures such as oR_4 and oR_5 at high filament temperatures. By contrast, D_4 films show a greater degree of incorporation of linear, unstrained structures (D) over the range of filament temperatures studied. Ring structures are generated from methyl abstraction processes, and are incorporated into the structure via silicon-silicon bonds. In contrast to organosilicon films produced by plasma processing, crosslinking via silicon-silicon bonding appears to predominate over that from ternary or quaternary siloxane bonds.

Acknowledgments. We gratefully acknowledge the support of the NIH under contract NO1-NS-9-2323, and the NSF/SRC Engineering Research Center for Environmentally Benign Semiconductor Manufacturing in funding this work. This work also made use of the MRSEC Shared Facilities supported by the National Science Foundation under Award Number DMR-9400334 and NSF Laser Facility grant #9708265-CHE.

3.6 References

-
1. A. M. Wróbel and M. R. Wertheimer, in *Plasma Deposition, Treatment, and Etching of Polymers*, R. d'Agostino, Editor, p. 163, Academic Press, San Diego, CA (1990).
 2. F. F. Shi, *Surf. Coat. Tech.*, **82**, 1 (1996).
 3. H. G. Pryce Lewis, D. J. Edell, and K. K. Gleason, *Chem. Mater.*, **12**, 3488 (2000).
 4. A. S. Chawla, *Biomaterials*, **2**, 83 (1981).

5. Z. Ogumi, Y. Uchimoto, and Z. Takehara, *J. Electrochem. Soc.*, **136**, 625 (1989).
6. M. Kusabiraki, *J. Appl. Polym. Sci., Appl. Polym. Symp.*, **46**, 473 (1990).
7. P. K. Tien, G. Smolinsky, and R. J. Martin, *Appl. Opt.*, **11**, 637 (1972).
8. Y. Ishikawa, S. Sasakawa, M. Takase, Y. Iriyama, and Y. Osada, *Makromol. Chem., Rapid Commun.*, **6**, 495 (1985).
9. H. Matsuyama, A. Kariya, and M. Teramoto, *J. Appl. Polym. Sci.*, **51**, 689 (1994).
10. L. Peters, *Semicond. Int.*, **23**, 108 (2000).
11. M. J. Loboda, *Microelect. Eng.*, **50**, 15 (2000).
12. A. Grill and V. Patel, *J. Appl. Phys.*, **85**, 3314 (1999).
13. H. Yasuda and T. Hsu, *J. Polym. Sci., Polym. Chem. Ed.*, **15**, 81 (1977).
14. C. R. Savage, R. B. Timmons, and J. W. Lin, in *Adv. Chem. Ser.*, 236, p. 745, American Chemical Society, Washington, DC (1993).
15. N. M. Mackie, N. F. Dalleska, D. G. Castner, and E. R. Fisher, *Chem. Mater.*, **9**, 349 (1997).
16. C. B. Labelle, S. M. Karecki, L. R. Reif, and K. K. Gleason, *J. Vac. Sci. Technol. A*, **17**, 3419 (1999).
17. K. K. S. Lau and K. K. Gleason, *J. Fluorine Chem.*, **104**, 119 (2000).
18. S. J. Limb, K. K. S. Lau, D. J. Edell, E. F. Gleason, and K. K. Gleason, *Plasmas Polym.*, **4**, 21 (1999).
19. M. C. Kwan and K. K. Gleason, *CVD*, **3**, 299 (1997).
20. W. K. Chang, M. Y. Liao, and K. K. Gleason, *J. Phys. Chem.*, **100**, 19653 (1996).
21. V. N. Khabashesku, Z. A. Kerzina, A. K. Maltsev, and O. M. Nefedov, *J. Organomet. Chem.*, **364**, 301 (1989).
22. N. Wright and M. J. Hunter, *J. Am. Chem. Soc.*, **69**, 803 (1947).
23. R. E. Richards and H. W. Thompson, *J. Chem. Soc.*, 124 (1949).
24. H. Kriegsmann, in *Advances in Molecular Spectroscopy; Proceedings*, A. Mangini, Editor, **3**, p. 1000, Pergamon Press, New York (1962).
25. A. L. Smith and D. R. Anderson, *Appl. Spectrosc.*, **38**, 822 (1984).
26. K. M. McNamara, B. E. Williams, K. K. Gleason, and B. E. Scruggs, *J. Appl. Phys.*, **76**, 2466 (1994).
27. C. Rau and W. Kulisch, *Thin Solid Films*, **249**, 28 (1994).
28. L. J. Bellamy, *The Infra-red Spectra of Complex Molecules*, 2nd ed., p. 334, John Wiley & Sons, Inc., New York, (1958).
29. T. Alvik and J. Dale, *Acta Chem. Scand.*, **25**, 2142 (1971).
30. G. G. Kirei and M. P. Lisitsa, *Opt. Spectrosc.*, **12**, 403 (1962).
31. I. Tajima and M. Yamamoto, *J. Polym. Sci., A, Polym. Chem.*, **25**, 1737 (1987).
32. A. T. Kohl, R. Mimna, R. Shick, L. Rhodes, Z. L. Wang, and P. A. Kohl, *Electrochem. Solid-State Lett.*, **2**, 77 (1999).

33. M. C. Kwan, Ph.D. Thesis, Massachusetts Institute of Technology, Cambridge, MA (1997).
34. M. Soutzidou, A. Panas, and K. Viras, *J. Polym. Sci., B, Polym. Phys.*, **36**, 2805 (1998).
35. G. Fogarasi, H. Hacker, V. Hoffmann, and S. Dobos, *Spectrochim. Acta.*, **30A**, 629 (1974).
36. F. L. Galeener, *J. Non-Cryst. Solids*, **49**, 53 (1982).
37. C. A. M. Mulder, R. K. Janssen, P. Bachmann, and D. Leers, *J. Non-Cryst. Solids*, **72**, 243 (1985).
38. C. J. Brinker, D. R. Tallant, E. P. Roth, and C. S. Ashley, *J. Non-Cryst. Solids*, **82**, 117 (1986).
39. B. Humbert, A. Burneau, J. P. Gallas, and J. C. Lavalley, *J. Non-Cryst. Solids*, **143**, 75 (1992).
40. T. Nakano, N. Mura, and A. Tsuzumitani, *Jpn. J. Appl. Phys.*, **34**, L1064 (1995).
41. A. L. Smith, *Spectrochim. Acta.*, **16**, 87 (1960).
42. D. M. Adams and W. S. Fernando, *J. Chem. Soc., Dalton Trans.*, **4**, 410 (1973).
43. U. G. Stolberg and H. P. Fritz, *Z. Anorg. Allg. Chemie.*, **330**, 1 (1964).
44. C. A. M. Mulder and A. A. J. M. Damen, *J. Non-Cryst. Solids*, **93**, 387 (1987).
45. M. Hayashi, *J. Chem. Soc. Japan*, **78**, 1472 (1957).
46. R. K. Harris, J. D. Kennedy, and W. McFarlane, in *NMR and the Periodic Table*, R. K. Harris and B. E. Mann, Editors, p. 309, Academic Press, New York (1978).
47. E. A. Williams, in *Annual Reports on NMR spectroscopy*, G. A. Webb, Editor, p. 235, Academic Press, London (1983).
48. D. J. Burton, R. K. Harris, K. Dodgson, C. J. Pellow, and J. A. Semlyen, *Polym. Commun.*, **24**, 278 (1983).
49. R. A. Assink, A. K. Hays, R. W. Bild, and B. L. Hawkins, *J. Vac. Sci. Technol. A*, **3**, 2629 (1985).
50. R. K. Harris and B. J. Kimber, *J. Organomet. Chem.*, **70**, 43 (1974).
51. H. Marsmann, in *NMR: Oxygen-17 and Silicon-29*, P. Diehl, E. Fluck, and R. Kosfeld, Editors, 17, p. 65, Springer-Verlag, New York (1981).
52. H.-G. Horn and H. C. Marsmann, *Makromol. Chem.*, **162**, 255 (1972).
53. S. Roualdes, N. Hovnanian, A. van der Lee, J. Sanchez, and J. Durand, *J. Phys. IV France*, **9**, 1147 (1999).
54. D. R. Anderson, in *Analysis of Silicones*, A. L. Smith, Editor, 41, p. 407, Wiley, New York (1974).
55. C. B. Labelle and K. K. Gleason, *J. Appl. Polym. Sci.*, **74**, 2439 (1999).
56. K. K. S. Lau, J. A. Caulfield, and K. K. Gleason, *Chem. Mater.*, **12**, 3032 (2000).
57. M. Sobolevskii, I. Skorokhodov, V. Ditsent, L. Sobolevskaya, and G. Moiseyeva, *Vysokomol. Soedin., Ser. A*, **12**, 2714 (1970).
58. L. E. Gusel'nikov, N. S. Nametkin, T. K. Islamov, A. A. Sobtsov, and V. M. Vdovin, *Izvest. Akad. Nauk SSSR, Ser. Khimi.*, **20**, 84 (1971).
59. I. M. T. Davidson and J. F. Thompson, *Chem. Comm.*, 251 (1971).
60. I. M. T. Davidson and J. F. Thompson, *J. Chem. Soc., Faraday Trans. 1*, **71**, 2260 (1975).
61. G. Raabe and J. Michl, *Chem. Rev.*, **85**, 419 (1985)

62. M. G. Voronkov, *J. Organomet. Chem.*, **557**, 143 (1998).
63. T. Howard Thomas and T. C. Kendrick, *J. Polym. Sci., A-2, Polym. Phys.*, **7**, 537 (1969).
64. L. E. Gusel'nikov and N. S. Nametkin, *Chem. Rev.*, **79**, 529 (1979).
65. N. Grassie and I. G. MacFarlane, *Eur. Polym. J.*, **14**, 875 (1978).
66. D. J. Bannister and J. A. Semlyen, *Polym.*, **22**, 377 (1981).
67. K. K. S. Lau, K. K. Gleason, and B. L. Trout, *J. Chem. Phys.*, **113**, 4103 (2000).
68. W. Noll, *Chemistry and Technology of Silicones*, 2nd ed., Academic Press, New York, (1968).
69. A. M. Wróbel, M. Kryszewski, and M. Gazicki, *J. Macromol. Sci. - Chem.*, **A20**, 583 (1983).
70. P. Favia, R. d'Agostino, and F. Fracassi, *Pure Appl. Chem.*, **66**, 1373 (1994).
71. G. Smolinsky and M. J. Vasile, *Int. J. Mass Spectrom. Ion Phys.*, **12**, 147 (1973).
72. S. W. Kantor and R. C. Osthoff, U.S. Patent No. 2,793,222 (1957).
73. R. A. Shaw, in *International Symposium on Organosilicon Chemistry*, p. 297, Butterworths, London (1966).



CHAPTER 4

E-Beam Patterning of HFCVD Fluorocarbon Films Using Supercritical CO₂ as a Developer

HG Pryce Lewis, GL Weibel, CK Ober, and KK Gleason, submitted to *CVD*

4.1 Abstract

As microelectronic feature sizes decrease to 100-nm and below, major advances in both interconnect and lithography technologies are necessary. Novel low-k candidates being assessed include fluorine- and silicon-containing materials produced by chemical vapor deposition (CVD). Fluorine- and silicon-containing polymeric materials, highly transparent to 157-nm radiation and developable in supercritical CO₂, are also ideal for advanced 157-nm lithography since, at this wavelength, conventional photoresists are opaque. We are investigating a direct dielectric patterning process in which a low-k fluorocarbon or organosilicon material is deposited by pyrolytic CVD, exposed, and developed using no wet chemistry. In our scheme, a film is deposited using CVD and then masked and exposed using e-beam or a 157-nm source. Development is accomplished using supercritical CO₂ as a dry developing medium. The patterned film then serves as a low-k material compatible with metallization schemes such as the damascene process. This technology would greatly simplify future device manufacture by reducing the number of steps involved in patterning. The dry CVD process and the use of non-flammable, non-toxic, recyclable supercritical CO₂ for development offers environmental, safety and health advantages over solvent-based spin-on coating and aqueous development. Supercritical CO₂ has high diffusivity, no surface tension, and solvating capabilities tunable through pressure and temperature control. It is thus an ideal solvent for development of small, high-aspect ratio features. Positive-tone contrast has been demonstrated in fluorocarbon CVD films and fully-developed images of 0.5-micron have been demonstrated from e-beam exposure. We are presently working to enhance sensitivity and optimize image resolution.

4.2 Introduction

Microelectronics processes are increasingly designed with environmental impact in mind. As technologies change, new process insertion points occur. While polymers have traditionally been employed as photoresist materials, their potential applications in microelectronics have expanded to include low dielectric constant (low-k) materials.¹ Non-plasma chemical vapor deposition (CVD) techniques, such as hot-filament CVD (HFCVD, also known as pyrolytic CVD), have been shown to offer the ability to tailor the chemistry of films with polymer-like structure.^{2,3} In particular, HFCVD allows for more control over precursor fragmentation pathways than conventional plasma-enhanced CVD (PECVD). Thermal activation is limited to the gas phase and independent control of the substrate temperature can be exercised. HFCVD using hexafluoropropylene oxide (HFPO; $\text{CF}_3\text{CF}(\text{O})\text{CF}_2$) as the precursor gas has been shown to produce fluorocarbon films spectroscopically similar to polytetrafluoroethylene (PTFE).³ Bulk PTFE has the lowest dielectric constant of any non-porous material ($k \sim 2.0$), making films produced by this method attractive candidates for interlayer dielectrics. Similar to other fluorine-containing materials, they are highly transparent at 157-nm⁴ but are insoluble in aqueous developers currently used.

Supercritical CO_2 (SCF CO_2) is a promising development medium for fluorinated polymer resists.⁵ Performance enhancement is possible due to the unique properties of the supercritical phase, including low viscosity, negligible surface tension, high diffusivity relative to the gas phase, and density similar to that of the liquid phase. Solvating capability can be fine-tuned by temperature and pressure control.⁶ Pattern collapse caused by surface tension in liquid developers can also be avoided. Indeed, superior performance in producing high aspect ratio features has already been demonstrated using SCF CO_2 as a drying agent following resist development.⁷ In this communication we present the results of a collaboration intended to merge the role of resist and dielectric material, resulting in directly-patterned low-k films. These patterned films serve as insulating material compatible with metallization schemes including the damascene process. In this way, it may be possible to eliminate multiple steps presently required in producing patterned insulators. Environmental, health and safety benefits are also earned by the elimination of wet chemistry in photoresist application and development steps. Using

such a scheme, we have demonstrated positive-tone contrast in fluorocarbon HFCVD films using e-beam exposure and SCF CO₂ development.

4.3 Experimental

HFCVD films for patterning were deposited on silicon wafers in a custom-built vacuum chamber. Undiluted HFPO, donated by DuPont, was used as the precursor gas. For the hot filament, Nichrome wire (28 AWG, 80% Ni, 20%Cr) was resistively heated using a constant voltage of 60 V. Filament temperature was 500±50°C. The filament to substrate distance was maintained at 2.5 cm. Using backside water cooling, substrate temperature was maintained below 48°C during deposition. Details of the reaction chamber and filament have been described elsewhere.⁸ An investigation of the effect of three major process variables (filament preconditioning time, precursor flow rate, and pressure) was undertaken.⁹ Preconditioning was accomplished by burning a virgin filament at deposition conditions for a predetermined period prior to deposition. Some effect of post-deposition annealing was also considered. Several samples were chosen for e-beam exposure and SCF CO₂ development. Those that showed contrast are summarized in Table 4-1.

Table 4-1. Deposition conditions for CVD films that showed sensitivity to e-beam exposure.

sample no.	preconditioning time (min)	deposition time (min)	anneal time / temp (min / °C)	HFPO flow rate (sccm)	chamber pressure (Torr)	film thickness (nm)
1	5	30	60 / ~400	17	0.5	753
2	5	5	no anneal	17	0.5	435
3	5	5	60 / ~200	17	0.5	300
4	15	30	no anneal	30	4.5	722
5	15	60	no anneal	30	1.0	450

Films were characterized while on the substrate by Fourier Transform Infrared Spectroscopy (FTIR), using a Nicolet Magna 860 spectrometer in normal transmission mode. Film thickness was determined by profilometry. Exposure was performed using a Leica/Cambridge EBMF 10.5/CS with 40 KeV beam energy and a current of 1-10 nA. Supercritical CO₂ development was carried out using a commercial supercritical fluid

extraction (SFE) system from Applied Separations, as described previously⁵. SCF grade 4.0 liquid CO₂ (99.99% pure) with less than 100 ppm compressible contaminants and a 1500 psi He headspace from Mattheson was used at a temperature of 80°C and a pressure of 6000 psi at a flow rate of 2-4 L (vapor CO₂)/minute.

4.4 Results and Discussion

Fourier Transform Infrared (FTIR) Spectroscopy. In Figure 4-1, FTIR spectra of four of the samples tested show strong absorption bands at 1,155 cm⁻¹ and 1,215 cm⁻¹, assigned to CF₂ symmetric and asymmetric stretching.^{10,11} Other bands typically associated with CF₂ moieties are also present below 700 cm⁻¹. The spectra differ from one another and from bulk PTFE primarily in the presence of a broad absorption band centered around 3,400 cm⁻¹, and in the presence of bands at ~1,680 cm⁻¹ (in samples 1, 2, and 3), 1,780 cm⁻¹ and 1,880 cm⁻¹. The broad band above 3,000 cm⁻¹ is usually assigned to bound OH and indicates the presence of hydroxyl groups within the film.¹² The ratio of OH/CF₂ for each sample was estimated by integrating the areas of the corresponding absorption bands in Figure 4-1. The absorptions between 1,700 cm⁻¹ and 1,900 cm⁻¹ are associated with C=O moieties, particularly those in COOH and COF.^{13,14}

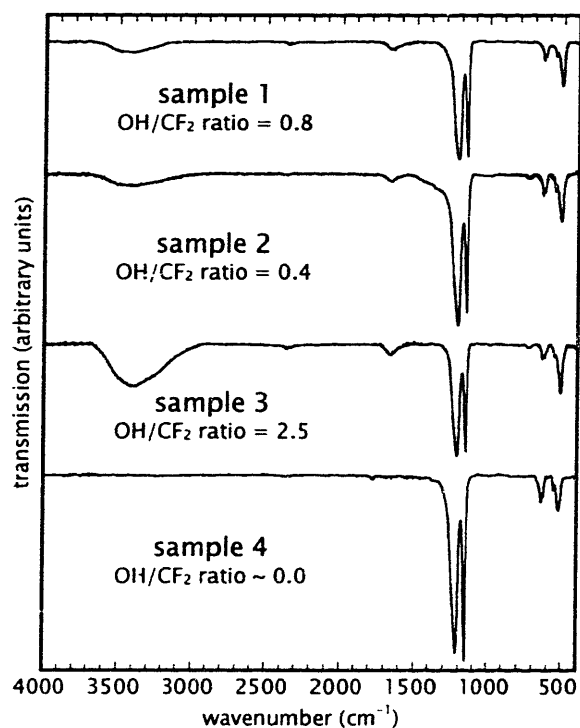


Figure 4-1. FTIR spectra of hot-filament CVD fluorocarbon films from HFPO, showing the change in –OH and –COOH content as a result of varying process conditions. OH/CF₂ ratios were estimated by integrating the area of each absorption stretch in the FTIR spectra.

The presence of groups such as COOH and COF is rationalized by considering the decomposition pathway of HFPO. During thermal activation, HFPO gas can decompose to form CF₂ radicals and the stable gaseous byproduct trifluoroacetyl fluoride (CF₃CFO; TFAcF).^{15,16} The CF₂ radicals can then polymerize to form linear chains and produce fluorocarbon films similar to PTFE. This decomposition pathway, however, does not provide a means of terminating the polymerization process. Unterminated radicals at the end of chains can readily react with oxygen to produce peroxy radicals, which can further decompose to form COF, or react with water to produce COOH⁹. This is analogous to the reactions that occur upon exposing irradiated bulk PTFE to air.^{13,14} From Figure 4-1, it is observed that the concentration of these groups can be minimized by careful design of the HFCVD process. OH and C=O moieties were undetectable in the FTIR spectra of sample 5 (not shown).

Exposure and Development. The films examined in Figure 4-1 were exposed to e-beam and developed using supercritical CO₂. Positive tone patterning was achieved as shown in the contrast curves, Figure 4-2. Complete development was observed in sample 4 with a dosage of 6,000 $\mu\text{C}/\text{cm}^2$. Sample 5 also showed complete development at 6,000 $\mu\text{C}/\text{cm}^2$. Contrast for each sample in the series correlates qualitatively with the concentration of OH and C=O species. It is observed that the lower the OH/CF₂ ratio, the higher the contrast under e-beam exposure.

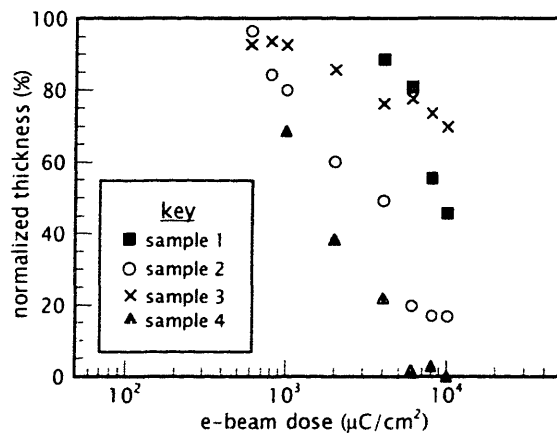


Figure 4-2. Contrast curves of samples 3, 4, 6, and 7, showing e-beam sensitivity following SCF CO₂ development. Sample 4 developed completely in positive-tone.

The high doses required for development suggest that the order-of magnitude increase in sensitivity desired for appropriate lithographic processing will require an explicit understanding of the contrast mechanism coupled with specific molecular design of future films. Addition of moieties for chemical amplification at e-beam (and eventually 157 nm) may also be necessary. An atomic force microscope image of 1.0 μm lines and spaces is shown in Figure 4-3. These 1.0 μm lines showed complete positive-tone development with high contrast. Sub-micron lines/spaces of 0.25 μm have also been obtained. AFM of the films after e-beam exposure and prior to development indicated that ablation was not responsible for the high contrasts observed. Rather, supercritical CO₂ acts as a developing medium to remove the irradiated material.

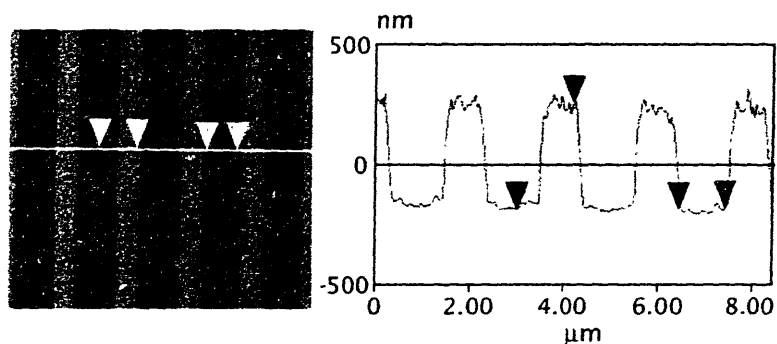


Figure 4-3. AFM image of 1.0 μm lines/spaces in sample 5. Left image is a top-down view, right plot is a cross-section through the line shown at left.

4.5 Conclusion

We have demonstrated successful patterning of 1.0 μm lines/spaces in fluorocarbon CVD films using a novel patterning process. Ongoing work includes the incorporation of moieties during the CVD process to improve sensitivity and resolution.

Acknowledgements. The authors of this paper would like to thank the Cornell Nanofabrication Facility, MIT Lincoln Labs, the NSF/SRC Engineering Research Center for Environmentally Benign Semiconductor Manufacturing, and the Semiconductor Research Corporation. This work also supported by the DOE and made use of MIT MRSEC Shared Facilities supported by the NSF (DMR-9400334).

4.6 References

-
1. See for instance, *MRS Bulletin*, **22** (1997).
 2. S. J. Limb, K. K. S. Lau, D. J. Edell, E. F. Gleason, and K. K. Gleason, *Plasmas Polym.*, **4**, 21 (1999).
 3. K. K. S. Lau and K. K. Gleason, *J. Fluorine Chem.*, **104**, 119 (2000).
 4. R. R. Kunz, T. M. Bloomstein, D. E. Hardy, R. B. Goodman, D. K. Downs, and J. E. Curtin, *J. Vac. Sci. Technol. B*, **17**, 3267 (1999).
 5. N. Sundararajan, S. Yang, K. Ogino, S. Valiyaveetil, J. Wang, X. Zhou, and C. K. Ober, *Chem. Mater.*, **12**, 41 (2000).
 6. C. F. Kirby and M. A. McHugh, *Chem. Rev.*, **99**, 565 (1999).

7. H. Namatsu, K. Yamazaki, and K. Kurihara, *Microelect. Eng.*, **46**, 129 (1999).
8. K. K. S. Lau and K. K. Gleason, *Mater. Res. Soc. Symp. Proc.*, **544**, 209 (1999).
9. K. K. S. Lau, J. A. Caulfield, and K. K. Gleason, *Chem. Mater.*, **12**, 3032 (2000).
10. C. Y. Liang and S. Krimm, *J. Chem. Phys.*, **25**, 563 (1956).
11. R. E. Moynihan, *J. Am. Chem. Soc.*, **81**, 1045 (1959).
12. W. K. Fisher and J. C. Corelli, *J. Polym. Sci., Polym. Chem. Ed.*, **19**, 2465 (1981).
13. N. P. G. Roeges, *A Guide to the Complete Interpretation of Infrared Spectra of Organic Structures*, John Wiley & Sons, New York., (1994).
14. W. Bürger, K. Lunkwitz, G. Pompe, A. Petr, and D. Jehnichen, *J. Appl. Polym. Sci.*, **48**, 1973 (1993).
15. W. Mahler and P. R. Resnick, *J. Fluorine Chem.*, **3**, 451 (1973).
16. P. J. Krusic, D. C. Roe, and B. E. Smart, *Isr. J. Chem.*, **39**, 117 (1999).

CHAPTER 5

Perfluorooctane Sulfonyl Fluoride as an Initiator in HFCVD of Fluorocarbon Thin Films

HG Pryce Lewis, JA Caulfield, and KK Gleason, submitted to *Langmuir*

5.1 Abstract

We have demonstrated the successful use of an initiator species in hot-filament chemical vapor deposition (HFCVD) of PTFE thin films. The introduction of PFOSF in small concentrations allows the enhancement of deposition rates, increased control over film composition, and control over film morphology. Endcapping by CF_3 groups is possible, which may provide benefits such as enhanced thermal stability and higher hydrophobicity for HFCVD films. Conversion of the PFOSF is high, and HFPO utilization efficiency can be increased significantly. The generation of an initiator radical via the pyrolysis of PFOSF may contribute to enhanced nucleation rates during film growth. Initiation and/or nucleation is rate-limiting at low filament temperatures, and mass transport limitations dominate at higher filament temperatures.

5.2 Introduction

Hot-filament chemical vapor deposition (HFCVD, also known as pyrolytic CVD), offers the ability to tailor the chemistry of films with polymeric structure.¹⁻⁴ In particular, HFCVD allows for more control over precursor fragmentation pathways than conventional plasma-enhanced CVD (PECVD).³ HFCVD uses thermal activation in the gas phase to generate reactive species⁵, and allows independent control of the substrate temperature to be exercised. The latter characteristic differentiates HFCVD from conventional thermal CVD, in which precursor breakdown temperature and substrate temperature are identical. The control over reaction pathways available via HFCVD make it possible to produce polymeric fluorocarbon films spectroscopically similar to poly(tetrafluoroethylene) (PTFE) with the precursor hexafluoropropylene oxide (HFPO; $\text{CF}_3\text{CF}(\text{O})\text{CF}_2$).³ PTFE has many desirable properties, including a low refractive index and dielectric constant, low coefficient of friction, excellent chemical resistance, and high thermal stability.⁶⁻⁸ Thin films of PTFE offer advantages for applications as diverse as optical coatings⁹, biopassivation coatings for implantable devices^{10,11}, and interlayer dielectrics (ILDs) in integrated circuits^{12,13} However, bulk PTFE's high melt viscosity and poor solubility make it difficult to process into thin, conformal, and uniform films.⁸ By contrast, HFCVD is capable of providing good control over film structure and morphology on wide range of substrates, including those that are thermally sensitive or of complex geometry.

Previously, we have reported on the characterization of films produced using this process^{2,3}, and on progress made in understanding the deposition chemistry of HFPO during HFCVD.⁵ In this paper, we report on the effects of adding an initiator species, perfluorooctane sulfonyl fluoride (PFOSF, $\text{CF}_3(\text{CF}_2)_7\text{SO}_2\text{F}$), to the HFCVD process. As in conventional polymer chemistry, the use of an initiator allows control over both growth rates and chemical composition of the resulting polymeric film. The use of PFOSF also allows further elucidation of the chemistry of this novel deposition process.

5.3 Experimental

Films were deposited on silicon wafer substrates in a custom built vacuum chamber, as described previously.¹⁴ Thermal excitation was accomplished by resistively heating 28 AWG Nichrome wire (80% Ni/20% Cr) strung on a filament holder. The filament holder straddled a cooled stage on which the silicon wafer was placed. The filament to substrate standoff was 1.0 cm. Pressure in the reactor was maintained at 1.0 Torr by a butterfly valve. Undiluted HFPO of 98% purity, donated by DuPont, was metered and controlled by a mass-flow controller. PFOSF was vaporized in a heated vessel and delivered through a needle valve to maintain flow rates of approximately 3 sccm, 6 sccm, and 11 sccm at three different valve settings. Experiments were performed at these valve settings and HFPO flow rates of 78 sccm and 158 sccm to evaluate the effect of the PFOSF/HFPO flow ratio on deposition rate. Filament temperature was measured using a 2.2 μm infrared pyrometer. For oxidized Nichrome, a spectral emissivity of 0.85 was estimated from direct contact thermocouple measurements. Temperatures were consistent from run to run and there was little variation in power requirements for heating the wire. Films were deposited at filament temperatures ranging from 435 °C to 580 °C. A single filament array was preconditioned for 15 minutes at 510 °C and used for all runs. Substrate temperature was maintained below 40 °C by backside water cooling. Deposition rates were monitored *in situ* using interferometry. A cycle thickness of 2,500 Å/min was calculated and confirmed by profilometry measurements. Nuclear Magnetic Resonance (NMR) experiments were performed on a home-built spectrometer tuned to 254.0 MHz for ¹⁹F detection. A Chemagnetics 3.2 mm double-resonance solids probe was spun at 23 to 25 kHz to perform high-resolution Magic-Angle Spinning (MAS). All spectral chemical shifts were referenced to CFC₃. Other experimental details have been described elsewhere.¹⁵ Atomic force microscopy (AFM) was performed on a Digital Instruments Dimension 3000. Images were taken under tapping mode with a standard etched silicon tip.

5.4 Results and Discussion

Deposition Rate. The addition of small quantities of PFOSF to the HFCVD process increases deposition rates significantly, as indicated in Figure 5-1a. This enhancement in deposition rate is sensitive to the ratio of PFOSF/HFPO for filament temperatures between 465 °C and 531 °C. With PFOSF present, the deposition rate is also found to be sensitive to filament temperature. In Figure 5-1b, deposition rates are plotted in Arrhenius form for films deposited at PFOSF/HFPO ratios greater than 0.07. Two kinetic regimes are observed, with the transition point occurring at a filament temperature of about 470 °C. Below this temperature, the deposition rate depends strongly on filament temperature, and an apparent activation energy of 256 kJ/mole is estimated. Above this temperature, the deposition rate is significantly less sensitive to temperature, and the apparent activation energy is close to zero.

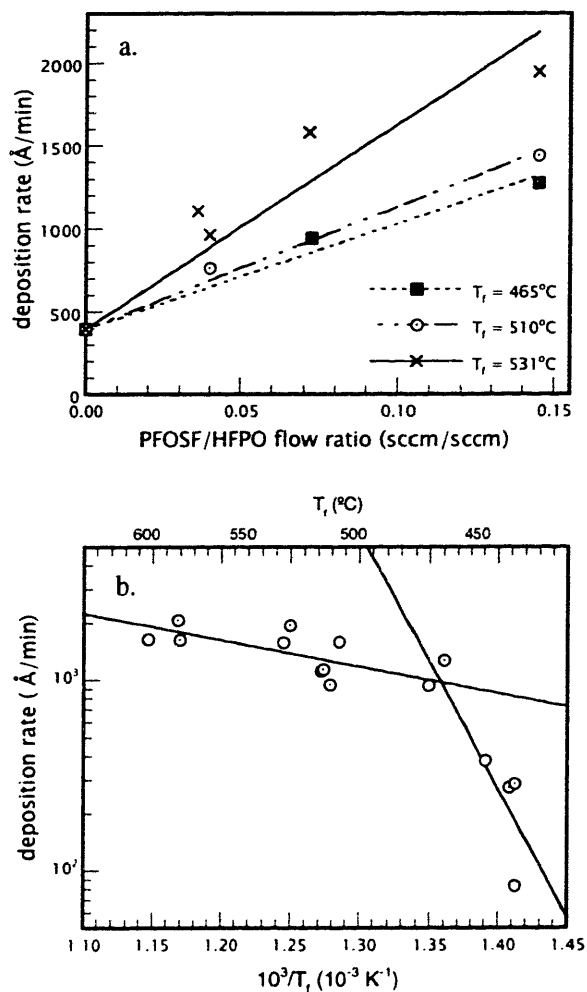


Figure 5-1. Deposition rates of HFCVD fluorocarbon films from PFOSF and HFPO, showing the effect of **a.** adding PFOSF, and **b.** changing filament temperature. Trend lines in Figure 5-1a are included for visual clarification. Figure 5-1b shows data for PFOSF/HFPO ratios greater than 0.07, and is plotted in Arrhenius form. Regression fits illustrate kinetic regimes above and below ~470°C.

Nuclear Magnetic Resonance (NMR) Spectroscopy. To elucidate differences in composition between films produced with and without PFOSF, solid-state ¹⁹F NMR spectroscopy was performed on the films (Figures 5-2a and 5-2b). Assignments are made from the literature.¹⁵

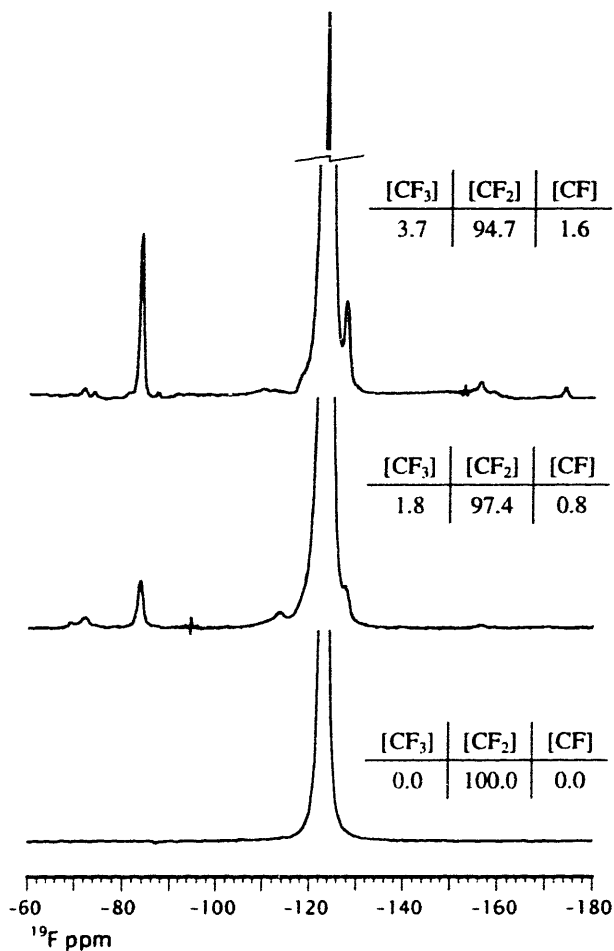


Figure 5-2. Nuclear Magnetic Resonance (NMR) spectra of **a.** HFCVD film from the precursors HFPO and PFOSF, **b.** HFCVD film from the precursor HFPO with no PFOSF, and **c.** bulk PTFE. Concentrations of CF₃, CF₂, and CF are shown in mol %.

As in bulk PTFE (Figure 5-2c), both films show a primary peak at -123 ppm assigned to CF₂CF₂CF₂. The HFCVD films (Figures 5-2a and 5-2b), however, show a shift at -84 ppm which is associated with the endgroup CF₃CF₂CF₂, and a corresponding shift at -128 ppm from CF₃CF₂CF₂. The HFCVD films also show evidence of CF near -156 ppm. No spectroscopic evidence was found indicating retention of the SO₂ group from PFOSF. The concentrations of each of the moieties CF, CF₂, and CF₃ have been tabulated in Figures 5-2a through 5-2c. The concentration of CF₃ in bulk PTFE is typically on the order of 0.01 mol %, below NMR sensitivity.⁶ Films deposited from HFPO with the addition of PFOSF have a higher CF₃ concentration than both bulk PTFE and films deposited from HFPO alone.

Atomic Force Microscopy (AFM). The morphology of films produced with the addition of PFOSF was investigated using Atomic Force Microscopy (AFM). Figure 5-3 shows the effect of filament temperature on films produced using a PFOSF/HFPO ratio of 0.145. Anisotropic, rodlike grain morphologies are observed in the film deposited at a filament temperature of 435 °C (Figure 5-3a) and an RMS roughness of 47 nm is calculated. The film deposited at a filament temperature of 580 °C (Figure 5-3c) shows nodular morphology and is much smoother with an RMS roughness of 6 nm. A roughness of 15 nm was measured for the film deposited at 510 °C (Figure 5-3b). By comparison, the underlying silicon wafer substrate has an RMS roughness of 0.5 nm.¹⁶ Previous work¹⁷ has shown that films grown from HFPO at low deposition rates possess high-aspect ratio grain structures similar to those observed in Figure 5-3c. Nodular structures comparable to those observed in Figure 5-3a were observed at higher deposition rates. Changes in morphology were attributed to competition between the rates of nucleation and propagation during the HFCVD process.¹⁷ By this reasoning, growth of films from PFOSF and HFPO at filament temperatures below 510 °C must be dominated by nucleation and/or initiation pathways rather than propagation events.

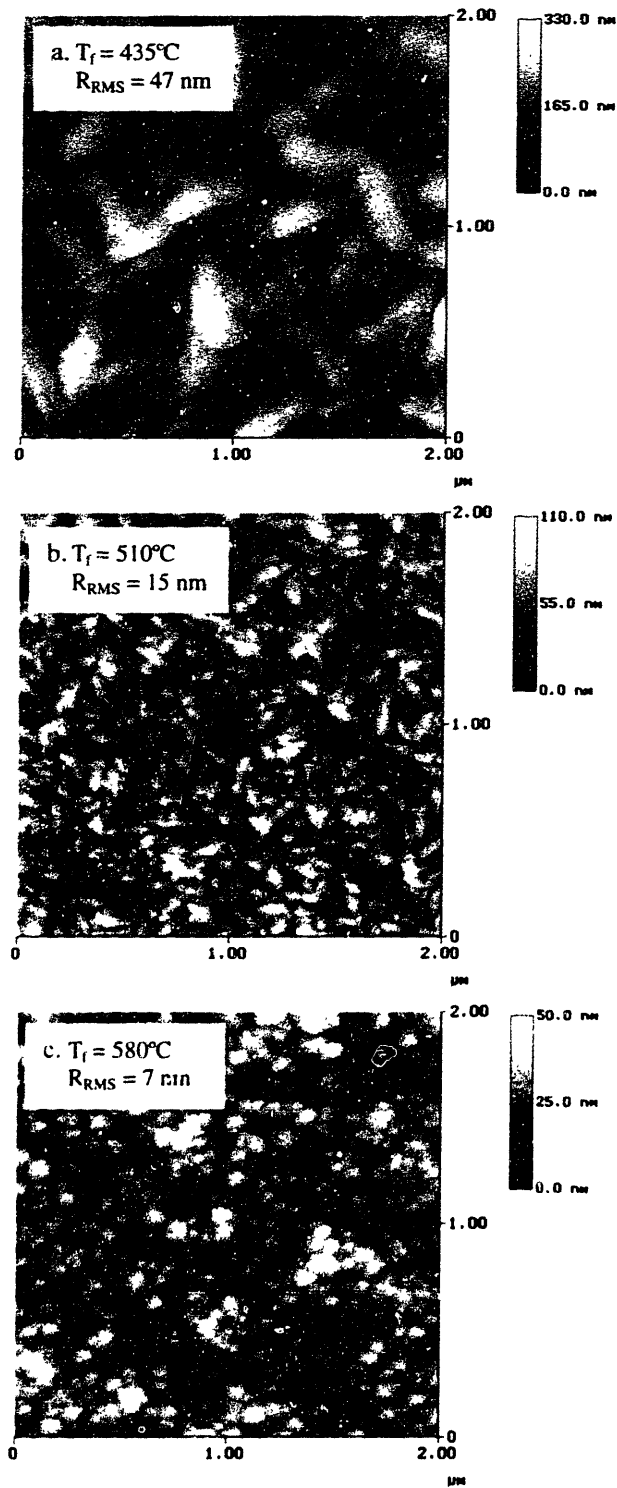


Figure 5-3. Atomic Force micrographs showing the effect of filament temperature on the morphology of HFCVD films from HFPO and PFOF. Films were deposited at a PFOF/HFPO ratio of 0.145 and filament temperatures of **a.** 435°C, **b.** 510°C, and **c.** 580°C. RMS roughnesses are also shown

Reaction Chemistry. The pyrolysis of PFOSF has been investigated by other workers over a temperature range of 460 °C to 550 °C, comparable to the range of filament temperatures used in our work.^{18,19} No activation energy was reported. Conversion of the PFOSF was found to increase with temperature, and conversions of greater than 90% were reported above 490 °C at all PFOSF flow rates considered.¹⁸ Observed products were perfluorinated straight chain molecules from C₈ to C₁₆. A free radical mechanism was postulated to account for the formation of these products, with CF₃(CF₂)₆CF₂· as the primary reactive species. Similar pyrolysis chemistry is expected to occur in our HFCVD system, and the formation of this radical species may constitute an initiation event analogous to that described in classical polymer chemistry. The diradical species, CF₂ (difluorocarbene), generated from the pyrolysis of HFPO would then constitute the propagating species. The proposed polymerization scheme is illustrated in Figure 5-4. Reaction (1) describes initiation via the pyrolysis of PFOSF. Reaction (2) describes the generation of polymerizable species from the pyrolysis of HFPO^{5,20-22}, and reaction (3) is the propagation step. Termination can occur via reaction with an oligomeric fragment or the initiator species, as illustrated in Reactions (4) and (5).

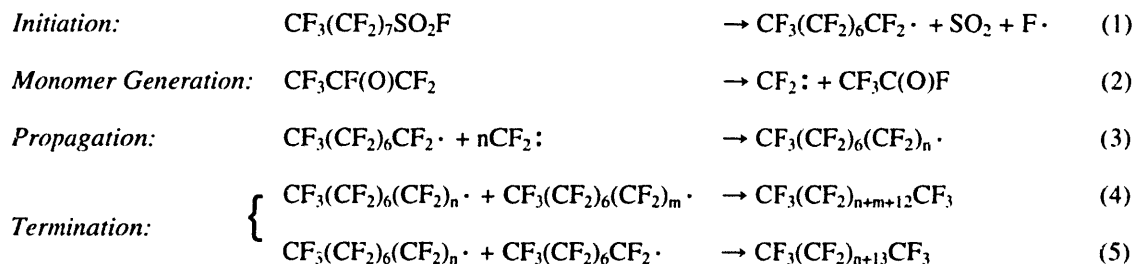


Figure 5-4. Proposed polymerization mechanism for HFCVD using HFPO and PFOSF.

The postulated mechanism provides an explanation for the results observed in our work. The enhanced deposition rate of the films from HFPO and PFOSF is consistent with a mechanism in which PFOSF contributes to initiation. The sensitivity to PFOSF flow rate shown in Figure 5-1a suggests that initiation may be rate-limiting. However, the sensitivity of deposition rate to filament temperature shown in Figure 5-1b indicates that there exists two kinetic regimes over the range of temperatures studied. Below about 470 °C, initiation via the pyrolysis of PFOSF is the rate-controlling step. Indeed, the apparent

activation energy of 256 kJ/mole for this region is close to the reported C-S bond energy of 272 kJ/mole.²³ Above 470 °C, the kinetics are dominated by mass transfer limitations, and deposition rate is relatively insensitive to filament temperature.²⁴ In previous work, the conversion of PFOSF at 470 °C has been reported as greater than 90% for low flow rates.^{18,19} The conversion was observed to reach a maximum of about 97 % at 530 °C, and was almost independent of flow rate above 550 °C.¹⁸ This suggests that above 470 °C, initiation via reaction (1) is no longer limiting.

Initiation by pyrolysis of PFOSF is also evidenced by the higher CF₃ concentrations observed in films deposited from both PFOSF and HFPO. These CF₃ moieties originate from the initiator radical produced by reaction (1) and are incorporated into PTFE chains as end groups during propagation and termination. When HFPO is used without PFOSF, initiation and termination by CF₃ groups is less likely, and films reveal the presence of OH and CO/COO moieties due to the reaction of unterminated CF₂ chain radicals with oxygen and moisture.¹⁴ Carboxyl end groups are observed in fluoropolymers produced using bulk processing methods, and are generally considered deleterious and unstable.²⁵⁻²⁷ CF₃ end groups can impart properties desirable for many applications, including thermal stability and hydrophobicity.^{26,28} The presence of the PFOSF initiator radical thus provides a means for selectively endcapping the PTFE chains.

The morphological effect induced by filament temperature suggests that initiation and nucleation may be related in our system. In previous work with only HFPO, it was proposed that nucleation was rate-limiting at low deposition rates, and propagation rate-limiting at higher deposition rates.¹⁴ In our system, the initiation step is found to be rate-limiting at low temperatures, and a rod-like morphology consistent with nucleation-limited film growth is observed. Conversely, at high temperatures when initiation is no longer limiting, nodular morphology is observed analogous to that observed for propagation-limited film growth. The pyrolysis of PFOSF may thus constitute both an initiation and a nucleation event. This may be due to a higher sticking coefficient for the PFOSF initiator radical than for CF₂. Indeed, the sticking coefficient for higher molecular-weight fluorocarbon radicals is expected to be higher than that for CF₂²⁹, which is typically on the order of 10⁻⁴ to 10⁻³ in the absence of low-energy ion

bombardment.^{30,31} The PFOSF initiator species may thus adsorb preferentially to the substrate surface and enable film growth. It is significant that morphological control that was previously available primarily by variation of filament condition and residence time can now be implemented by adding a secondary nucleating species.

5.5 Conclusions

In conclusion, we have demonstrated the successful use of an initiator species in HFCVD of fluorocarbon thin films. The introduction of PFOSF in small concentrations allows the enhancement of deposition rates, increased control over film composition, and control over film morphology. Endcapping by CF_3 groups is possible, which may provide benefits such as enhanced thermal stability and higher hydrophobicity for HFCVD films. Conversion of the PFOSF is high, and HFPO utilization efficiency can be increased significantly. The generation of an initiator radical via the pyrolysis of PFOSF may contribute to enhanced nucleation rates during film growth. Initiation and/or nucleation is rate-limiting at low filament temperatures, and mass transport limitations dominate at higher filament temperatures. The demonstration of PFOSF as an initiator species validates the argument that many techniques relevant to classical polymer chemistry may be applied to HFCVD.

Acknowledgments. We gratefully acknowledge the support of the NIH under contract NO1-NS-9-2323, and the NSF/SRC Engineering Research Center for Environmentally Benign Semiconductor Manufacturing in funding this work. This work also made use of the MRSEC Shared Facilities supported by the National Science Foundation under Award Number DMR-9400334.

5.6 References

-
1. M. C. Kwan and K. K. Gleason, *CVD*, **3**, 299 (1997).
 2. S. J. Limb, K. K. S. Lau, D. J. Edell, E. F. Gleason, and K. K. Gleason, *Plasmas Polym.*, **4**, 21 (1999).
 3. K. K. S. Lau and K. K. Gleason, *J. Fluorine Chem.*, **104**, 119 (2000).

4. H. G. Pryce Lewis, T. B. Casserly, and K. K. Gleason, *submitted*.
5. K. K. S. Lau, K. K. Gleason, and B. L. Trout, *J. Chem. Phys.*, **113**, 4103 (2000).
6. D. L. Kerbow, in *Polymeric Materials Encyclopedia*, J. C. Salamone, Editor, 9, p. 6884, CRC Press, Boca Raton (1996).
7. S. V. Gangal, in *Encyclopedia of Polymer Science and Engineering*, Vol. 16, H. F. Mark, N. M. Bikales, C. G. Overberger, G. Menges, and J. A. Kroschwitz, Editors, p. 577, John Wiley and Sons, New York (1989).
8. J. Scheirs, in *Polymeric Materials Encyclopedia*, J. C. Salamone, Editor, 4, p. 2498, CRC Press, Inc., Boca Raton (1996).
9. L. Martinu and D. Poitras, *J. Vac. Sci. Technol. A*, **18**, 2619 (2000).
10. D. E. Ocumpaugh and H. L. Lee, in *Biomedical Polymers*, p. 101, Marcel Dekker, New York (1971).
11. W. R. Gombotz and A. S. Hoffman, *Crit. Rev. Biocompat.*, **4**, 1 (1987).
12. T. Rosenmayer and W. Huey, *Mater. Res. Soc. Symp. Proc.*, **427**, 463 (1996).
13. K. K. S. Lau and K. K. Gleason, *Mater. Res. Soc. Symp. Proc.*, **544**, 209 (1999).
14. K. K. S. Lau, J. A. Caulfield, and K. K. Gleason, *Chem. Mater.*, **12**, 3032 (2000).
15. K. K. S. Lau and K. K. Gleason, *J. Phys. Chem. B*, **102**, 5977 (1998).
16. C. B. Labelle and K. K. Gleason, *J. Appl. Polym. Sci.*, **74**, 2439 (1999).
17. K. K. S. Lau, J. A. Caulfield, and K. K. Gleason, *J. Vac. Sci. Technol. A*, **18**, 2404 (2000).
18. M. Napoli, C. Fraccaro, A. Scipioni, R. Armelli, and M. Pianca, *J. Fluorine Chem.*, **24**, 377 (1984).
19. E. Traverso, *Chem. Ind. (Lond.)*, 523 (1986).
20. P. B. Sargeant, *J. Org. Chem.*, **35**, 678 (1970).
21. W. Mahler and P. R. Resnick, *J. Fluorine Chem.*, **3**, 451 (1973).
22. R. C. Kennedy and J. B. Levy, *J. Fluorine Chem.*, **7**, 101 (1976).
23. R. T. Sanderson, *Chemical Bonds and Bond Energy*, 2nd ed., Academic Press, New York, (1976).
24. A. S. Grove, *Physics and Technology of Semiconductor Devices*, p. 7, Wiley, New York, NY, (1967).
25. Y. I. Matveev, A. A. Askadskii, I. V. Zhuravleva, G. L. Slonimskii, and V. V. Korshak, *Vysokomol. Soedin., Ser. A*, **23**, 2013 (1981).
26. W. B. Farnham, A. E. Feiring, B. E. Smart, and R. C. Wheland, WO Patent No. 9702300 (1997).
27. M. Pianca, E. Barchiesi, G. Esposito, and S. Radice, *J. Fluorine Chem.*, **95**, 71 (1999).
28. A. W. Adamson, *Physical Chemistry of Surfaces*, 6th ed., p. 368, Wiley, New York, NY, (1997).
29. S. Samukawa and T. Mukai, *Thin Solid Films*, **374**, 235 (2000).
30. D. C. Gray, I. Tepermeister, and H. H. Sawin, in *Proceedings of the 2nd International Conference on Reactive Plasmas*, p. unpublished (1994).
31. K. Teii, M. Hori, T. Goto, and N. Ishii, *J. Appl. Phys.*, **87**, 7185 (2000).



CHAPTER 6

Hot-Wire Deposition (HWCVD) of Fluorocarbon and Organosilicon Thin Films

KKS Lau, HG Pryce Lewis, SJ Limb, MK Kwan, and KK Gleason, submitted to
Thin Solid Films

6.1 Abstract

Hot-wire or Hot-Filament Chemical Vapor Deposition (HWCVD or HFCVD) affords the capability to synthesize fluorocarbon and organosilicon thin films. These two classes of materials are of interest for a wide range of applications, including low dielectric constant coatings for microelectronic interconnection, “dry” photoresists, directly patternable dielectrics for lithographic production of integrated circuits, insulating biomaterials for implantable devices with complex topologies and small dimensions, low friction coatings, and semipermeable membranes. HWCVD from hexafluoropropylene oxide (C_3F_6O) dramatically reduces crosslink and defect concentrations in fluorocarbon coatings, producing films which are spectroscopically indistinguishable from bulk polytetrafluoroethylene (PTFE, Teflon™). Organosilicon films can be deposited from cyclic precursors such as octamethylcyclotetrasiloxane (D_4) at extremely high rates (>2 microns/min) by HWCVD. The bonding structure of HWCVD organosilicon films is substantially different from both their plasma enhanced chemical vapor deposition (PECVD) counterparts and bulk siloxane polymers, such as poly(dimethylsiloxane) (PDMS).

6.2 Introduction

Both fluorocarbon and organosilicon films find extremely diverse applications because of their unique electrical, chemical and surface properties. Fluorocarbon films are currently being evaluated as dielectric interconnects in microelectronic circuits and as passivation coatings in clinical devices.^{1,2} Potential applications of organosilicon CVD thin films include biocompatible coatings for medical implants³, semipermeable membranes⁴, integrated optical devices⁵, dielectric films⁶, and abrasion and corrosion resistant coatings⁷.

HWCVD represents an alternative to plasma-enhanced chemical vapor deposition (PECVD) for depositing both fluorocarbon⁸ and organosilicon⁹ thin films. Plasma exposure is entirely eliminated by HWCVD, a process in which a fluorocarbon or organosilicon gas is thermally decomposed over a hot surface while the substrate remains cool. In HWCVD, substrate temperature and gas precursor breakdown temperature are independently controlled. This is a distinct difference from conventional thermal CVD which involves heating the susceptor on which the substrate is placed.

HWCVD overcomes some of the processing constraints of having a directly heated substrate. The advantage of being able to achieve high temperature gas decomposition, yet film deposition on a substrate at room temperature, is three-fold. First, absorption limited deposition processes can be employed, since lower substrate temperatures enhance such mechanisms. Second, temperature sensitive substrates can be coated without difficulty, and film stresses due to temperature mismatch during and after deposition can be eliminated. Finally, significantly higher filament temperatures can be attained with low power consumption, permitting a more extensive range of CVD chemistries to be explored.

In this paper, HWCVD of fluorocarbon and organosilicon thin films in our laboratory⁸⁻¹⁵ is reviewed.

6.3 Experimental

For the fluorocarbon films, undiluted hexafluoropropylene oxide (HFPO; $\text{CF}_3\text{CF}(\text{O})\text{CF}_2$) was used as the precursor gas. Organosilicon thin films were grown from

octamethylcyclotetrasiloxane, $[(CH_3)_2SiO]_4$, also known as D_4 from the commonly used nomenclature of D for $-(CH_3)_2SiO-$. D_4 is a monomer which is commonly used in the base catalyzed, liquid phase ring-opening polymerization to PDMS.

Films were deposited onto silicon wafers by HWCVD in a custom built vacuum chamber (Figure 6-1) having backside water cooling on the substrate. The filament to substrate distance was maintained at 2.5 cm for the fluorocarbon films, and 1.0 to 1.5 cm for the organosilicon films. Table 6-1 summarizes the other HWCVD process parameters.

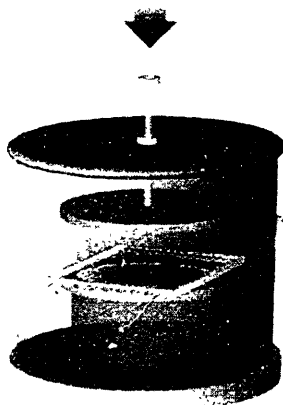


Figure 6-1. Schematic of the HWCVD Chamber. Showing gas inlet through upper showerhead, pyrolysis on square filament array, and deposition onto a wafer substrate resting on the bottom electrode. Gas pump out is toward the back side of the chamber.

Table 6-1. Typical process conditions for HWCVD.

CVD Parameter	Fluorocarbon	Organosilicon
Filament temperature (°C)	400 to 500	800 to 1000
Filament composition	NiCr (80%/20%)	Ta
Substrate temperature (°C)	25	25
Pressure (torr)	0.4 to 1.2	0.2 to 1.0
Flow rate (sccm)	10 to 400	1 to 15
Feed gas	HFPO	D_4

X-ray photoemission (XPS) survey and C1s scans were obtained at a takeoff angle of 45° using a Mg K $\alpha_{1,2}$ source on a Perkin Elmer 5100 instrument. Two spectra were run, a high resolution C1s and a low resolution (e survey) over a broader energy range. A Nicolet 860 was used to obtain the Fourier transform infrared (FTIR) spectra. High-resolution solid-state nuclear magnetic resonance (NMR) experiments were performed with a Chemagnetics 3.2 mm magic angle spinning probe at a field of 6.3 Tesla.

6.4 Results and Discussion

Figures 6-2 and 6-3 compare the ^{19}F NMR and FTIR spectra, respectively, for a film grown by HWCVD of HFPO to bulk PTFE, showing the similarity in chemical structure of the two types of materials.

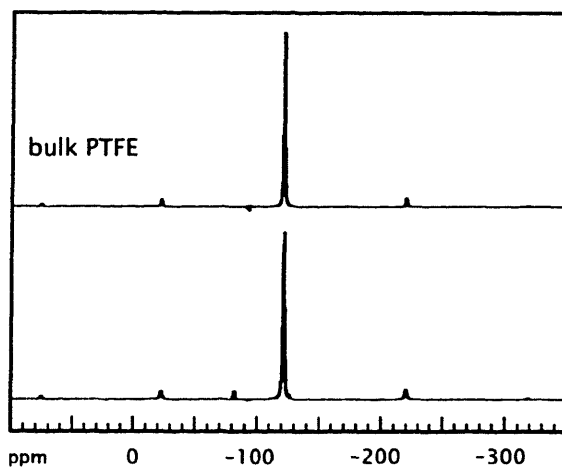


Figure 6-2. Solid state ^{19}F NMR of HWCVD fluorocarbon film (bottom) and PTFE (top).

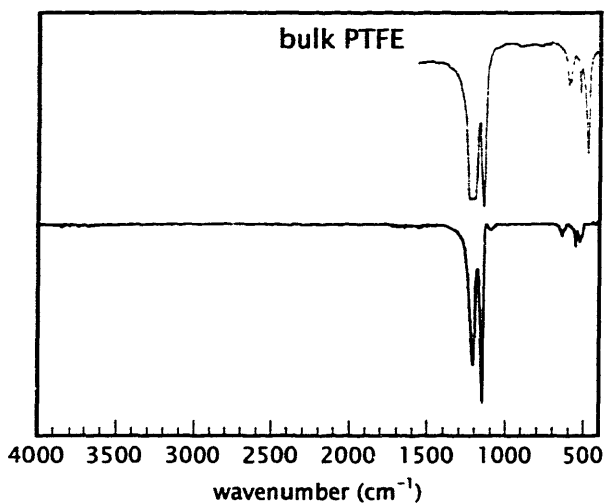


Figure 6-3. FTIR of HWCVD fluorocarbon film (bottom) and PTFE (top).

The precursor gas HFPO has a well-known thermal decomposition pathway (Figure 6-4), which commences at a fairly low temperature of 150°C.¹⁶

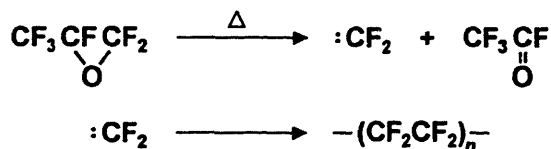


Figure 6-4. Reactions for the pyrolysis of HFPO and polymerization of difluorocarbene.

The product, difluorocarbene, can then polymerize to form linear CF₂ chains.¹³ Thus, HWCVD fluorocarbon films differ from their counterparts grown by PECVD. The PECVD films generally have a F/C ratio of ~1.5 as compared to 2 for PTFE [-(CF₂)-]. In addition, the PECVD films contain dangling bonds (free radicals), double bonds and crosslinks. These defects degrade the film electrical and mechanical properties, and also contribute to the aging of these materials.¹⁷ Exposure of the growth surface to the plasma plays a key role in defect formation. Plasma exposure is entirely eliminated by HWCVD.

Using HWCVD from D₄, high deposition rates (up to 2.5 μm/min) for organosilicon thin films could be achieved.⁹ FTIR (Figure 6-5) verified that the deposited films had the same functional groups as a poly(dimethylsiloxane) (PDMS) standard,

though with a measurably lower methyl concentration. Marked differences in the IR intensity can be seen at 2964 cm^{-1} (asymmetric methyl stretch), 2906 cm^{-1} (symmetric C-H methyl stretch), and at 1410 cm^{-1} (C-H methyl bending modes). No C-C crosslinking is detected, since such a rearrangement would result in the appearance of new peaks in the C-H stretch region at lower wavenumbers corresponding to $\text{sp}^3\text{-CH}_2$. Such $\text{sp}^3\text{-CH}_2$ peaks are often observed in PECVD films.¹⁸ Thus, the HWCVD materials differ from both PDMS and PECVD films.

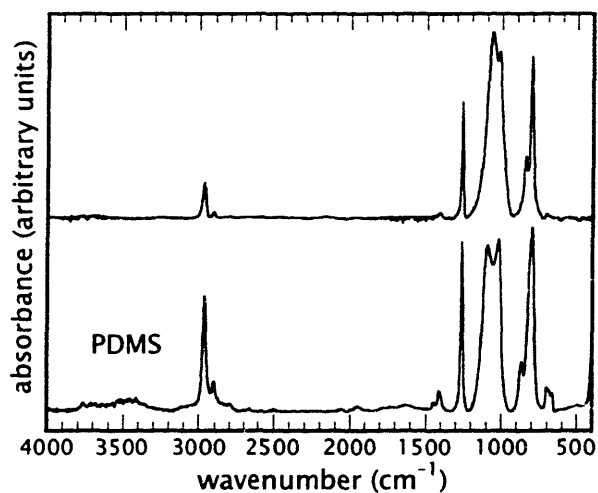


Figure 6-5. FTIR of HWCVD organosilicon film (top) and PDMS (bottom).

XPS showed that a typical film had an elemental composition of C:Si:O / 1.5:1:1, confirming the loss of methyl groups. ^{29}Si NMR suggested the existence of Si-Si crosslinking in the film, also consistent with the loss of methyl groups.¹⁵

The ability of HWCVD to extend the compositional range beyond that of PECVD films can ultimately improve the resulting properties. The molecular architectures uniquely achieved by HWCVD enable all-dry, resistless patterning of fluorocarbon low dielectric constant films, using supercritical CO_2 as the development medium.¹⁹ Lines and spaces defined by electron beam lithography at 0.25 micron resolution are shown in Figure 6-6.

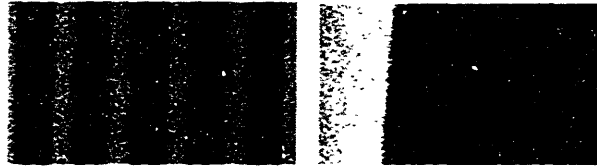


Figure 6-6. HWCVD fluorocarbon low dielectric constant film directly patterned at 1.0 (left) and 0.25 (right) micron resolution.

In addition, the absence of plasma driven densification processes can lead to the incorporation of porosity in the HWCVD films, further reducing their effective dielectric constant.¹⁴ Under HFCVD conditions which limit nucleation, a unique morphology can arise in HWCVD fluorocarbon films, as shown in Figure 6-7. This morphology clearly is the source of the porosity.



Figure 6-7. Scanning electron micrograph of HWCVD porous fluorocarbon film at the edge of the silicon wafer substrate (bottom right). The tilt angle makes it possible to observe both the surface morphology (top left) and porosity through the thickness of the layer.

6.5 Conclusions

Fluorocarbon films have been deposited by HWCVD and possess a chemical structure similar to poly(tetrafluoroethylene). Organosilicon films can be deposited from cyclic precursors such as octamethylcyclotetrasiloxane (D₄) at extremely high rates (>2 microns/min) by HWCVD. The bonding structure of HWCVD organosilicon films is substantially different from both their PECVD counterparts and bulk siloxane polymers, such as poly(dimethylsiloxane).

In contrast to PECVD, the HWCVD process does not involve any ion bombardment or UV irradiation, thus eliminating the possibility of related atomic rearrangements and defects. The ability to grow fluorocarbon and silicone thin films by hot wire CVD reveals that ion bombardment, which is often cited in discussions of PECVD mechanisms as being essential to the creation of active sites for film growth²⁰, is in fact not necessary for the deposition of these materials.

Acknowledgements. We gratefully acknowledge the NIH (Contract N01-NS-3-2301), NSF (CTS-9057119) and the NSF/SRC Engineering Research Center for Environmentally Benign Semiconductor Manufacturing for funding this work. This work made use of MRSEC Shared Facilities supported by the NSF (DMR-9400334).

6.6 References

-
1. K. Endo, T. Tatsumi, Y. Matsubara, and T. Horiuchi, *Jpn. J. Appl. Phys., Pt. 1*, **37**, 1809 (1998).
 2. B. D. Ratner, A. Chilkoti, and G. P. Lopez, in *Plasma Deposition, Treatment, and Etching of Polymers*, R. d'Agostino, Editor, p. 463, Academic Press, San Diego, CA (1990).
 3. A. S. Chawla, *Biomaterials*, **2**, 83 (1981).
 4. J. Sakata and M. Yamamoto, *J. Appl. Polym. Sci., Appl. Polym. Symp.*, **42**, 339 (1988).
 5. P. K. Tien, *Rev. Mod. Phys.*, **49**, 361 (1977).
 6. M. R. Wertheimer and T. S. Ramu, US Patent No. 4599678 (1986).
 7. T. Wydeven, *Appl. Opt.*, **16**, 717 (1977).
 8. K. K. S. Lau and K. K. Gleason, *J. Fluorine Chem.*, **104**, 119 (2000).
 9. M. C. Kwan and K. K. Gleason, *CVD*, **3**, 299 (1997).

10. S. J. Limb, C. B. Labelle, K. K. Gleason, D. J. Edell, and E. F. Gleason, *Appl. Phys. Lett.*, **68**, 2810 (1996).
11. S. J. Limb, K. K. S. Lau, D. J. Edell, E. F. Gleason, and K. K. Gleason, *Plasmas Polym.*, **4**, 21 (1999).
12. K. K. S. Lau, J. A. Caulfield, and K. K. Gleason, *Chem. Mater.*, **12**, 3032 (2000).
13. K. K. S. Lau, K. K. Gleason, and B. L. Trout, *J. Chem. Phys.*, **113**, 4103 (2000).
14. K. K. S. Lau, J. A. Caulfield, and K. K. Gleason, *J. Vac. Sci. Technol. A*, **18**, 2404 (2000).
15. H. G. Pryce Lewis, T. B. Casserly, and K. K. Gleason, *submitted*.
16. H. Millauer, W. Schwertfeger, and G. Siegemund, *Angew. Chem.*, **97**, 164 (1985).
17. H. Yasuda, *J. Macromol. Sci. - Chem.*, **A10**, 383 (1976).
18. H. G. Pryce Lewis, D. J. Edell, and K. K. Gleason, *Chem. Mater.*, **12**, 3488 (2000).
19. G. L. Weibel, H. G. Pryce Lewis, K. K. Gleason, and C. K. Ober, *Polym. Prepr.*, **41**, 1838 (2000).
20. A. M. Wróbel and M. R. Wertheimer, in *Plasma Deposition, Treatment, and Etching of Polymers*, R. d'Agostino, Editor, p. 163, Academic Press, San Diego, CA (1990).



CHAPTER 7

Conclusions and Future Work

7.1 Conclusions

The major accomplishment of this research is summarized in Figure 7-1. It is now possible to draw out an array of CVD material compositions accessible through the selection of an organosilicon or fluorocarbon molecule as a precursor and either PPECVD or HFCVD as the method of deposition. ^{29}Si and ^{19}F NMR spectra illustrate the range of chemical structures possible with any combination of choices. The top row of the array, representing the chemistry of organosilicon films deposited by PPECVD and HFCVD, was incomplete before the research described in this thesis was undertaken.

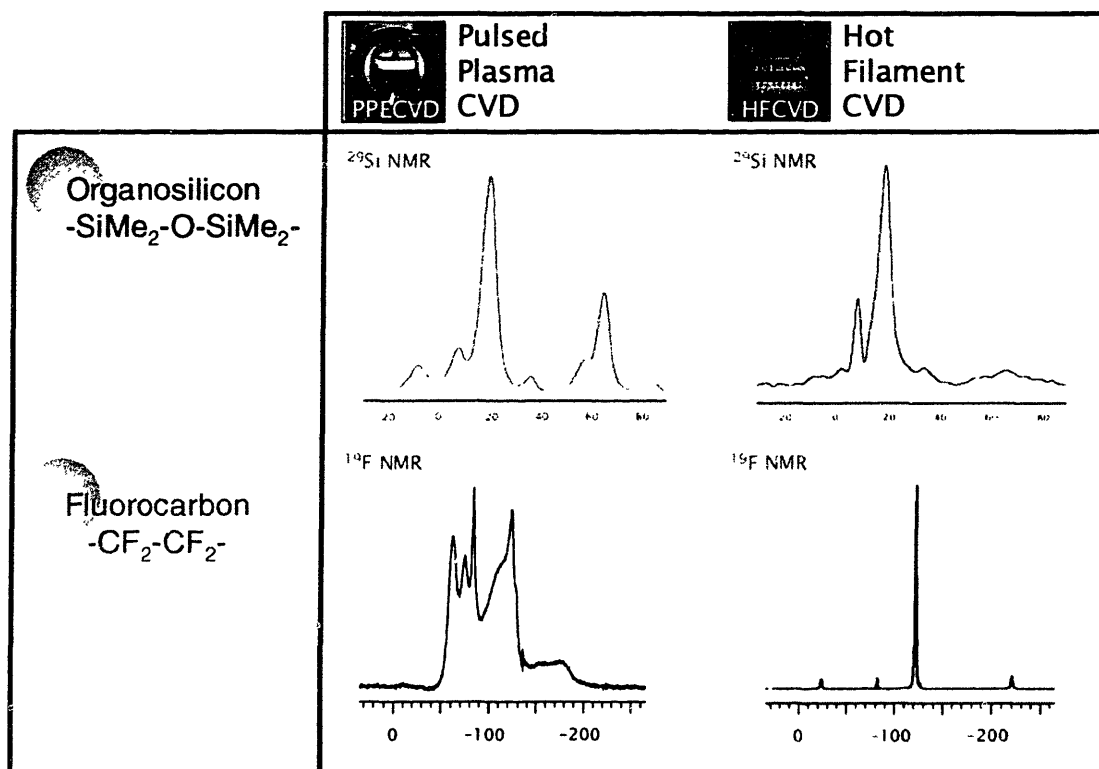


Figure 7-1. Compositional space available from CVD of organosilicon and fluorocarbon materials, as derived from ^{29}Si and ^{19}F NMR. This work filled in the top row of the matrix, and furthered our understanding of fluorocarbon HFCVD chemistry.

A number of unique bonding environments were identified in organosilicon films deposited by CVD, and these are enumerated in Table 7-1. Non-branched structures are shown in the first column, and environments in which silicon is branched are shown in the next three columns. These have been divided into three types. Type I branches are

typical of organosilicon materials prepared by conventional methods such as anionic polymerization.¹ They were observed in PECVD films from D₃, but were present only in low concentrations in HFCVD films. Type II branches involve methylene bonds between siloxane units, and were unique to PECVD films deposited from D₃ under continuous excitation. Type III branches consist of silicon-silicon bonds between siloxane units, and were observed in HFCVD films grown from D₃ and D₄. The proximity of these silicon-silicon bonds to siloxane bonds is remarkable, and probably the result of the incorporation of siloxane ring species in the film structure. HFCVD is thus capable of retaining much of the organic structure present in the precursor molecule.

Table 7-1. Silicon bonding environments in PPECVD and HFCVD organosilicon films.

Non-Branched	TYPE I	TYPE II	TYPE III
$\begin{array}{c} \text{CH}_3 \\ \\ -\text{O}_{\frac{1}{2}}-\text{Si}-\text{CH}_3 \\ \\ \text{CH}_3 \end{array}$	$\begin{array}{c} \text{O}_{\frac{1}{2}} \\ \\ -\text{O}_{\frac{1}{2}}-\text{Si}-\text{O}_{\frac{1}{2}} \\ \\ \text{CH}_3 \end{array}$	$\begin{array}{c} \text{CH}_3 \\ \\ -\text{O}_{\frac{1}{2}}-\text{Si}-\text{O}_{\frac{1}{2}} \\ \\ (\text{CH}_2)_x \end{array}$	$\begin{array}{c} \text{O}_{\frac{1}{2}} \quad \text{CH}_3 \\ \quad \\ \text{CH}_3-\text{Si}-\text{Si}-\text{O}_{\frac{1}{2}} \\ \quad \\ \text{O}_{\frac{1}{2}} \quad \text{CH}_3 \end{array}$
M	T	DCH₂	DM
$\begin{array}{c} \text{CH}_3 \\ \\ -\text{O}_{\frac{1}{2}}-\text{Si}-\text{O}_{\frac{1}{2}} \\ \\ \text{CH}_3 \end{array}$	$\begin{array}{c} \text{O}_{\frac{1}{2}} \\ \\ -\text{O}_{\frac{1}{2}}-\text{Si}-\text{O}_{\frac{1}{2}} \\ \\ \text{O}_{\frac{1}{2}} \end{array}$	$\begin{array}{c} (\text{CH}_2)_x \\ \\ -\text{O}_{\frac{1}{2}}-\text{Si}-\text{O}_{\frac{1}{2}} \\ \\ (\text{CH}_2)_x \end{array}$	$\begin{array}{c} \text{O}_{\frac{1}{2}} \quad \text{O}_{\frac{1}{2}} \\ \quad \\ \text{CH}_3-\text{Si}-\text{Si}-\text{CH}_3 \\ \quad \\ \text{O}_{\frac{1}{2}} \quad \text{O}_{\frac{1}{2}} \end{array}$
D	Q	D(CH₂)₂	D^D
		$\begin{array}{c} \text{O}_{\frac{1}{2}} \\ \\ -\text{O}_{\frac{1}{2}}-\text{Si}-\text{O}_{\frac{1}{2}} \\ \\ (\text{CH}_2)_x \end{array}$	
		TCH₂	

note : x = ½ or 1

A better understanding of the HFCVD chemistry of fluorocarbon thin films was also obtained, and we have demonstrated the use of an initiator species to control polymerization rates and influence film composition. We believe the latter result is

particularly novel and unique, and constitutes a significant contribution to our understanding of the possibilities of gas-phase chemistry processes such as HFCVD.

7.2 Future Work

I believe this research should proceed primarily in the direction of:

Development of new HFCVD materials. HFCVD has already proved itself as a powerful technique capable of producing fluorocarbon and organosilicon materials of unique composition and structure. This technique should be extended to new polymeric systems. The ability to produce polymeric materials on substrates of small and complex geometry will be a key enabler for many emerging technologies in optics, micro-electro mechanical systems (MEMS), and biomedical applications. This also has application for Direct Dielectric Patterning, where new materials of greater sensitivity to e-beam and 157-nm irradiation are required to prove viability and expedite integration of the process in the microelectronics industry.

7.3 References

-
1. W. Noll, *Chemistry and Technology of Silicones*, 2nd ed., Academic Press, New York, (1968).



APPENDIX A

Reactor Design and Construction

A.1 Description

A new CVD reactor system was built, and is shown in Figure A-1. The system was designed to operate in both PPECVD and HFCVD modes, and has a water-cooled stage on which substrates are placed during deposition. A single mechanical pump was used to sustain vacuum pressures down to about 30 mTorr. Flow into the chamber is controlled in two ways: volatile feeds are metered through a flow distribution manifold located in the hood and enter the chamber through the top o-ring sealed port; low vapor-pressure feeds are metered through an MKS 1153 heated mass-flow controller located at the rear of the reactor and enter through a Con-Flat (CF, or Del-Seal[®]) flange at the rear of the chamber. An access door is located at the front of the chamber, which allowed visual inspection of the deposition process for the first time. Film deposition rates can be measured *in situ* using an interferometry system, and filament temperature can be monitored during HFCVD by a pyrometer operating at a wavelength of 2.2-micron. Up to 500W RF power (at 13.56 MHz) is available for PPECVD applications, and a pulse generator can be used to modulate on- and off-times. DC power is available for filament heating.

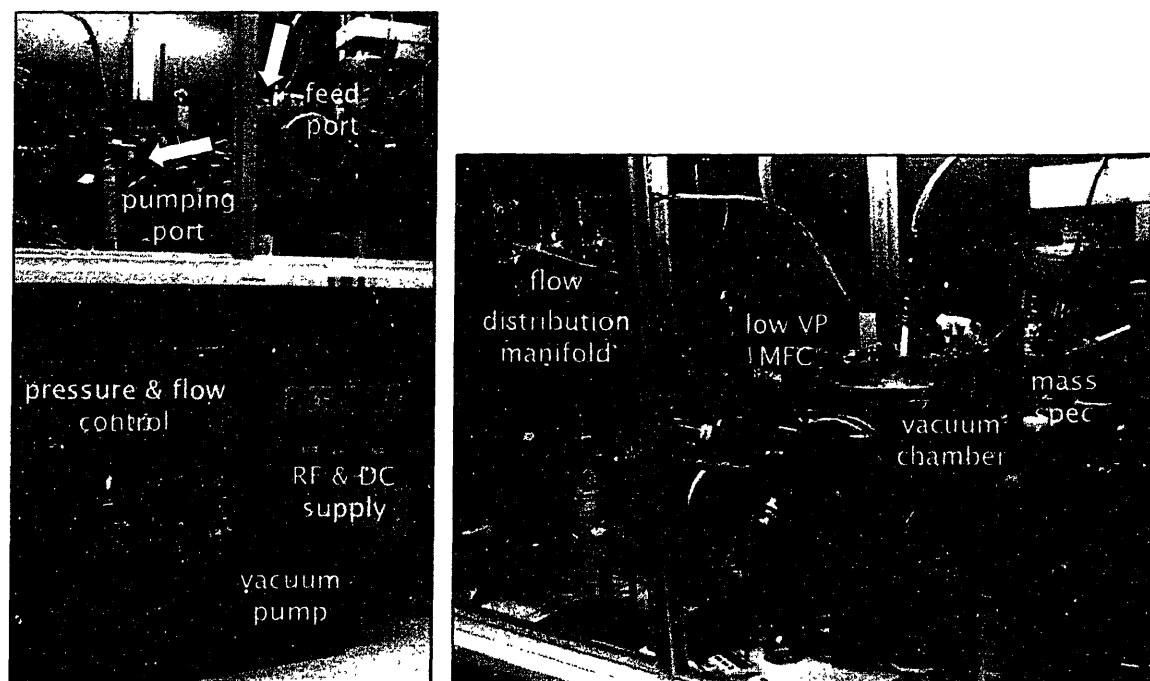


Figure A-1. Photographs of the dual-mode CVD reactor system known as *Pumpkin*.

Front, rear, top and side views of the main chamber are shown in Figures A-2 through A-4. These views show the positions of various ports and the features of the reactor lid. All dimensions are in inches.

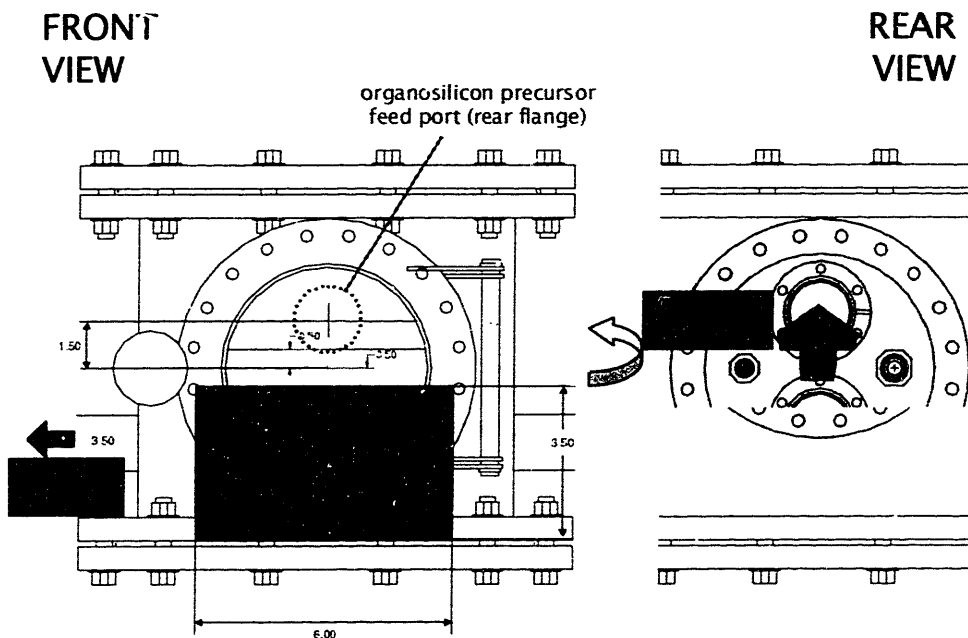


Figure A-2. Front and rear view of chamber, showing feed port and pumping port.

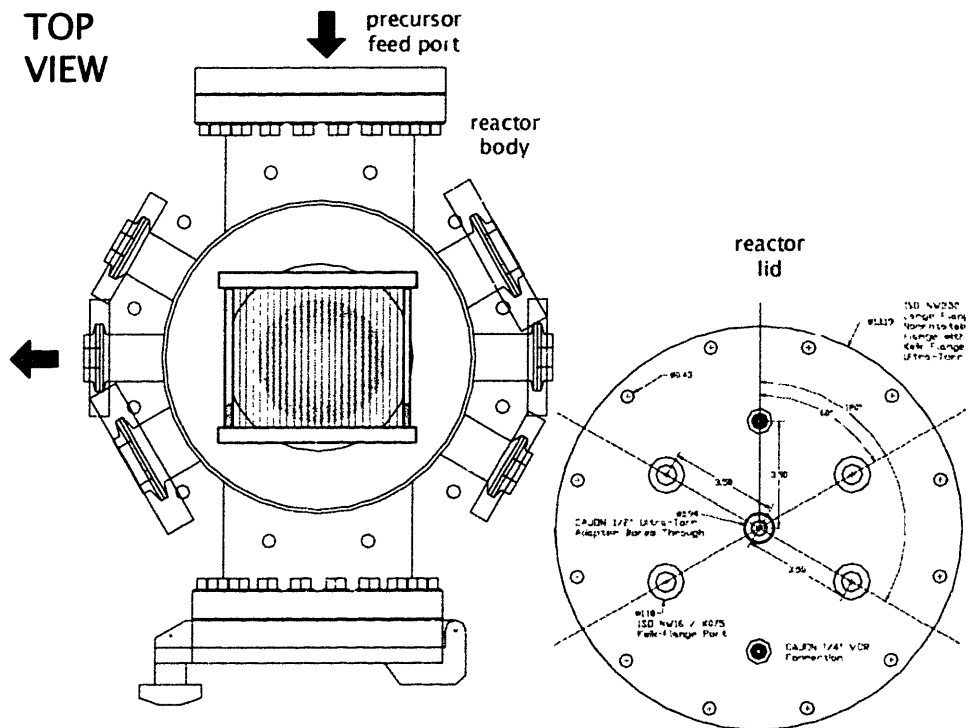


Figure A-3. Top view of chamber, showing lid design, and filament orientation for HFCVD.

SIDE VIEW

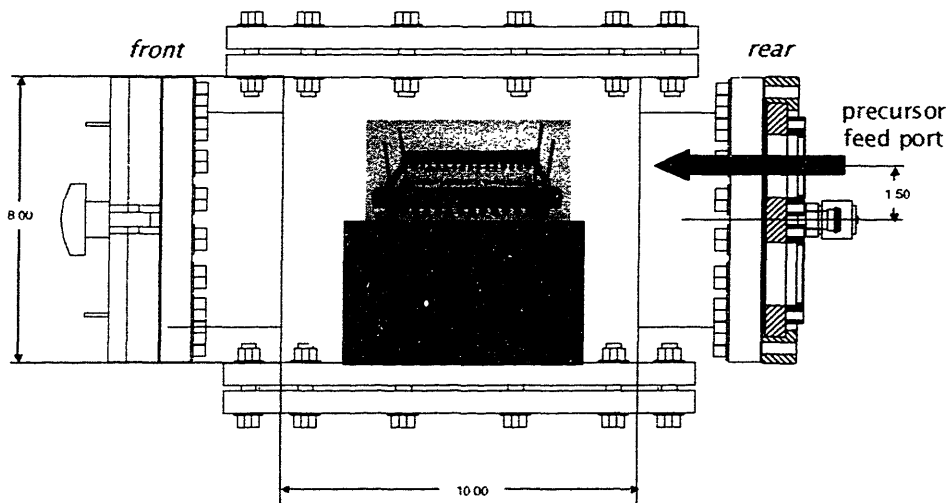


Figure A-4. Side view of chamber, showing water-cooled stage, pumping port and access door.

A.2 Main Chamber CAD Drawings

AutoCAD drawings of the main chamber are shown in Figures A-5 through A-10.

For these, and all other CAD drawings, all dimensions are in inches.

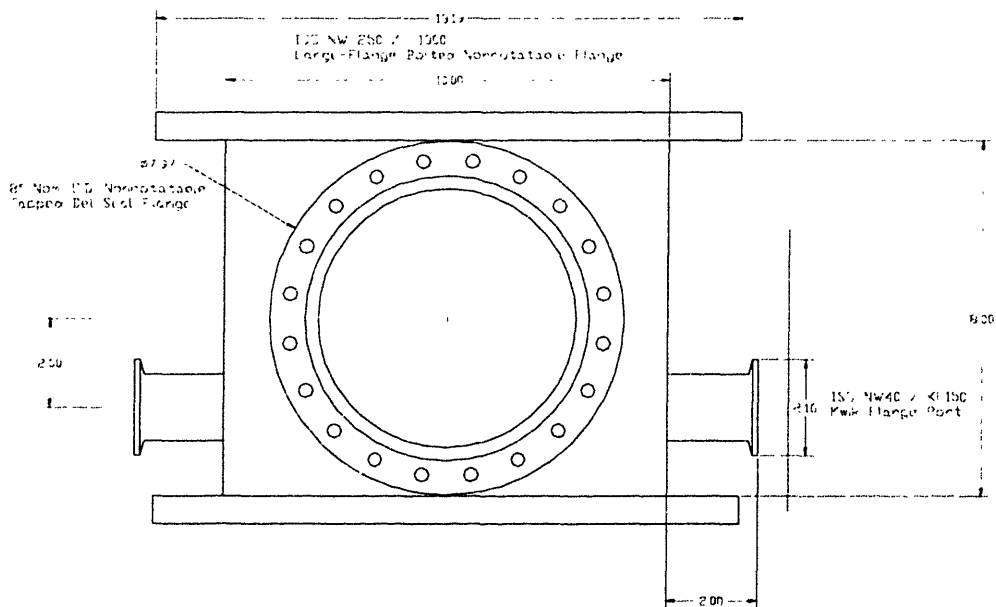


Figure A-5. Front view of chamber design.

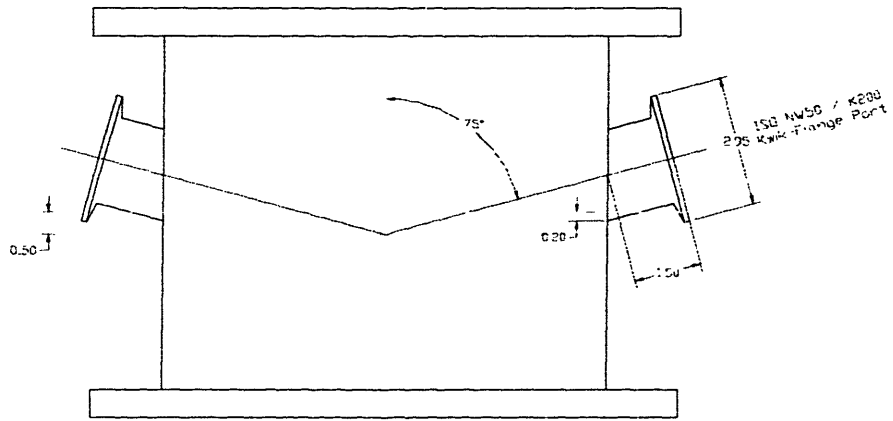


Figure A-6. Front view of chamber design, rotated 30° clockwise as observed from above.

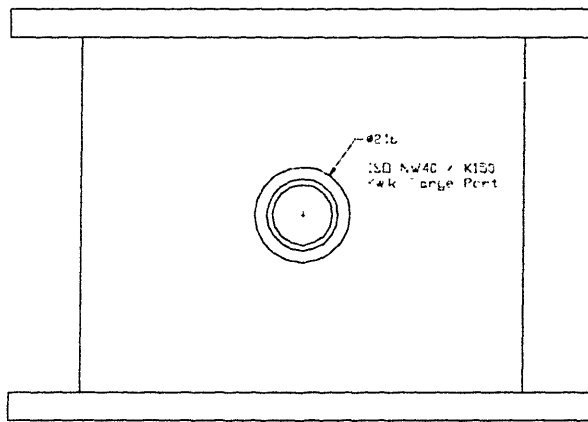


Figure A-7. Front view of chamber design, rotated 60° clockwise as observed from above.

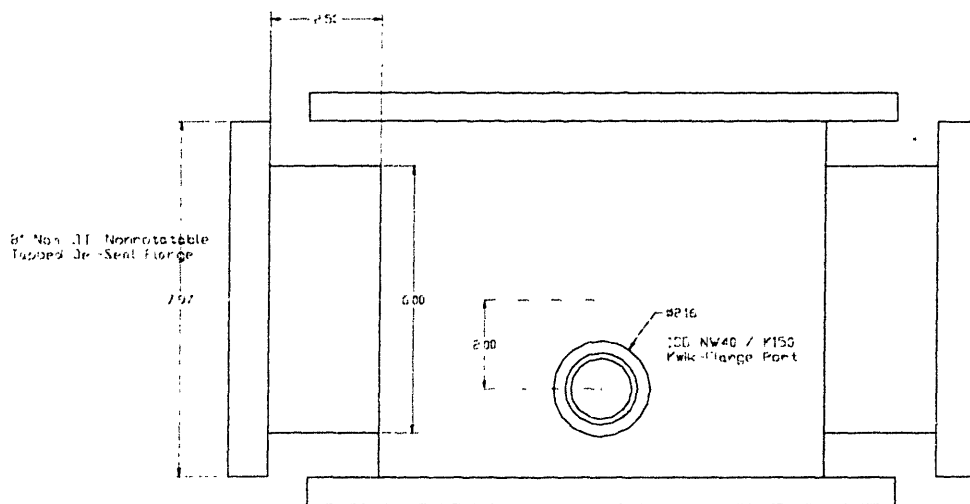


Figure A-8. Front view of chamber design, rotated 90° clockwise as observed from above.

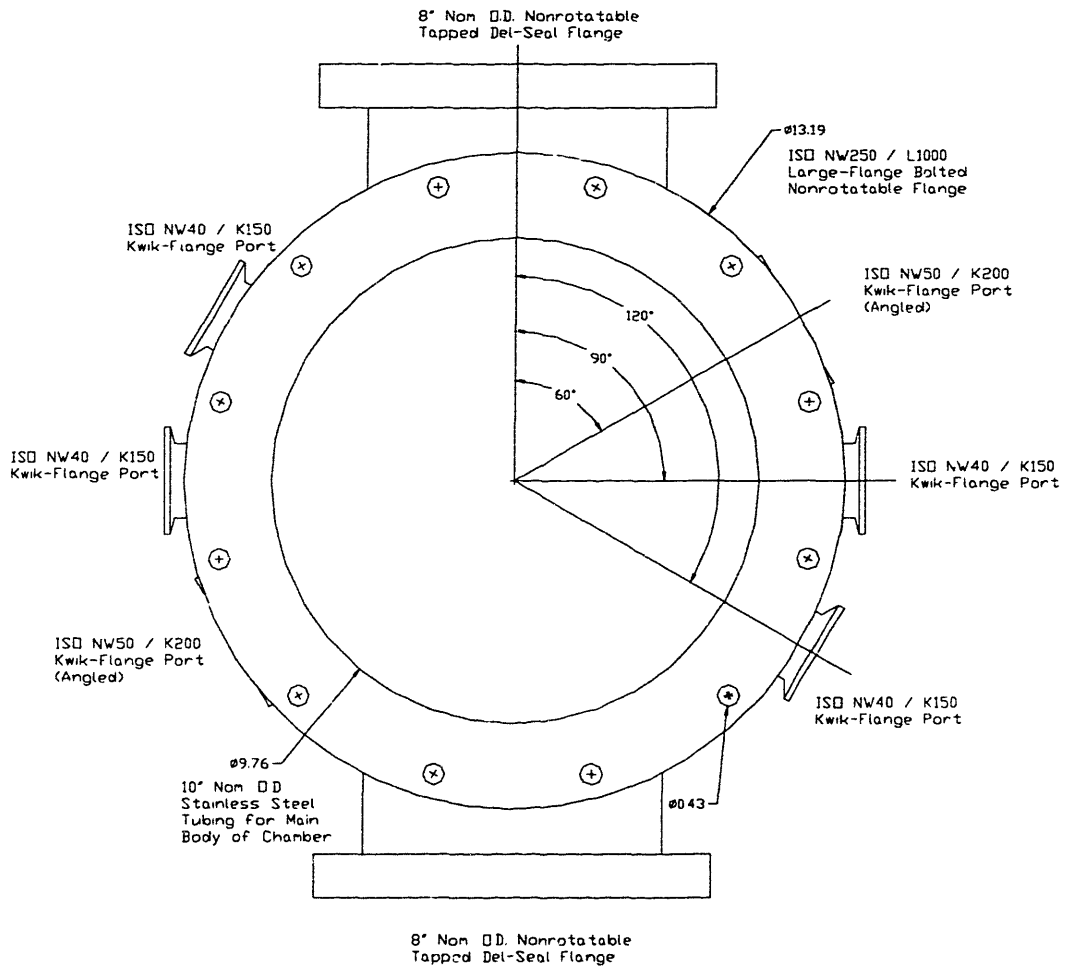


Figure A-9. Top view of chamber design, showing position of ports.

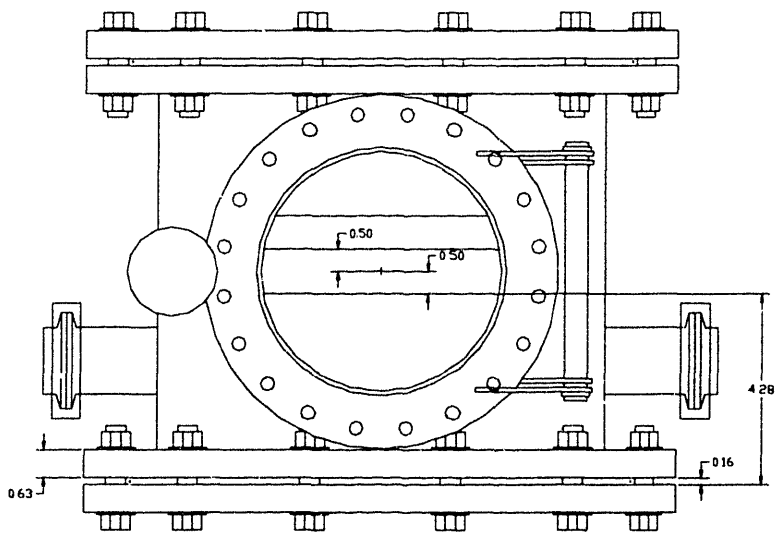


Figure A-10. Assembly view of main chamber design.

A.3 Bottom Plate CAD Drawing

The original design for the bottom plate is shown in Figure A-11. Upon the recommendation of MDC Vacuum, Inc., the copper tubing was replaced with a stainless steel plate 1-in. below the top of the stage to create a cooling water reservoir beneath the stage. Inlet and outlet tubing was welded into the reservoir.

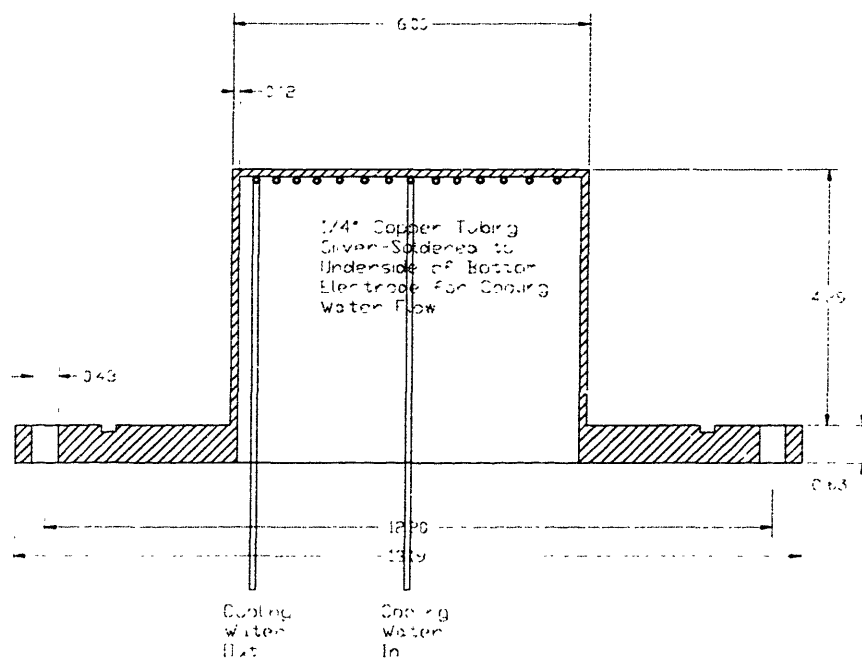


Figure A-11. Side cutaway view of original design of bottom plate. Note that copper tubing was replaced with a stainless steel reservoir 1-in. deep with inlet and outlet tubing in final construction.

A.4 Reactor Lid CAD Drawings

The reactor lid was designed to facilitate the use of a feedthrough Teflon tube to hold the showerhead during PPECVD applications. A central o-ring seal was designed for this purpose. 1/4-in. VCR fittings and NW16 ports were also provided for gas feeds and electrical/thermocouple feedthroughs. AutoCAD drawings are shown in Figures A-12 through A-14.

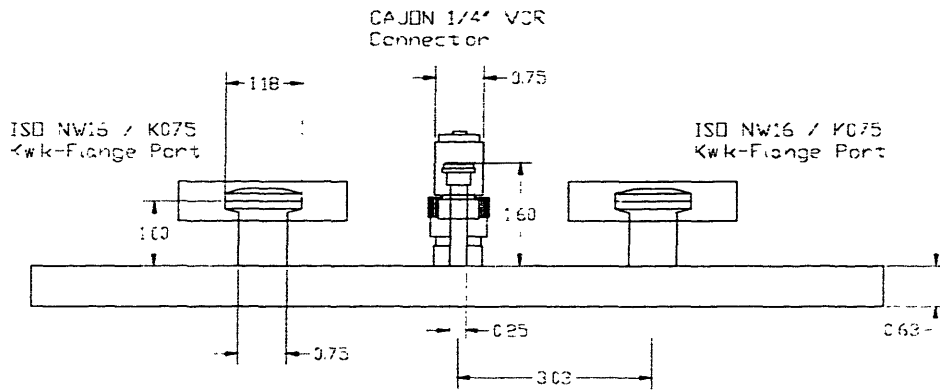


Figure A-12. Side view of reactor lid, showing 1/4-in. VCR and NW16 ports.

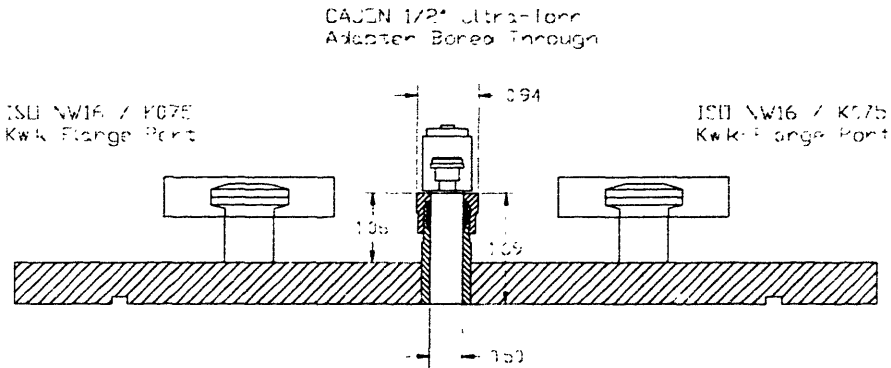


Figure A-13. Side cutaway view of reactor lid, showing 1/2-in. o-ring port and NW16 ports.

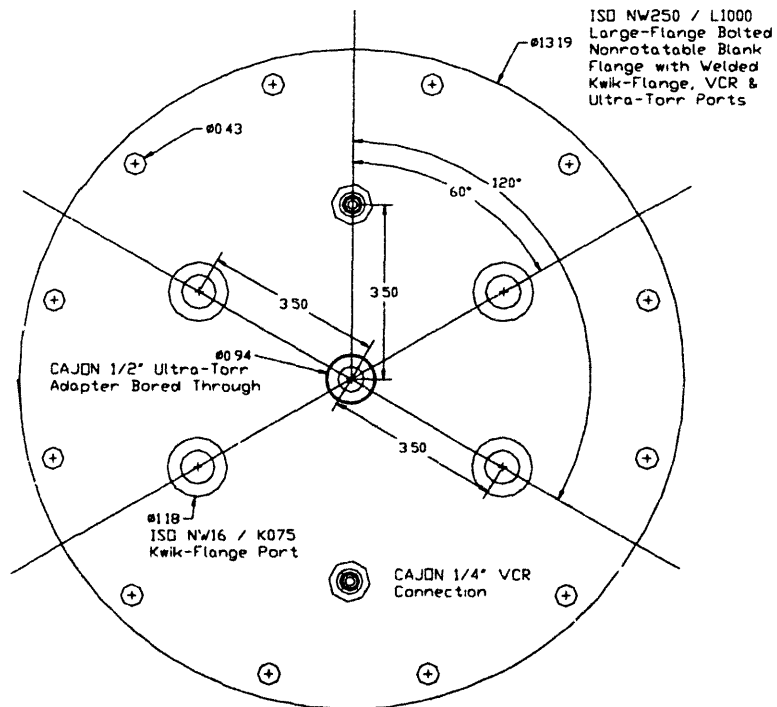


Figure A-14. Top view of reactor lid, showing all ports.

A.5 Rear Flange CAD Drawings

A rear flange was designed to accommodate extra feedthrough and feed ports. The 2-3/4-in. CF port was used as the feed port for low vapor-pressure precursors delivered through the MKS 1153 mass flow controller.

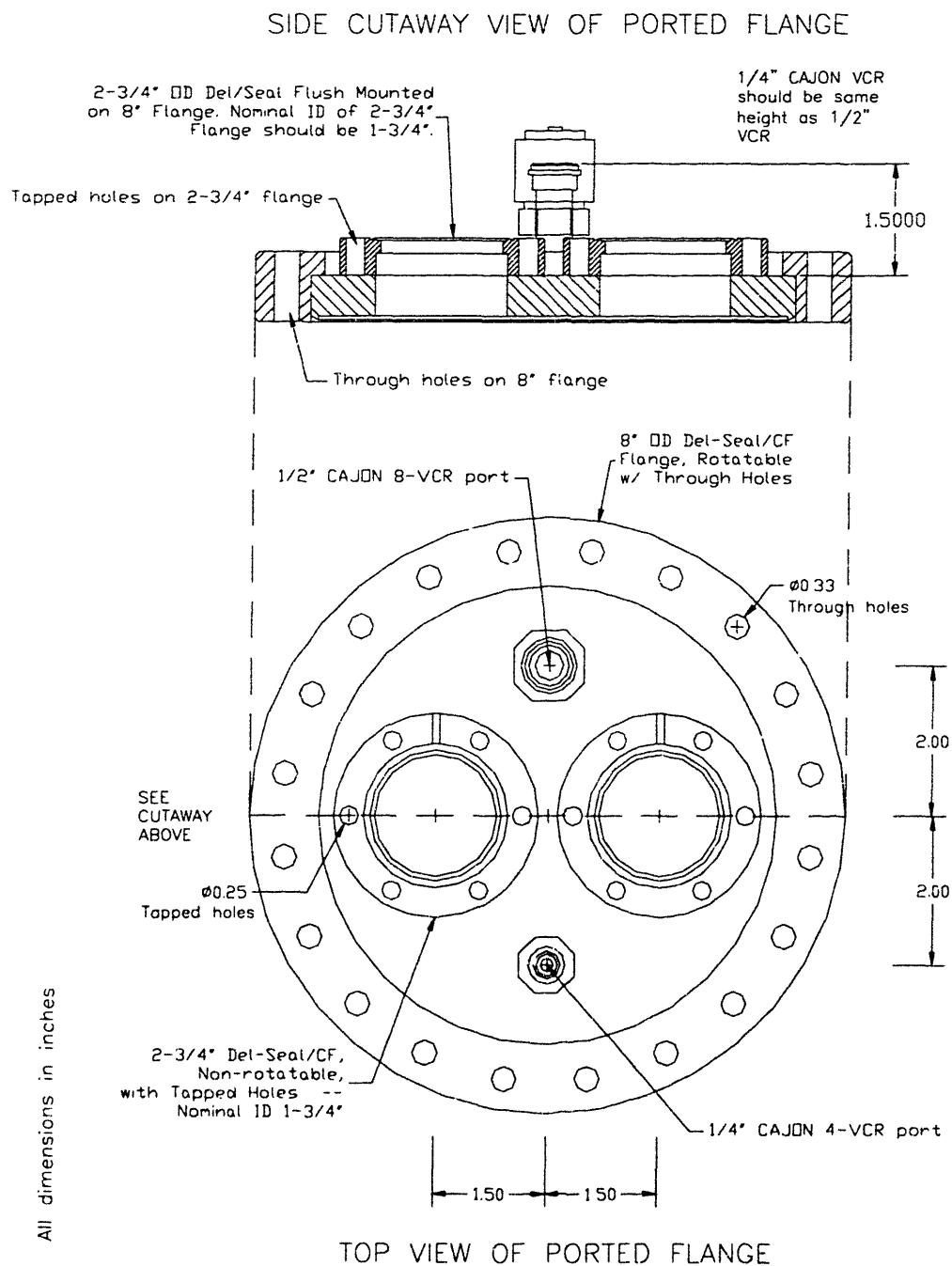


Figure A-15. Top and side views of rear flange.



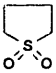
APPENDIX B

Additive Precursors Used in Combination with HFPO HFCVD

B.1 List of Additive Precursors

Table B-1 lists the precursors that were used in combination with HFPO in a screening program designed to test the effects of adding a secondary species during HFCVD. The incorporation of sulfone moieties was desired to increase the e-beam and 157-nm irradiation sensitivity of the basic fluorocarbon materials.

Table B-1. Precursors used in combination with HFPO HFCVD.

Desired Moiety	Secondary precursor	Structure
SULFONE	tetramethylene sulfone sulfolane	
	perfluorooctane sulfonyl fluoride PFOSF	$\text{CF}_3(\text{CF}_2)_6\text{CF}_2-\text{S}(=\text{O})_2\text{F}$
	dimethyl sulfone DMSO ₂	$\text{CH}_3-\text{S}(=\text{O})_2-\text{CH}_3$
	trifluoromethane sulfonic anhydride TFMSA	$\text{F}_3\text{C}-\text{S}(=\text{O})_2-\text{O}-\text{S}(=\text{O})_2-\text{CF}_3$

B.2 Deposition Rates with Additive Precursors

The addition of secondary species during HFPO HFCVD was found to increase deposition rates significantly, as illustrated in Figure B-1. This was attributed to the effect of initiation as described in Chapter 5 of this work.

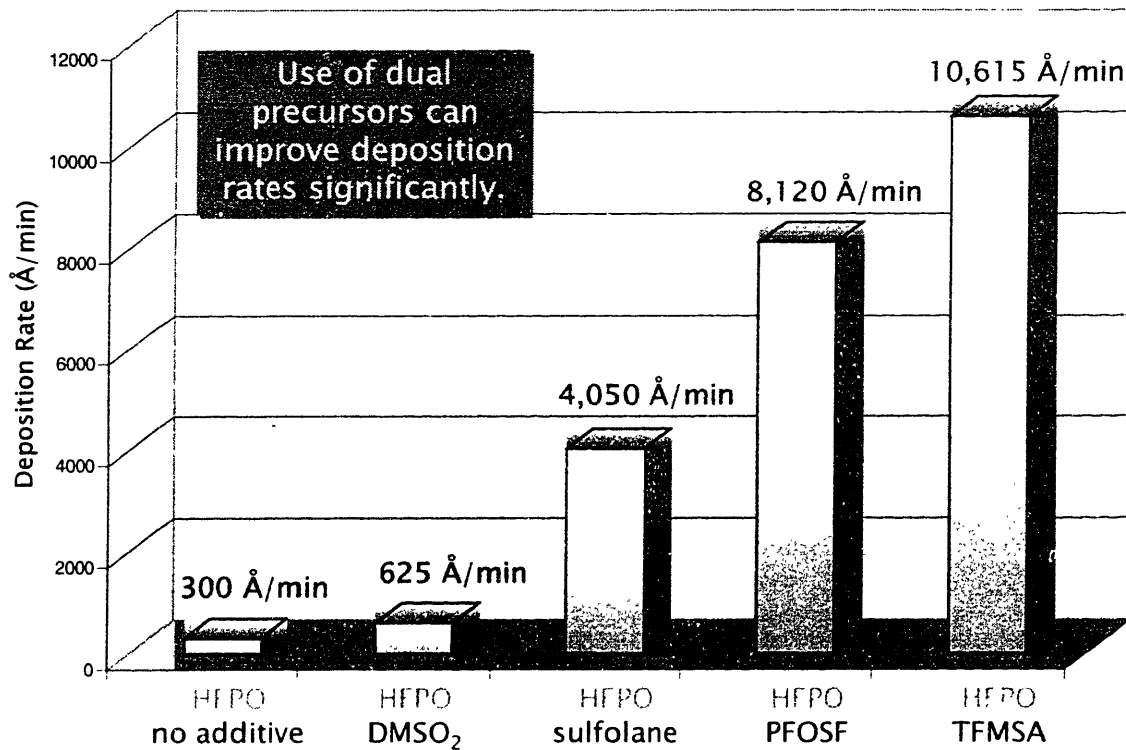


Figure B-1. Typical deposition rates obtained using HFPO with secondary precursor species.

B.3 New Chemistries Possible Using HFCVD with Dual Precursors

Selective endcapping of PTFE chains using HFCVD was demonstrated using HFPO and dimethyl sulfone together, as shown in the C1s XPS spectra in Figure B-2.

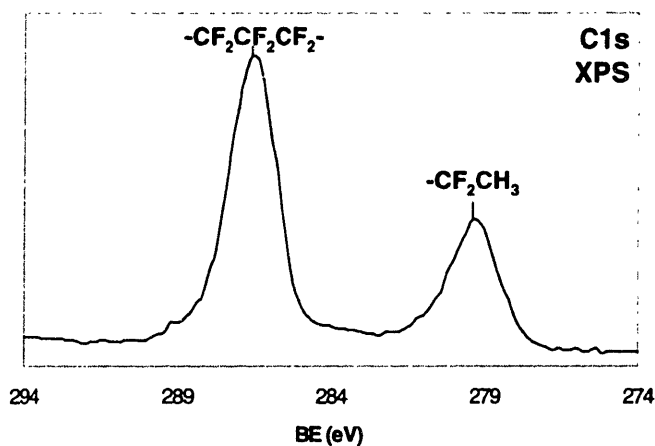


Figure B-2. C1s XPS spectra showing high surface concentrations of terminal CH₃ groups in PTFE films

These results suggest that HFCVD is a powerful technique for producing CVD films of novel composition. A more extensive investigation into the potential for development of materials that can be customized for specific applications is warranted.

THESIS PROCESSING SLIP

FIXED FIELD: ill. _____ name _____

index _____ biblio _____

► COPIES: Archives Aero Dewey ~~Baker~~ Hum
Lindgren Music Rotch Science Sche-Plough

TITLE VARIES: ► _____

NAME VARIES: ► Gavin

IMPRINT: (COPYRIGHT) _____

► COLLATION: _____

► ADD: DEGREE: _____ DEPT.: _____

► ADD: DEGREE: _____ ► DEPT.: _____

SUPERVISORS: _____

NOTES:

*10/2/00
PRYCE
HILLON*

cat'r: _____ date: _____
page: _____

► DEPT: Chem. Eng ► J179

► YEAR: 2001 ► DEGREE: Ph. D.

► NAME: ~~PRYCE~~ PRYCE LLWIS, Hillon

Gavin G.